University of Nevada, Reno

# Emergence of Mechanical Oscillations from Stochastic Simulations of a Discrete Chemical Thermodynamic Model of Force Generation

A dissertation submitted in partial
fulfillment of the requirements for the
degree of Doctor of Philosophy in
Biomedical Engineering

by

Vidya Murthy

Dr. Josh E. Baker/Dissertation Advisor

August, 2023

THE GRADUATE SCHOOL

We recommend that the dissertation
prepared under our supervision by

**VIDYA MURTHY**

entitled

**Emergence of Mechanical Oscillations from Stochastic Simulations of a Discrete Chemical Thermodynamic Model of Force Generation**

be accepted in partial fulfillment of the
requirements for the degree of

**DOCTOR OF PHILOSOPHY**

Josh E. Baker
*Advisor*

Christine Cremo
*Committee Member*

Indira Chatterjee
*Committee Member*

Jihwan Yoon
*Committee Member*

Frederick C. Harris
*Graduate School Representative*

Markus Kemmelmeier, Ph.D., Dean
*Graduate School*

August, 2023

**Abstract**

This dissertation provides a thermodynamic framework, to investigate collective behaviors and emergent mechanisms of muscle contraction. It emphasizes the need for a chemical thermodynamic approach to properly characterize muscle mechanics by presenting facts and historical context to show the inadequacies of the molecular mechanics' approach. A simple and comprehensive model is proposed to explain experimental findings that conventional models of muscle contraction are unable to explain by integrating quantifiable features backed by studies. This study extends our understanding of ensemble muscle function and addresses important issues in the field of muscle research by integrating theory, experimentation, and computer simulations.

**Acknowledgements**.

I want to begin by sincerely thanking Dr. Josh Baker for being such an excellent support. Dr. Baker trusted me and my skills from the beginning of our journey together. His commitment to quality, depth of knowledge, and enthusiasm for innovation and to contribute to science have inspired me to aim higher and to have a curious outlook in many aspects. Even in the busiest periods, you have made yourself available, and showed me a willingness to listen. You have shown genuine interest in my welfare outside of the classroom. Your patience, motivation, and support have been essential to me during this journey's highs and lows. I am really grateful to have you as my graduate advisor.

I am appreciative of Travis Stewart, a fellow lab member, for our brainstorming sessions, conversations, and enthusiasm for science. Learning from you has been a wonderful experience.

My sincerest thanks go out to my esteemed committee members for their valuable feedback, insightful suggestions, and critical evaluation, which enabled me to improve my quality of work. Dr. Indira Chatterjee, Associate Dean of the College of Engineering, has consistently been approachable and has provided invaluable insights and assistance with her thoughtful contributions. Having Dr. Fred Harris on my committee is an honor, as he constantly inspires me with his positive attitude and insightful insights that push me to think critically and deeply. It has been a pleasure to work with Dr. Jihwan Yoon throughout my research journey, as he has been a constant pillar of strength guiding me

through some of my toughest times. Dr. Christine Cremo has not only demonstrated her strength and expertise as a woman in academia but has also communicated her ideas with passion and clarity. In addition to her approachability, she has an exceptional teaching style that has left a lasting impression on me, and I will always cherish our interactions.

I want to thank my parents, brother, and dear friends and family for your belief in my abilities throughout my Ph.D. journey. I am also grateful to colleagues, and fellow students for their friendship, and to all those who have supported me. Your contributions have made this journey possible, and I am very thankful.

I am really grateful for the support provided by the University of Nevada, Reno, which has enabled me to do cutting-edge research, engage in meaningful conversation with distinguished professors, and collaborate with other scholars.

**Dedication**.

This dissertation is lovingly dedicated to Sharath, Viru, and Nidhi, who have been my pillars of support throughout my academic journey. Their belief in me, their encouragement, and their unwavering emotional support have been invaluable in helping me achieve my dream of becoming a Ph.D. holder. I am deeply grateful for their presence in my life and for making my academic pursuit a reality.

## Table of Contents

## List of Tables

## List of Figures

# Chapter 1

## Dissertation Introduction

### Background.

Muscle is an extraordinary structure that is capable of converting chemical energy into mechanical energy to do work. Muscle is a very dynamic system and vital for many physiological processes, including force generation and locomotion. Molecular motors facilitate conversion of chemical energy into mechanical energy and perform physiological functions.

### Muscles.

Muscle is a very complex structure which contains myofibrils, sarcomeres, and motor proteins which enables the contraction and relaxation of muscles and performs a wide range of physiological processes. Muscle tissue is made up of cells or fibers that, when stimulated, have the ability to contract, producing force and enabling movement[1]. The fundamental rod-like structures known as myofibrils, which are found in muscle cells, causes muscles to contract at the cellular level. Sarcomeres, which are fundamental contractile units of muscle contraction, are arranged sequentially within myofibrils. Sarcomeres consists of interdigitated actin and myosin filaments, which slide past one another during muscle contraction and relaxation[2]. The sliding of actin and myosin filaments past each other causes shortening of sarcomeres and, in turn, the overall contraction of the muscle fiber[2,3]. In addition to the structural components, motor proteins play a pivotal role in muscle function. These motor proteins are specialized biological machines that are capable of converting chemical energy, in the form of ATP, into mechanical energy[4]. Motor proteins use this mechanical energy to carry out a variety of

crucial biological processes, including cell division, cellular transport, and muscle contraction, vesicle transport among others[1].

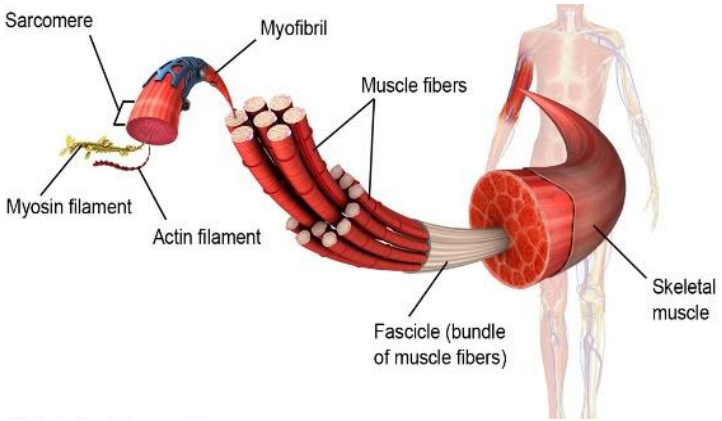


Figure 1-1: Organization of Skeletal Muscle. This figure illustrates the hierarchical levels of organization in skeletal muscle, including the structure of a single muscle fiber with its multiple nuclei and mitochondria, the arrangement of myofibrils within the muscle fiber composed of myosin thick filaments and actin thin filaments. *Source: Shutterstock*

**Sarcomere.**

Sarcomere is a building block of muscle comprising two types of filamentous proteins that play crucial roles in muscle contraction. These proteins are 1) thin filaments comprising two strands of actin and one strand of regulatory proteins 2) thick filaments comprising myosins[5, 6]. There are bands in sarcomere which are used to describe structural details. These bands are visible through electron microscopy and interference contrast microscopy. Z-line is the optically dense region which connects neighboring sarcomeres for mechanical transduction of force[7]. I-band (Isotropic-band) is adjacent to the Z-line which consists only of thin filaments and is a region of low optical density. A-band (Anisotropic-band) is adjacent to the I-band and consists of three zones[7]. H-zone is a region which is composed of only thick filaments, M-line is a region which is center to the bipolar thick filaments without any myosin heads.

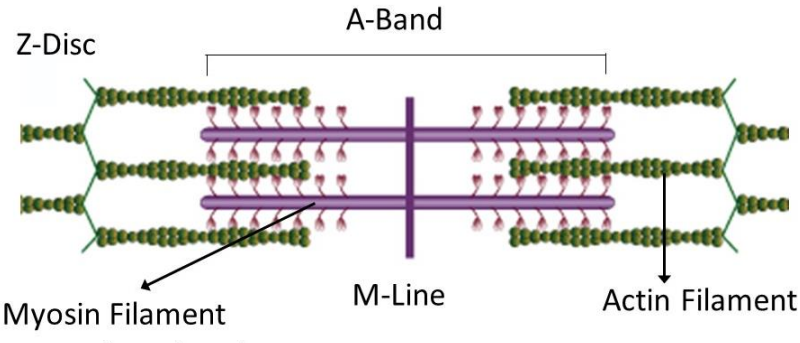


Figure 1-2: Cartoon to show arrangement of thick and thin filaments in the structure of Sarcomere. Sarcomere contains thick and thin filaments. They are composed of myosin thick filaments and actin thin filaments. Thick filaments extend from the M-line in opposite directions, as the actin thin filaments do from the Z disc. Contraction occurs as the myosin heads bind and pull the actin filaments towards the A-Band.

**Actin.** Actin polymerizes to form thin filaments. Actin exists in two forms: G-actin (globular monomer) and F-actin (filamentous polymer of G-actin). Actin filaments are flexible, and filaments have structural polarity due to polarized structure of globular F-actin and establishes the directionality for binding to myosins[8]. Structurally actin filaments are made up of seven actin monomers, actin filaments are 8 nm wide, 1.1 μm long and they extend inward from the Z-disks. The positive ends of the filaments are attached to the Z-disk and the negative end extends toward the middle of the sarcomere where it overlaps the ends of the myosin filaments[7,8].

. Myosin is a molecular motor, a protein that converts chemical energy in the form of ATP to mechanical energy, thus generating force and movement. Myosin was identified more than 100 years ago in muscle[9] . It is no wonder that myosins were the first proteins to be identified when muscle was treated with salt solution; myosin makes up about 38% of the total protein found in muscle. In the last three decades knowledge about myosin family has grown and now we can distinguish 35 different classes in the myosin

superfamily found across all eukaryotic cells[10]. The globular head domain contains actin binding site- and ATP-binding site and is responsible for generating force; this is the most conserved region among the various myosin families. Adjacent to the head domain lies the α-helical neck region, which is associated with the light chains. The latter regulates the activity of the head domain[11]. The tail domain contains the binding sites that determine the specific activities of a particular myosin. Structurally, thick filaments are bipolar polymers of myosin molecules which are 1.8 micrometer long that form clusters of myosin molecules which are bound tightly through their coiled-coil tails[12]. By binding together, the myosin-II molecules have a density of 120-150 molecules per half-sarcomere. Thick filaments are divided by M-line, which consists of only tails of bound myosin molecules[12,11,8].

**Features of Myosin.** Myosin heads are very dynamic in nature, and they are highly disordered and have the capacity to undergo large amplitude rotations in μs range[13]. Myosin head's internal-structure changes during force generation[13]. Myosin is involved in a wide range of transport and contractile activity. A single head functions through its ATPase reaction as a force generator and mechanosensor[14]. When two heads work together to move actin filament, the communication between them contributes to collective myosin behavior[14].

**Actin Myosin ATPase activity.** Figure 1-3 shows a simple five-state discrete chemical model with kinetic and mechanical transitions that are well characterized through single molecule mechanics[22,23,24] and kinetics[25,26] studies. Specifically, myosin displaces an actin filament a distance 8 nm upon strongly binding actin and displaces the actin

filament[24,27] an additional 2 nm upon ADP release[28]. Affinity of myosin to actin decreases from “strong” to “weak” (AM to MT) upon ATP (T) binding to myosin[27,29]. While bound to myosin ATP is hydrolyzed (MT to $MDP_i$) to form the products ADP (D) and $P_i$. Following ATP hydrolysis, a transition from weak-to-strong actin-myosin attachment ($AMDP_i$ to AMD) occurs upon release of $P_i$[29,15]. A large and distinct rotation of the myosin lever arm associated with the $AMDP_i$ to AMD transition generates force[30] and displaces the actin filament[24,31,32,33].

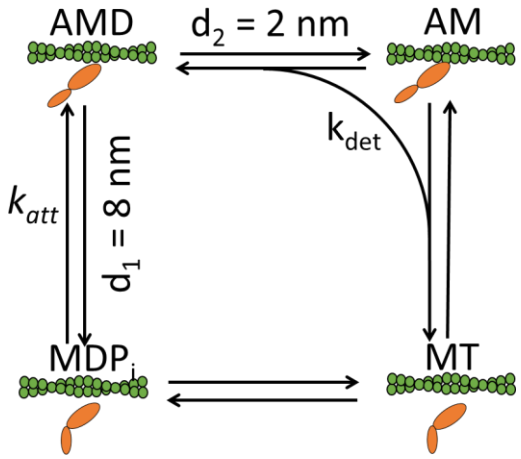


Figure 1-3: ATPase cycle of muscle contraction. The cartoon illustrates the Actin (A) and Myosin (M) interaction during muscle contraction. In the rigor state (AM), A and M are tightly bound. Upon addition of ATP, ATP binds to M, causing dissociation from the actin filament, resulting in the MT biochemical state. ATP is hydrolyzed to ADP and $P_i$ on M, transitioning to the MDP state. The release of inorganic phosphate leads to the $AMDP_i$ state, where the molecule attaches to the actin filament before lever-arm rotation. With the generation of force, the actin filament is displaced, and it enters the AMD state. ADP release returns the molecule to the rigor state, and the cycle repeats.

**Models of muscle Contraction.**

The fundamental basis of muscle contraction involves actin and myosin filaments moving past one another[4]. In certain cases, researchers are interested molecular mechanics rather than ensemble mechanochemistry[3]. The models proposed by A.V. Hill[15] and A.F. Huxley[16,3] offer two distinct and mutually exclusive physical explanations for the mechanochemical coupling that occurs in muscle. These models have served as the cornerstone for research in the field of muscle contraction.

**A.V. Hill's model of muscle contraction.** A.V. Hill played a pioneering role in advancing our understanding of muscle contraction. During a time when technological limitations and the mechanisms of muscle contraction were still unknown, Hill conducted groundbreaking experiments on muscle shortening. Based on his experimental findings,

Hill formulated an original equation that correlates the force and velocity of the system with the heat released during muscle contraction known as the Hill equation:

$$(F + a)(V + b) = c \qquad \text{Eq (1)}$$

Force-Velocity relationship defined in equation 1 is used to describe the inverse relationship of force and velocity, *F* denotes force, *V* is the velocity, *a, b and c* are constants that determine the hyperbolic curve of the force generation, these can be used to determine the force-velocity relation for the contracting muscle. Due to the unavailability of myosin's crystal structure during A.V. Hill's time, his model treats the molecular interactions within the sarcomeres as a "black box."

**A.F. Huxley's model of Muscle Contraction.** X-ray crystallography and advancements in microscopic technologies like electron micrographs (EM) enabled the view of structure of myosin and understanding of molecular mechanisms of muscle contraction and led to the development of sliding filament theory. Huxley described muscle contraction in microscopic detail describing dynamic elements in muscle filaments. Huxley described that myosin heads projects from thick filament and upon stimulation attaches itself to the actin filament and generates force and displaces the thin filament. In 1957, following the observation of myosin crossbridges in EM images of muscle, A.F. Huxley proposed a model in which a myosin head generates force within itself, resulting in models of muscle contraction where muscle force is the sum of independently generated molecular forces, each individual myosin head is treated as a "system" and it neither exchanges energy with the other myosin heads nor it interacts with neighboring myosin heads.

**Thermodynamics Model.** In single molecule experiments, we have learned how single molecules work, but how do the mechanics and chemistry of a single molecule relate to the mechanics and chemistry of muscles? It does not appear that the current models of muscle contraction adhering to the molecular mechanics of A.F. Huxley's model of muscle contraction explaining how molecular motors links muscle mechanics are valid. The connection between molecular mechanics and muscle mechanics is still like a black box, and the only way to establish a connection between those is through thermodynamic models of muscle contraction. A.V. Hill's chemical thermodynamics model was abandoned and was not developed by scientists in muscle field as they followed molecular mechanics model of muscle contraction.

The difference between Molecular Mechanics and Thermodynamics: Molecular mechanics formalism was conceptualized by R. Boyle in 1662[35]. He referred to it as corpuscular mechanics philosophy, in which the property of a system directly results from the property of the individual molecules in that system. According to Boyle, volume of air decreases with increasing pressure and he compared the tiny air molecules within the system to coiled springs and suggested that the with applied force air molecules (i.e., the springs) contracts and decreases the volume and increases the pressure. Later in 1699, Amontons[36] described that the pressure of the gas varies directly with temperature. Consistent with corpuscular mechanics, he thought heat in the form of phlogiston tensioned the springs of air increasing force. Then in 1730, Bernoulli proposed the kinetic theory of gases, which described system force as a thermodynamic property (not the property of a corpuscle/molecule). Since then, corpuscular mechanics has been widely viewed as an obsolete scientific idea.

Bernoulli to Carnot[37], who corrected Amontons by describing the work performed by a heat engine in terms of thermodynamic (not molecular mechanic) parameters such as temperature, T, entropy, and system force. Gibbs described chemical reactions in terms of thermodynamics describing reaction free energy in terms of temperature, T, entropy, and system force, F. In his studies of muscle, A.V. Hill described muscle contraction using thermodynamics describing muscle mechanics in terms of temperature T, system force, and system free energy. Then in 1957[3], crossbridges were observed in electron micrographs of muscle, and the muscle field returned en mass to the obsolete philosophy of molecular mechanics, imagining that myosin molecules contained tiny molecular springs that account for muscle force and that shorten when muscle shortens to perform work. The muscle field remains mired in this corpuscularian worldview to this day.

## Methods

**In-Vitro motility assay:** The in-vitro motility assays are widely used assays to study actin myosin interaction[17]. It is the in vitro model for sarcomere shortening. Myosins are attached to the coverslip, fluorescently labelled actin filaments are run over a bed of myosin molecules. The actin sliding velocities are visualized using a fluorescence microscope (Fig 1-4). There are several advantages of using motility assays. They are a simple system, it efficiently collects large amounts of data, in addition to measuring actin filament velocities, we can measure number of moving filaments. This assay is convenient to measure many different types of perturbations, such as the number of myosin, varying nucleotides, kinetic inhibitors[18,19,20] and buffer conditions[21].

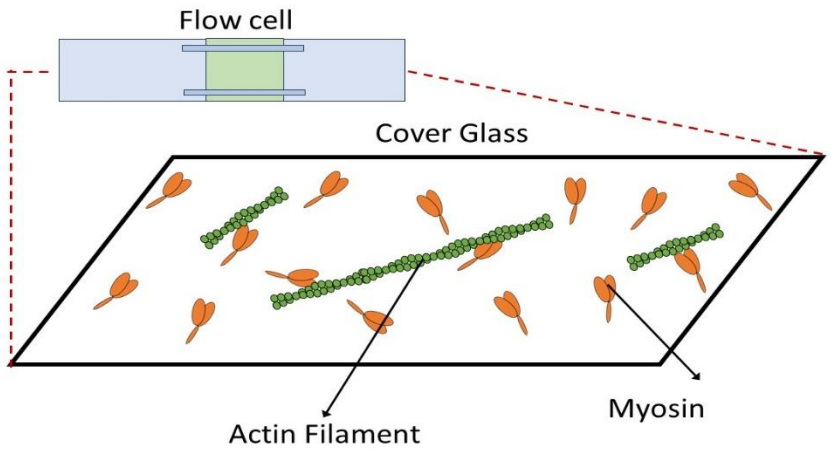


Figure 1-4: In vitro motility Assay. Flow cells with glass coverslips coated with nitrocellulose are coated with myosin molecules. TRITC labeled actin filaments flowed onto the bed of myosin molecules. Motility buffer containing ATP is flowed which induces the ATPase cycle by cyclically interacting with actin and propels the actin filament forward on the surface of the cover slip. Actin filament movement can be imaged under the microscope and the velocities of actin filaments can be measured.

**Computational Model.** We have developed a simple kinetic model based on well-established interaction between actin and myosin in the ATPase cycle (Fig. 1-4), explaining the mechanism underlying muscle contraction. Myosin binds to actin by releasing phosphate and undergoing lever-arm rotation, thereby generating force and displacing actin filaments. The mathematical model will guide us as a predictive tool for experimental outcomes, which are then verified through experiments. We can then refine the model that allows for the prediction of complex behaviors in muscle contraction. We use discrete stochastic simulations, utilizing myosin heads as agents in a Markov Chain with four states that correspond to biochemical states of the ATPase cycle. These simulations enable us to study collective force generation and incorporate both mechanical and kinetic aspects of muscle contraction. The probability of simultaneous transitions is restricted due to their impact on system variables, which arises from coupling the mechanical system state variables with the chemistry of individual myosin heads in this model. Our statistical model reveals emergent behaviors when applied to a ensemble molecules. These molecules are distributed based on the equations defined in the model and they are distributed in the biochemical states. The interactions between the molecules are influenced by strain-dependent kinetics and mechanics. Our objective is to develop a minimalistic model that ensures consistency with known myosin structure and chemistry, while also being capable of explaining complex mechanochemical behaviors exhibited by muscle and flow cell motility assay experiments[34].

**References**


1. Block, S. M. Fifty ways to love your lever: Myosin motors. *Cell* **87**, 151–157 (1996).

2. Huxley, A. F. Muscular contraction. *J. Physiol.* **243**, 1–43 (1974).

3. HUXLEY, A. F. Muscle structure and theories of contraction. *Prog. Biophys. Biophys. Chem.* **7**, 255–318 (1957).

4. Lymn, R. W. & Taylor, E. W. Mechanism of Adenosine Triphosphate Hydrolysis by Actomyosin. *Biochemistry* **10**, 4617–4624 (1971).

5. Walcott, S. & Sun, S. X. Hysteresis in cross-bridge models of muscle. *Phys. Chem. Chem. Phys.* **11**, (2009).

6. Seow, C. Y. Hill's equation of muscle performance and its hidden insight on molecular mechanisms. *J. Gen. Physiol.* **142**, 561–573 (2013).

7. Burgoyne, T., Morris, E. P. & Luther, P. K. Three-Dimensional Structure of Vertebrate Muscle Z-Band: The Small-Square Lattice Z-Band in Rat Cardiac Muscle. *J. Mol. Biol.* **427**, (2015).

8. Chase, P. B., Macpherson, J. M. & Daniel, T. L. A spatially explicit nanomechanical model of the half-sarcomere: Myofilament compliance affects Ca 2+-activation. *Annals of Biomedical Engineering* vol. 32 (2004).

9. Wittinghofer, A. & Geeves, M. A. Review: The ATPase mechanism of myosin and actomyosin. *Biopolymers* **105**, 483–491 (2016).

10. Wittinghofer, A. & Geeves, M. A. Review: The ATPase mechanism of myosin and actomyosin. *Biopolymers* vol. 105 (2016).

11. Cooper, G. M. & Hausman, R. E. *The Cell: A Molecular Approach 2nd Edition*. *Sinauer Associates* (2007).

12. Melli, L. *et al.* Bipolar filaments of human nonmuscle myosin 2-A and 2-B have distinct motile and mechanical properties. *Elife* **7**, (2018).

13. Thomas, D. D. *et al.* The mechanism of force generation in myosin: A disorder-to-order transition, coupled to internal structural changes. *Biophys. J.* **68**, (1995).

14. Jackson, D. R. & Baker, J. E. The energetics of allosteric regulation of ADP release from myosin heads. *Phys. Chem. Chem. Phys.* **11**, 4808–4814 (2009).

15. Hill, A. V. The heat of shortening and the dynamic constants of muscle. *Proc. R. Soc. London. Ser. B, …* **126**, 136–195 (1938).

16. Huxley, A. F. & Simmons, R. M. Proposed mechanism of force generation in striated muscle. *Nature* **233**, 533–538 (1971).

17. Uyeda, T. Q. P., Warrick, H. M., Kron, S. J. & Spudich, J. A. Quantized velocities at low myosin densities in an in vitro motility. *Nature* **352**, (1991).

18. Ostap, E. M. 2,3-Butanedione monoxime (BDM) as a myosin inhibitor. *J. Muscle Res. Cell Motil.* **23**, (2002).

19. Shaw, M. A., Ostap, E. M. & Goldman, Y. E. Mechanism of inhibition of skeletal muscle actomyosin by N-Benzyl-p-toluenesulfonamide. *Biochemistry* **42**, (2003).

20. Cheung, A. *et al.* A small-molecule inhibitor of skeletal muscle myosin II. *Nat. Cell Biol.* **4**, (2002).

21. Greenberg, M. J. & Moore, J. R. The molecular basis of frictional loads in the in vitro motility assay with applications to the study of the loaded mechanochemistry of molecular motors. *Cytoskeleton (Hoboken).* **67**, 273–85 (2010).

22. Guilford, W. H. H. *et al.* Smooth muscle and skeletal muscle myosins produce similar unitary forces and displacements in the laser trap. *Biophys. J.* **72**, 1006–21 (1997).

23. Finer, J. T., Simmons, R. M., Spudich, J. A. & others. Single myosin molecule mechanics: piconewton forces and nanometre steps. *Nature* **368**, 113–119 (1994).

24. Molloy, J. E., Burns, J. E., Kendrick-Jones, B., Tregear, R. T. & White, D. C. S. Movement and force produced by a single myosin head. *Nature* **378**, (1995).

25. Lymn, R. W. & Taylor, E. W. Mechanism of adenosine triphosphate hydrolysis by actomyosin. *Biochemistry* **10**, 4617–4624 (1971).

26. Cremo, C. R. & Geeves, M. A. Interaction of actin and ADP with the head domain of smooth muscle myosin: Implications for strain-dependent ADP release in smooth muscle. *Biochemistry* **37**, 1969–1978 (1998).

27. Baker, J. E., Brosseau, C., Joel, P. B. & Warshaw, D. M. The biochemical kinetics underlying actin movement generated by one and many skeletal muscle myosin molecules. *Biophys. J.* **82**, 2134–2147 (2002).

28. Veigel, C., Molloy, J. E., Schmitz, S. & Kendrick-Jones, J. Load-dependent kinetics of force production by smooth muscle myosin measured with optical tweezers. *Nat. Cell Biol.* **5**, (2003).

29. White, H. D. & Taylor, E. W. Energetics and Mechanism of Actomyosin

Adenosine Triphosphatase. *Biochemistry* **15**, (1976).

30. Linari, M. *et al.* Force generation by skeletal muscle is controlled by mechanosensing in myosin filaments. *Nature* **528**, (2015).

31. Baker, J. E., Brosseau, C., Joel, P. B. & Warshaw, D. M. The biochemical kinetics underlying actin movement generated by one and many skeletal muscle myosin molecules. *Biophys. J.* **82**, 2134–47 (2002).

32. Reedy, M. K., Holmes, K. C. & Tregear, R. T. Induced changes in orientation of the cross-bridges of glycerinated insect flight muscle. *Nature* **207**, 1276–80 (1965).

33. Warshaw, D. M. *et al.* The light chain binding domain of expressed smooth muscle heavy meromyosin acts as a mechanical lever. *J. Biol. Chem.* **275**, (2000).

34. Duke, T. Cooperativity of myosin molecules through strain-dependent chemistry. *Philos. Trans. R. Soc. B Biol. Sci.* **355**, 529–538 (2000).

35. Boyle, R. A Defence of the Doctrine Touching the Spring and Weight of the Air. (1662).

36. Amontons, G. Method of Substituting the Force of Fire for Horse and Man Power to Move Machines. Hist. Mem. R. Acad. Sci. Paris. Transl. by Martyn Chambers.London (1742).

37. Carnot, S. Reflections on the Motive Power of Fire. Dover (2005).

## Chapter 2

### Velocity of myosin-based actin sliding depends on attachment and detachment kinetics and reaches a maximum when myosin-binding sites on actin saturate.

Stewart, T. J., Murthy, V., Dugan, S. P. & Baker, J. E. Velocity of myosin-based actin sliding depends on attachment and detachment kinetics and reaches a maximum when myosin binding sites on actin saturate. *J. Biol. Chem*. 101178 (2021) doi:10.1016/j.jbc.2021.101178.

### Abstract

Molecular motors such as kinesin and myosin often work in groups to generate directed movements and forces critical for many biological processes. Although much is known about how individual motors generate force and movement, surprisingly, little is known about the mechanisms underlying the macroscopic mechanics generated by multiple motors. For example, the observation that a saturating number, *N*, of myosin heads move an actin filament at a rate that is influenced by actin–myosin attachment and detachment kinetics is accounted for neither experimentally nor theoretically. To better understand the emergent mechanics of actin–myosin mechanochemistry, we use an *in vitro* motility assay to measure and correlate the *N*-dependence of actin sliding velocities, actin-activated ATPase activity, force generation against a mechanical load, and the calcium sensitivity of thin filament velocities. Our results show that both velocity and ATPase activity are strain dependent and that velocity becomes maximized with the saturation of myosin-binding sites on actin at a value that is 40% dependent on attachment kinetics and 60% dependent on detachment kinetics. These results support a chemical thermodynamic model for ensemble motor mechanochemistry and imply

molecularly explicit mechanisms within this framework, challenging the assumption of independent force generation.

**Keywords**: myosin, actin, collective force, velocity, mechanics

**Abbreviation**: TRITC, tetramethyl-rhodamine isothiocyanate

**Introduction**

Molecular motors such as myosin and kinesin often work in groups to perform diverse biological functions such as vesicle transport, cell division, wound healing, and muscle contraction[1,2,3] .The mechanochemistry of individual motors is in many instances well characterized[4,5,6,7,8] , and determining how molecular motor mechanics scale from single molecule to ensemble mechanochemistry is the next step in understanding the macroscopic mechanics of biological systems. Our understanding of the factors that influence macroscopic mechanics is currently underdeveloped. These factors include basic relationships between motor kinetics, energetics, force generation, force transmission, compliant linkages, and external loads. The goal of this study is to better define these relationships in order to more accurately describe the emergent mechanics of molecular motor ensembles.

Optical traps and *in vitro* motility experiments have been used to study how force and motion generation change with increasing numbers, *N*, of motors[9,10,11] and in general show that the mechanics of many motors working together is not a simple sum of the molecular mechanics of individual motors[4,12,13]. Consistent with the chemical thermodynamic model that we first proposed over 20 years ago[14], many studies now indicate that force is collectively generated and thermally distributed within systems of motors[12,13,15]. This leads to emergent mechanochemical properties[12,13,16] that are more accurately described by the thermodynamics of a motor ensemble than by molecular mechanics[14,17,18].

With thousands of myosin molecules working together to generate force and movement, muscle is an ideal system in which to study emergent motor behaviors. In the 1920s and 1930s, early pioneers in biophysics like A.V. Hill and W.O. Fenn made precise measurements of muscle power and heat output[19,20,21] that established macroscopic energetic constraints (like muscle force) on muscle mechanics and chemistry using classical chemical thermodynamics. Since then, researchers have focused more on reductionist approaches using electron microscopy, X-ray diffraction, spectroscopic techniques, stopped flow kinetics, crystal structures, and single molecule mechanics measurements[22,23,24,25,26,27,28,29] to provide detailed structural, biochemical, and mechanical descriptions of the molecules involved in muscle contraction. For example, from these studies we now know that the basic molecular mechanism for muscle contraction involves a discrete displacement of an actin filament generated by a myosin structural change induced by strong actin binding. However, despite these remarkable insights into basic molecular mechanisms, it is still unclear how these observable, simple, discrete molecular mechanisms scale up to the mechanics and chemistry of muscle in a way that is consistent with the macroscopic energetic constraints described by Hill and Fenn[19,21] and more recently implied by our observation that the free energy for the discrete myosin working step is a function of muscle force[17].

The conventional independent force model of muscle contraction assumes that actin sliding velocities, $V_{max}$, are limited by detachment of individual myosin motors from actin[30]. However, this model does not account for the thermal equilibration of forces that exists in most chemical systems and is inconsistent with the observation that $V_{max}$ is influenced by both actin–myosin attachment[4,10,16,18,31] and detachment kinetics[30,32]. Here

we use mathematical modeling and an *in vitro* motility assay to better understand how both attachment and detachment kinetics contribute to $V_{max}$.

In an *in vitro* motility assay, the velocity, *V(N)*, at which actin filaments slide over a bed of myosin molecules increases with increasing numbers, *N*, of myosin molecules, saturating at a maximum velocity, $V_{max}$, through a mechanism that continues to be disputed. For decades, it has widely been assumed that—in accord with independent force models— $V_{max}$ is limited by what are effectively molecular mechanical barriers to force transmission between independent force generators[30,32]. Specifically, a single strongly bound myosin head is assumed to prevent the working step of other myosin heads from moving actin and transmitting forces between them, and thus movement is limited by detachment of the resistive myosin head.

To describe this hypothetical mechanical limit to $V_{max}$, we consider the probability, *P(N)*, that *N* myosin heads stall actin movement by myosin working steps. According to the independent force model, *P(N)* is simply the probability that at least one myosin head is bound to actin[32]. According to a collective displacement model that we recently developed, *P(N)* is the probability that at least one myosin head is bound to actin and has reached the end of its mechanical tether[33]. Here we develop a thermodynamic force model in which *P(N)* is the probability that an ensemble of myosin heads collectively reaches an internal stall force. Of importance, *P(N)* in the latter two models is clearly less than that in the independent force model. In all models, when $P(N) = 1$, actin movement can only occur with the detachment of the resistive head(s) (see Experimental procedures), at which point *V(N)* saturates at a $V_{max}$ that is limited by actin–myosin

detachment kinetics. Although this solid-state, detachment limit is theoretically possible within any of the above models, here we show that experimentally it is never reached (*P(N)* is always less than one) by myosin ensembles under physiological conditions.

We determine the chemical kinetics underlying *V(N)*, *P(N)*, and $V_{max}$ using an *in vitro* motility assay to directly measure and correlate, under nearly identical conditions, the *N*-dependence of actin sliding velocities, *V(N)*; actin-activated ATPase activity, *v(N)*; small molecule inhibition of ATPase activity; force generation against a mechanical load, *F(N)*; and calcium sensitivity of thin filaments, $pCa_{50}$*(N)*. In all cases, we observe that these *N*-dependent measurements saturate at an *N* similar to that at which *v(N)* saturates, consistent with saturation of myosin-binding sites on actin.

According to an independent force model this means that, at saturating *N*, there is an insufficient number of myosin heads for processive movement (*P(N)* < 1). Here we show that, according to a thermodynamic force model, a peak *V* is reached well before the detachment limit (*P(N)* < 1) with at least one myosin head strongly bound to actin.

Our data and analysis support a classic chemical thermodynamic framework for describing motor ensemble mechanochemistry, demonstrating that force generation is thermally equilibrated within ensemble motor systems. Here, within this formal framework, we continue to develop the first molecularly explicit models for how myosin working steps, resistive myosin heads, and external loads influence *V(N)* and how their relative contributions change with changes in *N*, linker compliance, and actin–myosin kinetics and energetics. These chemical thermodynamic mechanisms are broadly applicable to any molecular motor ensemble and account for our observations that both

*V(N)* and *v(N)* are influenced by the strain-dependent kinetics of the myosin working step and that *V(N)* saturates at a $V_{max}$ that is influenced 40% by attachment kinetics and 60% by detachment kinetics.

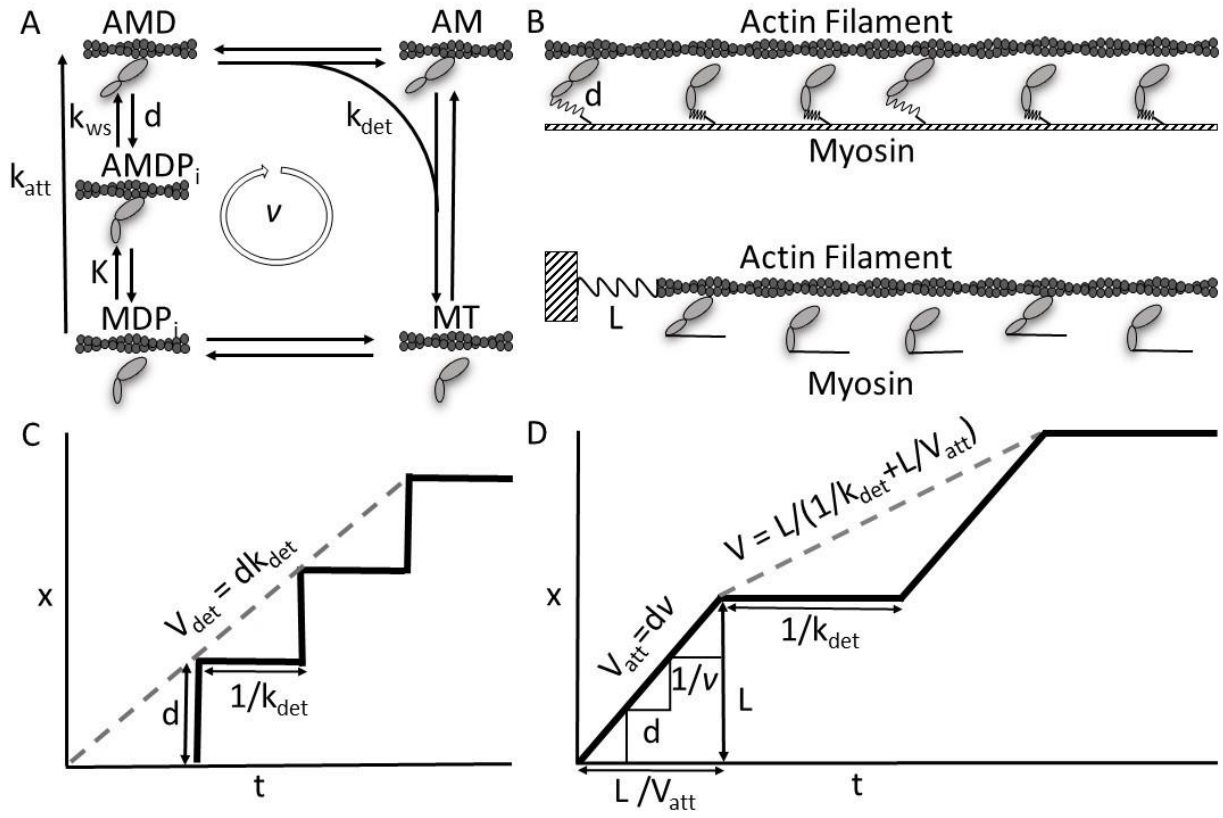


Figure 2-1: **Models for attachment- and detachment-limited myosin-based actin movement**. (A) A five-state kinetic scheme for the actin–myosin ATPase reaction. Myosin displaces an actin filament a distance d, with a working step (a lever arm rotation) induced by strong binding to that actin at a rate $k_{att}$. Actin–myosin detachment occurs with ADP (D) release followed by ATP (T) binding at an overall rate, $k_{det}$. (B) in an independent force generator model (top) the working step of a myosin head generates force that is localized to that head independent of the system force. The system force is calculated as a sum of molecular forces. In a thermodynamic model (bottom) the working step of a myosin head generates force that equilibrates with and directly contributes to the system force. (C) Actin sliding velocities in an independent force generator model are described as the mechanical step, *d*, of a single myosin head divided by the length of time that myosin head remains bound to actin, $1/k_{det}$. (D) Actin sliding velocities in a thermodynamic force model are described as the distance, *L*, myosin heads (through steps of size *d*) collectively move an actin filament before reaching a stall force divided by the bulk (*N*-dependent) time it takes those myosin heads to detach from actin.

**Results**

Figure 2-1A is a kinetic scheme of the actin–myosin ATPase reaction showing that the working step of a myosin head displaces an actin filament a distance *d*, upon strong actin binding at a rate $k_{att}$, and a myosin head detaches from actin at a rate $k_{det}$.

In an independent force model (Fig. 2-1B, top) actin sliding velocities are described in terms of the kinetics and mechanics of an individual myosin head, $V_{max} = d \cdot k_{det}$. According to this model, $V_{max}$ is fully determined by the displacement, *d*, generated by a single myosin head and by a single rate constant, $k_{det}$ (Fig. 2-1C), and thus $V_{max}$ is inherently detachment-limited. The *N*-dependence of *V* is determined by the probability that at least one myosin head is strongly bound to actin (i.e., one strongly bound myosin head is sufficient to prevent the working step of other myosin heads from moving actin).

In a chemical thermodynamic model (Fig. 2-1B, bottom) multiple myosin heads collectively move an actin filament at $V_{att} = d \cdot v$ (Fig. 2-1D) where *v* is the bulk (*N*-dependent) ATPase rate. A myosin head strongly bound to an actin filament imposes a resistive but nonarresting load against actin movement, and with increasing *N* a detachment-limited $V_{det} = L \cdot k_{det}$ is approached when a stall force is reached at the bulk (*N*-dependent) average maximum displacement, *L*. Movement resumes when myosin heads detach from actin at a bulk (*N*-dependent) rate (Fig. 2-1D). Figure 2-1D shows that, according to a thermodynamic model, actin sliding velocities are influenced by both attachment and detachment kinetics.

The *N*-dependent velocities, *V(N)*, predicted by these two models are fundamentally different. Figure 2-2, A–C show the effects of attachment kinetics ($k_{att}$ of 55, 8, and 2 $s^{-1}$) on *V(N)* predicted by three models (see Experimental procedures): independent force (equation), collective displacement (equation), and thermodynamic force (discrete state simulation). According to all three models, when *N* is increased without bound (no saturation of binding sites), *V(N)* eventually saturates at a $V_{det}$ that is independent of *N* and $k_{att}$ and decreasing $k_{att}$ increases the myosin $K_M$ (*N* at half $V_{det}$) without affecting $V_{max} = V_{det}$.

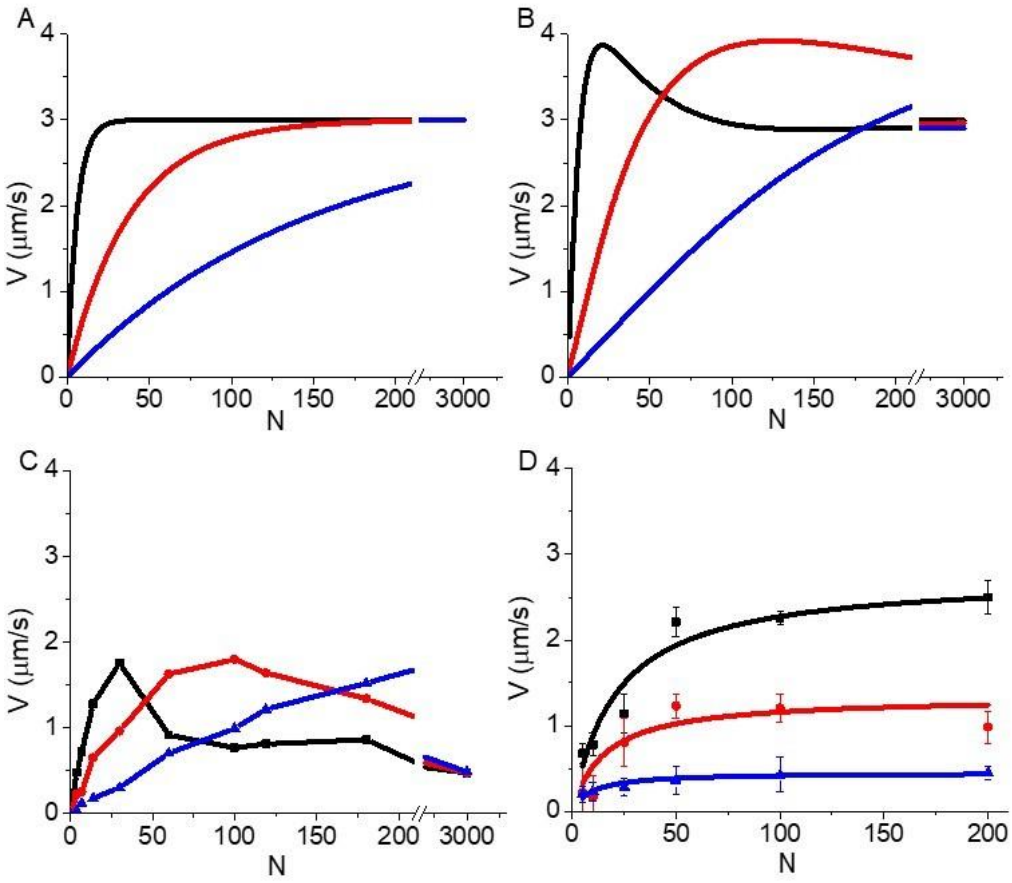


Figure 2-2: **Experimental and theoretical effects of (-)-blebbistatin on the N-dependence of *V*.** (A) mathematical expression for *V(N)* developed by Uyeda and Spudich based on the independent force model[32] with $d$ = 10 nm, $k_{det}$ = 300 $s^{-1}$, $k_{att}$ = 55 $s^{-1}$ (black lines), 8 $s^{-1}$ (red lines), and 2 $s^{-1}$ (blue lines). (B) mathematical expression for *V(N)* based on a collective displacement model[33] with $L$ = 10 nm, $k_{det}$ = 300 $s^{-1}$, $d$ = 10 nm, $k_{att}$ = 55 $s^{-1}$ (black line), 8 $s^{-1}$ (red line), and 2 $s^{-1}$ (blue line). (C) a thermodynamic force computer simulation (see Experimental procedures) with strain-dependent, reversible kinetics and stiffness of a collective spring of 0.04 pN/nm, reverse weak-to-strong rate 0.01 $s^{-1}$, $k_{det}$ = 300 $s^{-1}$, $d$ = 10 nm, $k_{att}$ = 55 $s^{-1}$ (black square), 8 $s^{-1}$ (red circle), and 2 $s^{-1}$ (blue triangle). (D) the effects of $k_{att}$ on *V(N)* were measured in an in vitro motility assay using (-)-blebbistatin to inhibit $k_{att}$. The plot shows $V$ measured at different myosin surface densities ($N$) in the presence of 0 (black squares), 10 (red circles), and 50 μM (blue triangles) (-)-blebbistatin (decreasing $k_{att}$) with least squares fits (lines) giving values for $K_M$ and $V_{max}$ of 16.1 ± 4.9 and 2.9 ± 0.3 μm/s for control, 13.3 ± 90.6 and 1.4 ± 0.3 μm/s for 10 μM, and 6.4 ± 1.3 and 0.5 ± 0.02 μm/s for 50 μM.

We use an *in vitro* motility assay to directly test whether decreasing katt increases $K_M$ without affecting $V_{max} = V_{det}$. Counter to predictions of all three models, Figure 2-2D shows that blebbistatin inhibition of $k_{att}$[34] inhibits $V_{max}$ without increasing $K_M$. This is consistent with previous studies showing that, at saturating *N*, $V_{max}$ is influenced by $k_{att}$[35]. These results suggest that $V_{max}$ in a motility assay is not detachment-limited (i.e., is not equal to $V_{det}$) and indicate that *V(N)* saturates before a detachment limit is reached (when $P(N) < 1$). Here we test an alternative hypothesis that *V(N)* saturates not at the detachment limit but with the saturation of myosin-binding sites on actin.

According to this hypothesis, *V(N)* and the actin–myosin ATPase rate, *v(N)*, should exhibit similar saturation kinetics ($K_M$) and correlated maximal activities ($V_{max}$ and $v_{max}$) (Equation 2). To test this prediction, we directly measured the *N*-dependence of both *V* and *v* in motility assays to determine $V_{max}$ and $v_{max}$ and the myosin $K_M$ for *V* and *v* at two different ionic strengths.

Figure 2-3 shows the *N*-dependence of *v* in an *in vitro* motility assay both with and without actin filaments. Because both experiments were prepared identically with the exception of the addition of actin, the difference in these activities is the actin-activated activity. From the activities in Figure 2-3 and the myosin densities and flow cell geometry described[36], we estimated the baseline Mg-ATPase activity of myosin on the motility surface to be approximately 2 $s^{-1}$, which is more than 30-fold higher than that measured in solution studies[37]. This suggests that binding of myosin to the surface partially activates Mg-ATPase and/or that some of the basal activity comes from myosin

in solution (not bound to the surface) that was not completely removed with the washes. Previous studies[36] have shown a linear increase in myosin ATPase activity (no actin) with increasing *N* similar to that shown in Figure 2-3, suggesting that saturation of the motility surface contributes to neither the saturation of *V(N)* nor *v(N)*.

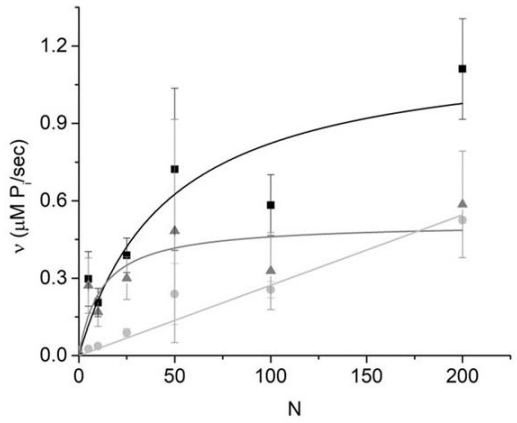


Figure 2-3: **The N-dependence of actin-activated ATPase activity, *v(N)*, measured in a motility assay**. The baseline myosin ATPase activity (light gray circles) was measured in the absence of actin at different *N* and fit to a line (light gray). The ATPase activity measured in the presence of 0.15 μM actin (black squares) is the total ATPase activity of myosin heads interacting with actin (actin-activated ATPase) and the majority of myosin heads that are not interacting with actin (baseline myosin ATPase). Subtracting the baseline ATPase (light gray circles) from the total ATPase (black squares) gives the actin-activated ATPase rate, v(N) (gray triangles), which is fitted to a hyperbolic function (gray line).

To maximize the *v* signal, we used higher concentrations of actin in this assay than typically used in a motility assay, and we confirmed that the majority of actin filaments were still moving under these conditions. Assuming an actin-activated ATPase activity of 40 $s^{-1}$ (20-fold over 2 $s^{-1}$), the ~4-fold actin activation of ATPase activity observed at low *N* in Figure 2-3 suggests that ~20% of myosin on the surface are activated by actin in this assay.

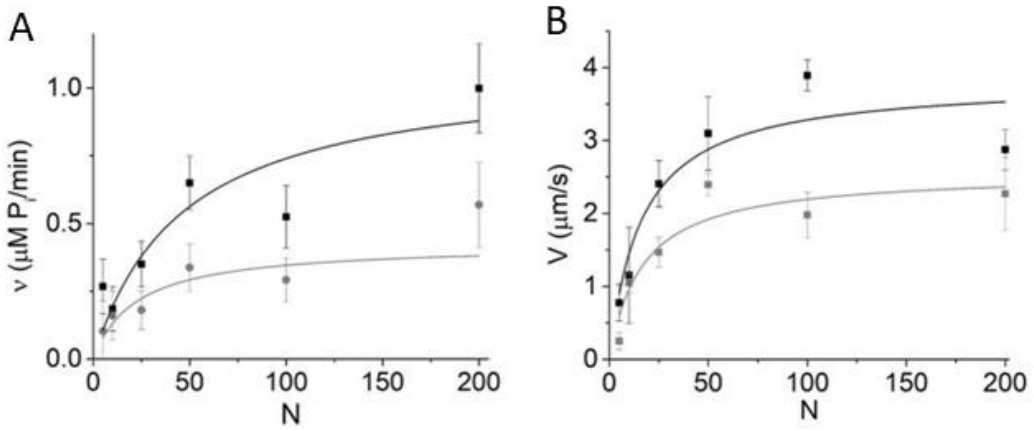


Figure 2-4: ***v(N)* and *V(N)* measured at two different ionic strengths in similar in vitro motility assays**. (A) *v(N)* was measured at both 50 (black squares) and 100 (gray circles) mM KCl and fitted to hyperbolic functions (lines) giving $K_M$ values of 46 ± 32 and 23 ± 13 for 50 and 100 mM KCl, respectively. (B) *V(N)* measured under nearly identical conditions (only with 0.15 μM instead of 0.01 μM actin) to those in (A) at both 50 (black squares) and 100 (gray circles) mM KCl and fitted to hyperbolic functions (lines) giving $K_M$ values of 16 ± 8 and 17 ± 9 for 50 and 100 mM KCl, respectively.

Figure 2-4 shows *v(N)* and *V(N)* measurements obtained in a motility assay at two different ionic strengths fit to hyperbolas. These data show that increasing KCl from 50 to 100 mM results in similar decreases in both $V_{max}$ and $v_{max}$ (32 ± 20% and 51 ± 28%, respectively), consistent with $V_{att}$ influencing $V_{max}$ (Equation 2). The observed decrease in $V_{max}$ with increasing KCl at high ionic strength is consistent with previous studies[38]. Both *V(N)* and *v(N)* exhibit similar saturation kinetics with $K_M$ values of 16 ± 8 and 46 ± 32, respectively, at 50 mM KCl and 17 ± 9 and 23 ± 13, respectively, at 100 mM KCl. To further test the saturation kinetic hypothesis and its implications for the models in Figure 2-2C, we measured the *N*-dependence of *V(N)* against a mechanical load. Force generation by myosin molecules along an actin filament increases linearly with the number, *N*, of myosin available to bind that actin filament. Thus, according to our

hypothesis, the $K_M$ for myosin force generation in a motility assay should resemble that of both *V(N)* and *v(N)* determined above. We tested this prediction by measuring the *N*-dependence of myosin force generation against a mechanical load imposed by alpha-actinin in a motility assay.

Alpha-actinin binds to actin and when adhered to a motility surface imposes a mechanical load against actin movement by weakly linking actin to the surface. In effect, alpha-actinin acts as a frictional load[39] that slows *V*. Assuming that the force, *F(N)*, collectively generated by myosin molecules against this load increases with *N* as $F(N) = F_{uni} \cdot N \cdot r$ (where *r* is the fraction of strongly bound, force-generating myosin heads) the *N*-dependence of *V(N)* is described by Equation 1.

$$V(N) = \left(\frac{1}{\gamma}\right) \cdot F_{uni} \cdot N \cdot r \qquad \text{Eq (1)}$$

where $F_{uni}$ is the average force generated per myosin head and γ is a frictional coefficient that, according to a molecular model for friction (2), equals $N_\alpha \cdot \kappa_\alpha \cdot t_\alpha$ where $N_\alpha$, $\kappa_\alpha$, $t_\alpha$ are the bound number, stiffness, and bound lifetime of alpha-actinin molecules. According to a classical chemical thermodynamic formalism, $F_{uni} = \Delta G/d$, where $\Delta G$ is the free energy for the working step[14,17]. Equation 1 is analogous to the myosin detachment-limited model illustrated in Figure 2-1D; only here at sufficiently high alpha-actinin concentrations *V* is influenced by alpha-actinin detachment kinetics. Specifically, the distance alpha-actinin compliant linkages are collectively displaced at stall *is* $L_\alpha = F_{uni} \cdot N \cdot r / N_\alpha \cdot \kappa_\alpha$ and the detachment rate of alpha-actinin is $k_{det\alpha} = 1/t_\alpha$. Thus, the alpha-actinin equivalent of the myosin detachment-limited velocity illustrated in Figure 2-1D is $V = L_\alpha/(1/k_{det\alpha} + L_\alpha/V_{att})$, which at relatively high $V_{att}$ approaches the alpha-actinin

equivalent of Equation 2.

The collective force formalism provides a clear working-step influenced mechanism for *V(N)* against a mechanical load (Equation 1). This is in contrast to the independent force generator equivalent of Equation 3, which inverts the actual physical agency in this relationship. Because the independent force formalism requires that myosin heads generate force locally, myosin working steps can neither directly move actin filaments nor directly generate force, *F(N)*, in external compliant linkages such as alpha-actinin (see Discussion); instead, the detachment-limited movement of actin subsequent to the working step stretches alpha-actinin linkages to generate a frictional force, $F_f$. In this way a detachment-limited *V* determines $F_f$[39], and because $F_f$ must be equal and opposite to the net force exerted by myosin heads ($F_f = -F_{uni} \cdot N \cdot r$), it follows that *V* determines $-F_{uni} \cdot N \cdot r$, which is simply not true. Myosin working steps actively generate $F_{uni} \cdot N \cdot r$ (and the opposing $F_f$) against alpha-actinin linkages, and $F_{uni} \cdot N \cdot r$ determines *V* as described by Equation 1 (and Fig. 2-1D), not the other way around.

Figure 2-5A is a graph of *V(N)* measured in an *in vitro* motility assay with and without alpha-actinin on the motility surface. These data show that, at sub saturating myosin ($N < 50$), *V(N)* slowed by an alpha-actinin load (increasing $\gamma$) can be recovered by increasing *N*, consistent with Equation 1. However, at *N* values above those at which *V(N)* and *v(N)* saturate, *V(N)* inhibited by alpha-actinin cannot be recovered by further increasing *N*, implying that *F(N)* saturates with *V(N)* and *v(N)*. Fits of the alpha-actinin data to a hyperbolic function give $K_M$ values for *F(N)* ($16 \pm 7$ at 0.5 μg/ml alpha-actinin and $38 \pm 13$ at 1.0 μg/ml alpha-actinin) that are not significantly different from the $K_M$

values for *V(N)* and *v(N)* (Table 1), further supporting our hypothesis.

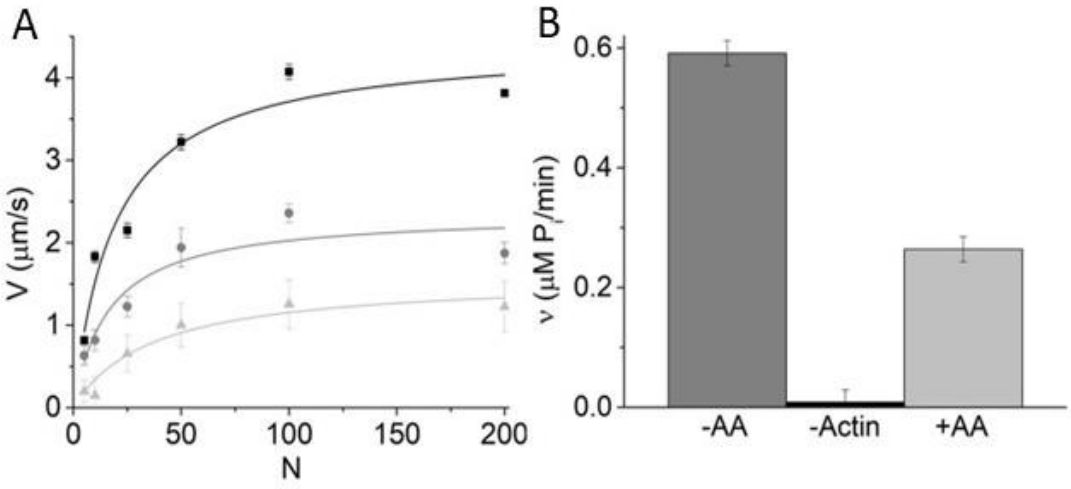


Figure 2-5: **The effects of a mechanical load on *V(N)* measured in an in vitro motility assay**. (A) *V(N)* measured in an in vitro motility assay after incubating motility flow cells with 0 (black squares), 0.5 (dark gray circles), and 1 (light gray circles) μg/ml alpha-actinin. The data were fitted to hyperbolic functions (lines), giving values for $K_M$ of 19 ± 5, 16 ± 7, and 38 ± 13. (B) actin-activated ATPase activity, *v*, measured in an in vitro motility assay (*N* = 5 and 1.0 μM actin) with (light gray bar) and without (dark gray bar) 1 μg/ml alpha-actinin shows v decreases from 0.59 to 0.26 μM $P_i$/min upon addition of 1 μg/ml alpha-actinin (p = 0.018). The 1 μg/ml alpha-actinin control (myosin without actin) is indicated with the black bar.

Table 2-1: Summary of parameters determined in figures.

| **Experiment** | **$K_M$ for V** | **$K_M$ for v** |
|---|---|---|
| 50 mM KCl | 16 ± 8 | 46 ± 32 |
| 100 mM KCl | 17 ± 9 | 23 ± 13 |
| 0.5 μg/ml alpha-actinin | 16 ± 7 | |
| 1.0 μg/ml alpha-actinin | 38 ± 13 | |
| Actin breaking rate | 13 ± 11 | |
| $pCa_{50}$ 50 mM KCl | 24 | |
| $pCa_{50}$ 100 mM KCl | 26 | |

Because the independent force model requires that myosin working steps generate force locally, strain-dependent kinetics of the working step, $k_{ws}$, can in theory only be a function of local strain, independent of the external alpha-actinin load. In contrast, we previously showed that working step energetics are a function of an external muscle load[17], and the collective force model we developed to account for that observation predicts that $k_{ws} = k_{ws}° \cdot exp(-w/k_BT)$, where $w$ is the work performed in collectively stretching external compliant linkages like those introduced by alpha-actin[14].

According to Equation 2, the slope of the low $N$ data in Figure 2-5A is $V/N = k_{att} \cdot d$. The addition of 1.0 μg/ml alpha-actinin decreases this slope by 73% (Fig. 2-5A), suggesting that alpha-actinin decreases $k_{att}$ by decreasing the rate-limiting $k_{ws}$. This interpretation is supported by the data in Figure 2-5B. We measure the actin-activated ATPase activity with and without alpha-actinin during a motility assay at low $N$ (= 5), conditions under which $V$ is primarily limited by $k_{att}$. We observe that the load imposed by 1.0 μg/ml alpha-actinin inhibited actin-activated ATPase activity by 55% (Fig. 2-5B), consistent with the external alpha-actinin load inhibiting kws, as predicted by collective force models.

To further test the kinetic saturation hypothesis, we consider the $N$-dependence of myosin activation of thin filaments. In 2010 we developed and tested experimentally a simple two-state model for thin filament activation of thin filament motility by calcium and myosin[9,40,41]. Our simulations and experimental data imply a simple relationship between $pCa_{50}$ (the calcium concentration at half-maximal activation), $N$, and the actin–

myosin duty ratio, *r* (the fraction of time myosin spends strongly bound to an actin filament). Specifically, we showed that $pCa_{50}$ is proportional to $N \cdot r$. Previously we showed that $pCa_{50}$ increases linearly with $N$[40,41] up to $N = 100$ (100 μg/ml myosin incubation), but we never measured $pCa_{50}$ at $N > 100$. Here, using an *in vitro* motility assay, we measured the calcium dependence of *V* at both 50 and 100 mM KCl and obtained $pCa_{50}$ values from Hill fits to pCa–*V* curves (Fig. 2-6, inset) as previously described[41]. We repeated these experiments at different *N* up to 150. Figure 2-6 shows that $pCa_{50}$ values saturate at high myosin densities, which according to our model indicates that the number of myosin, *N*, available to strongly bind and activate a thin filament saturates at N values similar to those that saturate *V(N)*, *v(N)*, and *F(N)*.

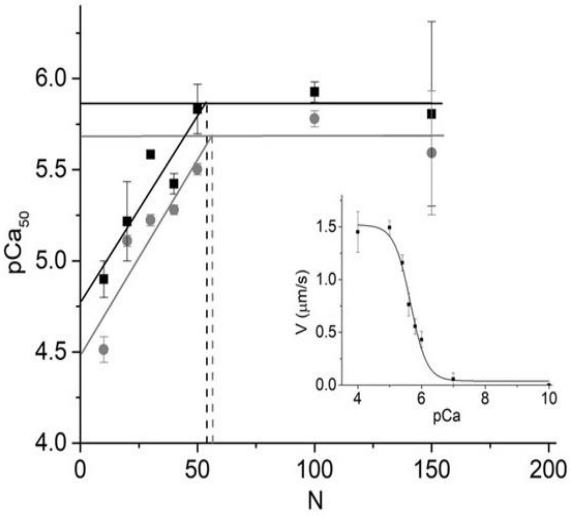


Figure 2-6: ***N*-Dependence of $pCa_{50}$ in a motility assay.** The calcium dependence of thin filament sliding velocities was measured in an in vitro motility assay, and the data were fit to a Hill equation to obtain the calcium concentration at half-maximal activation reported as the $pCa_{50}$ (inset) as previously described[41]. These experiments were repeated at different N to obtain $pCa_{50}$(N) at both 50 (black squares) and 100 (gray circles) mM KCl. The data at or below $N = 50$ were fit to lines with y-intercepts of 4.8 and 4.5 and slopes of 0.02 and 0.02 for 50 and 100 mM KCl, respectively. The data above $N = 50$ were averaged (horizontal lines) to estimate maximum $pCa_{50}$ values of 5.9 and 5.7 at 50 and 100 mM KCl. The *N* at saturation is the intercept of the maximum $pCa_{50}$ and the linear fit, and the pseudo $K_M$ is half the *N* at saturation.

A hyperbolic fit is not well constrained by these data because the y-intercept is non-zero, and so we fit data obtained at $N < 100$ to a line (our two-state model) where according to our model the y-intercept is the $pCa_{50}$ for calcium binding to TnC in the absence of myosin and the slope is proportional to the actin–myosin duty ratio[40]. The horizontal lines in Figure 2-6 are the average $pCa_{50}$ values measured at or above $N = 100$. The $N$ at saturation was determined from the intercept of the linear fit and the average saturated $pCa_{50}$ value, and the $N$ at half saturation (a pseudo $K_M$) is half the $N$ at saturation. Using this approach, the pseudo $K_M$ for $pCa_{50}$ is 24 for 50 mM KCl and 26 for 100 mM KCl, similar to $K_M$ values for $V(N)$, $v(N)$, and $F(N)$ (Table 2-1).

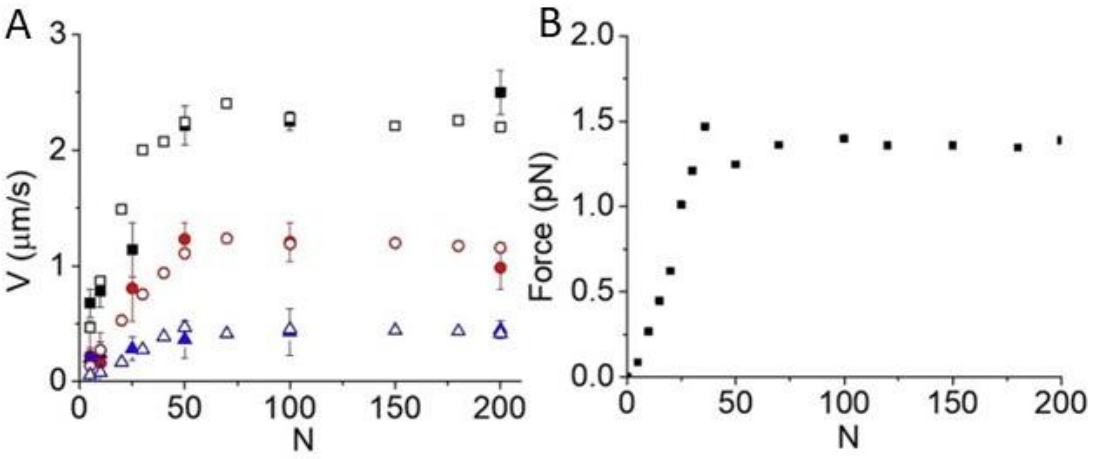


Figure 2-7: **Collective force model with saturation kinetics**. (A) Computer simulations of V(N) obtained at different $k_{att}$ values based on a collective force model with saturation attachment kinetics (open symbols) are overlaid with V(N) data from Figure 2-2D obtained at different blebbistatin concentrations (solid symbols). Parameters of the simulation are $d$ = 10 nm, $k_{det}$ = 400 $s^{-1}$, and $k_{att}$ of 30 $s^{-1}$ (black symbols), 5 $s^{-1}$ (red symbols), and 1.5 $s^{-1}$ (blue symbols). (B) in computer simulations of *F(N)* based on a collective force model with saturation attachment kinetics, force is generated collectively by myosin heads when they displace a single mechanical spring with spring constant κ = 0.04 pN/nm. *F(N)* increases linearly with *N* and saturates at the same *N* as *V(N)* when myosin heads saturate.

Figure 2-7 shows collective force computer simulations with a finite number of myosin-binding sites per micron actin and an infinite *K*. In Figure 2-7A, simulations of *V(N)* at different $k_{att}$ values are compared with the blebbistatin data from Figure 2-2D. Figure 2-7B shows simulations of *F(N)*. Although these results suggest that in a standard motility assay actin–myosin binding saturates at a $V_{max}$ prior to *P(N)* saturating at 1, *P(N)* is not zero at $V_{max}$. In other words, detachment kinetics still contributes to $V_{max}$. This is supported by numerous studies that have demonstrated a correlation between $V_{max}$ and $k_{det}$[42]. The extent to which $V_{max}$ is influenced by $V_{det}$ depends on experimental conditions, which is to say many factors influence *P(N)*. For example, we have previously shown that $V_{max}$ is influenced more by $V_{det}$ in a myosin monomer–based motility assay than in a

myosin filament–based motility assay[10,33], and we have shown that $V_{max}$ is influenced more by $V_{det}$ at low [ATP] than at high [ATP][16].

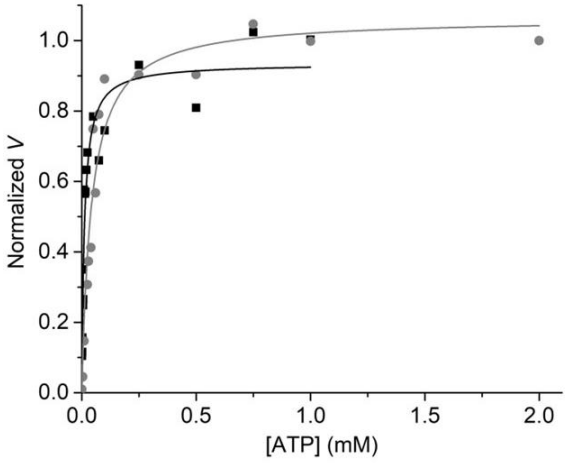


Figure 2-8: ATP dependence of *V* at 5 and 100 μg/ml myosin. The [ATP] dependence of *V* at high (100 μg/ml; gray circles) and low (5 μg/ml; black squares) myosin fitted to a hyperbola (lines), giving $K_M$ values of 0.01 ± 0.002 at 5 μg/ml and 0.04 ± 0.007 at 100 μg/ml.

Here we estimate the extent to which $V_{max}$ is influenced by $V_{det}$—the *P(N)* when actin–myosin binding saturates—in a standard motility assay. At *P(N)* = 0, $V = V_{att}$ is attachment-limited (Equation 2) and the [ATP]-dependence of V has a $K_{M(ATP)}$ ([ATP] at half $V_{max}$) of $k_{att}/k_T$, where $k_T$ is the second-order ATP binding constant. Figure 2-8 (gray circles) shows the [ATP] dependence of *V* measured in an *in vitro* motility assay at low *N* (= 5) and low *P(N)*. A hyperbolic fit to these data gives a $K_{M(ATP)} = k_{att}/k_T$ of 0.01 mM. At *P(N)* = 1, $V = V_{det}$ is detachment-limited (Equation 3) and the [ATP]-dependence of *V* has a $K_{M(ATP)}$ of $k_{-D}/k_T$, which is ($k_{-D}/k_{att}$)-fold greater than the $K_{M(ATP)}$ at *P(N)* = 0. Here $k_{-D}$ is the rate constant for ADP release. Assuming a duty ratio of $k_{att}/k_{-D} = 0.1$, we expect the $K_{M(ATP)}$ for $V_{det}$ to be 10-fold greater than the $K_{M(ATP)}$ for $V_{att}$. Figure 2-8 (black squares) shows the [ATP] dependence of *V* obtained at saturating *N* (= 100) fitted to a hyperbola

with a $K_{M(ATP)}$ of 0.04 mM. This is 40% of the $K_{M(ATP)}$ predicted for $V_{det}$, implying that $P(N) = 0.4$ at saturating $N$.

**Discussion**

Many biological processes rely on collections of molecular motors to generate macroscopic forces and movement[1,2,3]. The mechanics and chemistry of different molecular motors have been well characterized at the level of a single molecule[4,5,6,7,8] often with an expectation that single motor mechanics will directly translate to ensemble motor mechanics to reveal the molecular mechanisms of macroscopic biological processes. This expectation is largely fueled by the independent force generator model[30] that describes ensemble motor mechanics as the sum of its molecular mechanical parts. However, data presented here and elsewhere imply that forces are collectively generated and thermally equilibrated within motor systems, leading to emergent behaviors that are not readily inferred from single molecule measurements[14,17,18]. A system in which forces are thermally equilibrated is best described by Gibbs' chemical thermodynamics[43], and here we continue to develop the first explicit models for *V(N)* and *F(N)* within this classical framework.

In an *in vitro* motility assay, myosin-generated actin sliding velocities, *V(N)*, increase with increasing *N*, saturating at a $V_{max}$ that is influenced by both actin–myosin attachment and detachment kinetics. The conventional assumption of a detachment-limited $V_{max}$ is based more on adherence to the formal constraints of the independent force model than on experimental data, as the influence of v on $V_{max}$ was long ago demonstrated[31].

Not only is the independent force model not incontrovertible but it also challenges Gibbs' classical chemical thermodynamics. T.L. Hill developed the independent force formalism in the 1970s[44] specifically to address the problem that the assumption of

independent force generation[30] is inconsistent with classical chemical thermodynamics. For the past 20 years we have argued that instead of abandoning chemical thermodynamics a different assumption was needed[14]; specifically, that force generated by a myosin head is equilibrated with the force of the muscle system. Although evident and principled, this argument has been challenged[45,46] and otherwise simply disregarded. Here, we highlight the fundamental differences between these two formalisms.

The independent force generator model[30] assumes that force generated with a myosin working step is locally equilibrated[47] , which means that multiple myosin heads through their working steps cannot collectively generate force in external compliant elements (they generate force independently). Placed in a broader context, this model assumes that myosin force generation within the macromolecular assembly of multiple actin-bound myosin heads does not equilibrate within the assembly but instead equilibrates within a single protein (myosin) component of that assembly. This highly unconventional view requires an unconventional chemical thermodynamic formalism. Because Gibbs free energies describe the energetics of a system within which molecular forces are equilibrated, T.L. Hill developed a new form of chemical thermodynamics to describe molecular free energies of individual proteins thermally isolated from the assembly with which they interact. The independent force definition of *P(N)*—that a single actin-bound myosin head prevents actin movement and force transmission—is the purported mechanism by which myosin heads are thermally isolated in shortening muscle despite there being no known molecular mechanisms for such a barrier to thermal force. Within this framework, motor kinetics and energetics are only influenced by the work individual motors perform locally and are uncoupled from any work performed on

external compliant elements through subsequent actin movement. Thus, unique to this model is the definition of molecular stress-strain curves, a characteristic feature that identifies most models of muscle contraction to date as independent force generator models[48,49,50,51].

In 1999, we directly measured mechanochemical coupling in isometric muscle and observed that the free energy for the myosin working step varies proportionally with muscle force, implying that the myosin working step equilibrates with muscle force[17] . This led us to develop a thermodynamic model of muscle force[14] that predicts that a myosin working step (generated by a discrete myosin lever arm rotation induced by strong actin binding) directly moves a given actin filament and directly displaces and generates force in all crossbridges, compliant linkages, and external loads that oppose that movement[16]. Here, the Gibbs free energy and rate constant for the myosin working step, $k_{ws}$, are functions of the average work, $w$, performed on all external loads and compliant linkages stretched by that transition, e.g., $k_{ws} = k_{ws}^{\circ} \cdot exp(-w/k_BT)$ [14,43] , consistent with the observed effects of an external alpha-actinin load on $k_{ws}$ in Figure 2-5.

The Gibbs' chemical thermodynamic and Hill's molecular mechanics formalisms are fundamentally different. They are based on fundamentally different assumptions with fundamentally different formal constraints, resulting in fundamentally different predictions. The data and analysis herein highlight some of those differences and further demonstrate that motor ensemble mechanochemistry is consistent with Gibbs' chemical thermodynamics not Hill's molecular mechanics.

The observation that $k_{ws}$ contributes to $V_{max}$ implies that myosin working steps

directly contribute to actin movement and perform work on all external compliant elements stretched by that movement, challenging the independent force generator formalism. The observation that myosin-binding sites on actin saturate before a detachment limit is reached implies that kws contributes to $V_{max}$ in any actin–myosin system, including muscle. The data and analyses herein infer explicit mechanisms for a classical chemical thermodynamic model. Equations 2 and 3 along with collective force definitions of *P(N)* and *L* (see Experimental procedures) provide a clear description of how myosin working steps and resistive myosin heads both contribute to $V_{max}$ and how these contributions change with *N*, actin–myosin attachment and detachment kinetics, and linkage compliance as opposed to the relatively rigid independent force prediction that $V_{max}$ depends only on two parameters. The working step contribution to movement and force generation also provides a clear mechanism for *V(N)* against a load (Equation 1) as opposed to the convoluted inverse agency predicted by independent force models (see Results).

The observation in Figure 2-5 that an alpha-actinin load in a motility assay similarly slows *V(N)* (limited by $k_{att}$ at low *N*) and *v(N)* (limited by $k_{att}$) implies that the work performed by myosin working steps in stretching alpha-actinin linkages slows $k_{ws}$. Although we cannot rule out that the alpha-actinin load diminishes to some extent *d* and/or $k_{det}$, the observation that it decreases $k_{ws}$ by more than 50% (Fig. 2-5B) is inconsistent with the independent force model, whereas this external strain dependence is predicted by a collective force model[18].

In the same way that the independent force model formally precludes myosin

working steps from collectively performing work against an external load[17] and stretching external alpha-actinin linkages (Fig. 2-5, Equation 1), it formally precludes myosin working steps from collectively stretching compliant linkages associated with other strongly bound myosin heads. In contrast, in a thermodynamic force model, myosin working steps can collectively generate force by stretching compliant linkages associated with other strongly bound myosin heads, analogous to how force is collectively generated in muscle[17] or in stretching alpha-actinin linkages (Fig. 2-1D, Equation 1). Thus, one myosin head strongly bound to actin is not sufficient to stall actin movement. Instead, actin movement stalls when compliant linkages associated with strongly bound myosin heads are collectively displaced until a stall force is reached at a net displacement, *L*. *P(N)* is then the probability that a stall force is reached by *N* myosin heads, which occurs when many myosin heads are strongly bound to actin (Fig. 2-2C).

We have previously shown that many factors influence *L* and *P(N)*, including the Gibbs free energy for the working step (16), the number of strongly bound heads resisting movement[16], and the compliance of resistive linkages[33] . Our recent observation that the myosin S2 tether dramatically increases *L*[33,52] allowed us to develop an idealized collective displacement model (linkages with infinitely high compliance and a hard stop at a displacement *L*) from which we developed an analytical expression for *P(N)*. In general, however, a more realistic model requires strain-dependent kinetics and collective force generation in stretching compliant linkages. Here we have developed the simplest possible discrete state collective force model (see Experimental procedures) in which all resistive linkages are treated as a single effective spring with an effective spring constant, κ (Fig. 2-2C). It is worth noting that our computer simulations of collective force in

Figure 2-2C resemble our mathematical model of collective displacements plotted in Figure 2-2B. We continue to refine and test this model through experiments like those presented here.

Our observation that $P(N)$ = 0.4 when myosin-binding sites on actin are saturated (Fig. 2-8) is also inconsistent with the independent force model for $P(N)$. Assuming that there are 28 myosin-binding sites on actin along the pseudo repeat of a 1-μm actin filament and a duty ratio of 0.1, we would expect on average 2.8 strongly bound myosin heads not 0.4 as inferred by the independent force model. In muscle, this discrepancy is even greater considering the myosin S2 tether further decreases $P(N)$[33] . In addition, because the independent force definition of $P(N)$ is the probability that at least one myosin head is strongly bound to actin, the fraction of time no myosin heads are strongly bound to actin is $[1 - P(N)]$. This would imply that a 1-μm actin filament sliding at $V_{max}$ in a motility assay spends 60% of its time with no myosin heads strongly bound and even more time with no heads strongly bound in muscle, which is inconsistent with sustained muscle contractions. Clearly, the probability that actin-bound myosin heads stall actin movement, $P(N)$, is much smaller than the probability that at least one myosin head is strongly bound to actin, which is to say that a strongly bound myosin head does not prevent actin movement or force transmission; myosin working steps directly move actin filaments and generate force in external elements; and multiple myosin heads collectively generate force against common actin-bound myosin heads, compliant linkages, and external loads that resist that movement, inconsistent with independent force generation.

The extent to which detachment kinetics influences $V_{max}$ has mechanistic

significance. For example, near the attachment limit [$P(N) << 1$], muscle shortens at a maximum velocity per myosin head with minimal energy lost to myosin head–head interactions and internal force generation, whereas near the detachment limit [$P(N) = 1$] myosin head–head interactions generate internal strain during shortening that can provide functionally significant cooperative mechanisms involving strain-dependent kinetics[8,30,53] [8,30,53].

Similarity between the $K_M$ for myosin reported here and the number of myosin-binding sites along the pseudo repeat of a 1-μm actin filament (see Results) implies that the weak-binding affinity of myosin for actin is high. Increasing ionic strength should decrease this weak-binding affinity, resulting in an increase in the $K_M$ for myosin; however, a significant increase in $K_M$ with addition of 50 mM KCl was not observed in Figure 2-4. This could be because the change in $K_M$ is relatively small and within the error of our measurements. It could also be because ionic strength affects other kinetic steps in the reaction cycle that result in an offsetting decrease in the apparent $K_M$.

The data and analysis reported herein provide explicit mechanisms for our observations that $V(N)$ and $v(N)$ are both strain dependent, and that $V(N)$ saturates at a $V_{max}$ that is influenced 40% by attachment kinetics and 60% by detachment kinetics, filling an important gap in our basic understanding of ensemble actin–myosin mechanics. The observation that myosin-binding sites on actin saturate prior to a detachment limit precludes a detachment-limited $V_{max}$ in any actin–myosin system, including muscle. The impact of these results extends well beyond this basic observation, however. These results inform our continuing development of the first explicit models for $V(N)$ and $F(N)$ within

a classical chemical thermodynamic framework that is broadly applicable to any molecular motor ensemble, providing insights into how motor working steps, resistive motors, and other resistive external loads all influence and contribute to *V(N)* and how the relative contributions of these mechanisms change with changes in *N*, motor kinetics and energetics, and linker compliance.

## Methods

**Protein preparations.** Skeletal muscle myosin was prepared from rabbit psoas muscle as described and stored in glycerol at −20 °C[54,55]. F-actin was purified from rabbit psoas muscle and stored on ice at 4 °C[56]. To stabilize and label actin for *in vitro* motility assays, actin (1 μM in actin buffer) was incubated with 1 μM tetramethyl-rhodamine isothiocyanate (TRITC)-phalloidin (Sigma) overnight at 4 °C prior to dilution to the experimental concentration (see below). Skeletal tropomyosin and troponin (Tm-Tn) were purified as described[57,58]. Regulated thin filaments were reconstituted by combining 250 nM Tm and Tn to 0.015 μM TRITC-actin and incubating on ice for 20 min as described[41].

**Buffers.** Myosin buffer contained 300 mM KCl, 25 mM imidazole (pH 7.4), 1 mM EGTA, 4 mM MgCl2, and 10 mM DTT. Actin buffer contained 50 mM KCl, 50 mM imidazole (pH 7.4), 2 mM EGTA, 8 mM MgCl2, and 10 mM DTT. Motility buffer contained 50 mM imidazole (pH 7.4), 2 mM EGTA, 8 mM MgCl2, 10 mM DTT, 0.5% methylcellulose and KCl, and 1 mM ATP. Motility buffer also contained an oxygen scavenger system (stock [c] of 2.9 mg/ml glucose, 1.6 mg/ml glucose oxidase, 2.3 mg/ml catalase) that was added immediately prior to imaging[59].

**In vitro motility assays.** Velocities of TRITC-labeled actin filaments were measured at 30 °C as they moved over surface-attached monomeric skeletal muscle myosin. Flow cells were made by attaching a nitrocellulose-coated coverslip to a microscope slide with double-sided ¼-inch-thick tape (3M). Myosin solutions of different concentrations in myosin buffer were applied to the flow cell followed by 2 × 50-μl

aliquots in sequence of 5 mg ml−1 bovine serum albumin in actin buffer, 10 nM TRITC-actin in actin buffer prepared as described above, actin buffer, and motility buffer. Each solution was incubated in the flow cell for 1 min before adding the next. Blebbistatin experiments were performed using 10 and 50 μM (-)-blebbistatin (Sigma-Aldrich) in the motility buffer[60]. For loaded motility assays, alpha-actinin (Sigma Aldrich) in actin buffer was added to the flow cell following the addition of myosin at the indicated concentrations in 2 × 50-μl aliquots with 1-min incubation. Calcium experiments were performed by adding calcium to the motility buffer at concentrations determined from an algorithm based on Fabiato and Fabiato to obtain the free calcium concentrations reported here as pCa[61]. A total of three experiments (N = 3) were averaged per data point. Motility assays were performed using a Nikon TE2000 epifluorescence microscope, and images were digitally acquired with an Andor iXon Ultra camera (Oxford Instruments).

**Tracking and image analysis.** MetaMorph software (Molecular Devices) was used for image acquisition. For each flow cell, 30-s image sequences from three different fields were recorded. Actin velocities were manually tracked using the MTrackJ plug-in for ImageJ (NIH). Only smoothly moving filaments with trajectories greater than 3 μm were selected for analysis. An average velocity for a given trajectory meeting the above criteria was determined using ImageJ. For a given experiment (one flow cell) 45 to 100 trajectories were recorded and analyzed (n = 1). Reported *V* values are averages of at least three (n = 3) independent experiments with standard error reported with error bars.

**Measurement of actin-activated ATPase activity, v, in an in vitro motility assay.** Actin-activated ATPase activity, v, was measured in a motility flow cell having the

geometry described above with three minor differences: (i) tape was added to only one side of the flow cell to allow access to the solution within, (ii) higher concentrations of TRITC-actin (see Figure legends) were used to increase the ATPase signal, and (iii) ATPase measurements were made over longer periods than motility measurements. Specifically, solutions and proteins were added as described above for the motility assay, but instead of mounting the slide on a microscope, slides were placed on a slide warmer set to 30 °C. At 5, 10, 15, 30, 35, 45, and 60 min time points, an individual flow cell was opened (side without the tape was lifted) and 25 µl of solution was removed and added to 250 µl of malachite green (20 ml 0.045% malachite green, 6.6 ml 1% sterox, and 2.2 ml 4.2% ammonium molybdate) and mixed with a positive displacement pipette. The reaction was quenched with 30 µl of 34% sodium citrate solution, and absorbance was read at 650 nm in a 96-well plate reader using Gen5 (Biotek) software. In all experiments, the time course of absorbance was well fit to a line with the slope being a proportional measure of the total ATPase activity in that flow cell. Because the total ATPase activity is the sum of the ATPase activity of myosin heads interacting with actin (actin-activated ATPase) and the activity of myosin heads not interacting with actin (basal ATPase), we subtract the basal ATPase from the total ATPase to obtain the actin-activated ATPase activity. We measured the basal (myosin) ATPase activity for each experimental condition by repeating all of the steps above except no TRITC-actin was added. Because we were unable to quantitate the amount of actin interacting with myosin in these experiments, we were only able to measure relative changes in actin-activated ATPase activity not absolute values. One-hour time courses obtained both in the presence and absence of actin constitute one experiment (n = 1), and a total of three experiments (N =

3) were averaged per data point.

**Calculating N.** Based on previous studies[36] and basal myosin ATPase data in Figure 2-3, we assumed a linear relationship between the surface density of myosin on a motility coverslip and the myosin concentration, [M], used to incubate a flow cell for 2 min. The number, *N*, of myosin available to bind a unit length (1 μm) of actin is proportional to the myosin surface density. To calculate *N*, we multiply [M] by a conversion factor 1 (myosin per μm actin) (ml/μg) consistent with estimates in Harris and Warshaw[36]. Within multiple experiments performed within days of each other, variability in *N* can occur with a combination of very subtle changes in temperature, denaturing of protein over days, differences in flow cell preparation, etc. Because we performed our experiments within days of each other, we estimated variability in *N* by measuring the intensity of fluorescently labeled myosin on a coverslip among different coverslips at different *N* values on the same day. We measured a standard deviation in fluorescence intensity for all *N* of less than ±80%. This error would contribute to the measured error in *V* over the range of *N* where *V* increases with *N* and would be reflected in the reported error in $K_M$ (Table 2-1).

**Molecular models for V(N).** Actin and myosin catalyze the hydrolysis of ATP through intermediate steps illustrated in Figure 2-1A. Upon myosin weak-to-strong binding to actin and release of inorganic phosphate, $P_i$[24], a discrete rotation of the myosin lever arm displaces an actin filament a distance *d* [28,62,63]. This mechanochemical step, which we refer to as the working step, occurs at a rate $k_{ws}$. The effective attachment rate, $k_{att}$, includes the weak association of actin and myosin, *K*, that precedes *kws*, or $k_{att}$ =

$K{\cdot}k_{ws}$. Following ADP release and ATP binding, myosin detaches from actin with an effective detachment rate, $k_{det}$.

A single myosin head ($N$ = 1) moves an actin filament a distance, $d$, with a working step every time it completes one actin–myosin ATPase reaction cycle[64,65,66] (Fig. 2-1, A and B). In theory, the speed at which one myosin head can move an actin filament is $V = d{\cdot}v$, where $v$ is the actin–myosin ATPase rate[2,4,35]. $V$ doubles when two myosin heads are moving the same actin filament, triples for three myosin heads, and for $N$ myosin heads is in theory

$$V_{att}\,(N) = v(N) \cdot d \qquad \text{Eq (2)}$$

At saturating [ATP], $v(N)$ is limited by $k_{att}$ [24], and so we refer to $V_{att}$ as being attachment-limited[31] (Fig. 2-1C). At low $N$, $v(N)$ increases linearly as $N{\cdot}k_{att}$, and at sufficiently high $N$, $v(N)$ saturates at $N_{actin}{\cdot}k_{ws}$, where $N_{actin}$ is the number of myosin-binding sites per 1 μm actin filament. We use 1 μm because it is roughly the length above which segmental actin movements become redundant, a length beyond which the force generated by a given myosin head is not transmitted[32,35]. Thus, with saturation of myosin-binding sites on actin, $V_{att}(N)$ saturates at a maximum velocity, $V_{max}$, of $k_{ws}{\cdot}N_{actin}{\cdot}d$.

This simple kinetic model for saturation of $V(N)$ does not take into consideration the mechanical effects of actin-bound myosin heads that impose mechanical loads against actin sliding at high $N$. The probability, $P(N)$, that actin-bound myosin heads stall actin sliding increases with increasing $N$, and when $P(N)$ = 1, actin movement can only occur with the detachment of resistive myosin heads at which point $V$ reaches a detachment limit[33,67]. In general, the detachment limit occurs when actin-bound myosin heads are

stretched a distance *L* before actin movement is stalled at which point actin movement can only resume with the detachment of resistive head(s) at a rate $k_{det}$ [67]. The time it takes an actin filament to move to the point of stall, *L*, is $L/V_{att}$, and once stalled the average time it takes resistive head(s) to detach from actin is $1/k_{det}$. Thus the detachment-limited *V* is $L/(1/k_{det}+L/k_{cat}\cdot N\cdot d)$ (Fig. 2-1B)[33], which for large *N* becomes $V_{det} = L\cdot k_{det}$

One goal of this study is to determine the *N*-dependence of the relative contributions of attachment (Equation 2) and detachment kinetics (Equation 3) to actin sliding velocities. Because definitions of *P(N)* and *L* are model dependent, achieving this goal requires discriminating between two fundamentally different models: the independent force generator model and the collective force model (see Discussion for a more detailed description of model differences).

According to the independent force generator model, actin movement stalls when one myosin head is strongly bound to actin and displaces it a distance *d*. *P(N)* is then the probability that at least one myosin head is strongly bound to actin, and $L = d$ [30,67,68] (Fig. 2-1B). Equation 3 becomes $V_{det}=k_{det}\cdot d$ (Fig. 2-2A) and the *N*-dependence of *V* is $V(N) = V_{det}\cdot P(N)$ [32].

According to a collective force model (Fig. 2-2C) actin movement stalls when the compliant linkages associated with myosin heads strongly bound to actin are collectively displaced a distance *L* by the working steps of *N* myosin heads before reaching a stall force, *F(N)*, which increases linearly with *N* [16]. Thus, *P(N)* is the probability that a collectively generated internal stall force is reached, and $L = F(N)/\kappa$, where κ is the effective stiffness of the compliant linkages associated with strongly bound heads.

According to this model, $V(N) = V_{det} \cdot P(N) + V_{att} \cdot (1 - P(N))$ (Fig. 2-2C). Based on our recent observation that the myosin S2 tether significantly increases $L$ in a myosin filament motility assay, we previously developed an idealized model in which the compliant linkage was infinitely compliant with a hard stop when stretched a distance $L$ (the length of the tether) from which we developed an analytical expression (Fig. 2-2B) for $P(N)$ [33]. We refer to this as a collectively displacement model. In general, however, a more realistic model requires strain-dependent kinetics and collective force generation in stretching compliant linkages. For this we develop a simple discrete state computational model for collective force generation (below).

**Collective force computational model.** Our collective force model is based on the ATPase kinetic scheme in Figure 2-1A with forward and reverse rate constants set to values consistent with those measured in skeletal muscle myosin. A single elastic element of stiffness κ is collectively displaced by myosin heads a distance 8 nm with each actin–myosin weak-to-strong binding step and 2 nm with each ADP release step. Strain-dependent kinetics are incorporated by multiplying the rate constants for each of the two mechanochemical steps by $exp(-w/k_BT)$, where $w$ is the work performed displacing the elastic element. Here, $k_B$ is Boltzmann's constant and $T$ is temperature. Monte Carlo simulations were run with 1-μs time steps. Simulations were run either without saturation kinetics (assuming an infinite number, $N_{actin}$, of actin-binding sites per micrometer of actin) or with saturation kinetics (assuming an infinitely high weak-binding affinity, $K$, and a fixed number, $N_{actin}$, of actin-binding sites per micrometer of actin).

## References


1. Bray, D. *Cell Movement From Molecules to Motility*. (2001).

2. Howard, J. *Mechanics of motor proteins and the cytoskeleton*. (Sinauer Associates, 2001).

3. Phillips, R., Kondev, J. & Theriot, J. *Physical Biology of the Cell*. (Garland Science, 2010).

4. Baker, J. E., Brosseau, C., Joel, P. B. & Warshaw, D. M. The biochemical kinetics underlying actin movement generated by one and many skeletal muscle myosin molecules. *Biophys. J.* **82**, 2134–47 (2002).

5. Palmiter, K., Tyska, M. J., Dupuis, D. E., Alpert, N. R. & Warshaw, D. M. Kinetic differences at the single molecule level account for the functional diversity of rabbit cardiac myosin isoforms. *J. Physiol.* **519 Pt 3**, 669–78 (1999).

6. Veigel, C., Molloy, J. E., Schmitz, S. & Kendrick-Jones, J. Load-dependent kinetics of force production by smooth muscle myosin measured with optical tweezers. *Nat. Cell Biol.* **5**, (2003).

7. Svoboda, K. & Block, S. M. Force and velocity measured for single kinesin molecules. *Cell* **77**, 773–84 (1994).

8. Baker, J. E. *et al.* Myosin V processivity: Multiple kinetic pathways for head-to-head coordination. *Proc. Natl. Acad. Sci. U. S. A.* **101**, 5542–5546 (2004).

9. Kad, N. M., Kim, S., Warshaw, D. M., VanBuren, P. & Baker, J. E. Single-myosin crossbridge interactions with actin filaments regulated by troponin-tropomyosin. *Proc. Natl. Acad. Sci. U. S. A.* **102**, 16990–16995 (2005).

10. Brizendine, R. K. *et al.* Velocities of unloaded muscle filaments are not limited by drag forces imposed by myosin cross-bridges. *Proc. Natl. Acad. Sci.* 201510241 (2015) doi:10.1073/pnas.1510241112.

11. Walcott, S., Warshaw, D. M. & Debold, E. P. Mechanical coupling between myosin molecules causes differences between ensemble and single-molecule measurements. *Biophys. J.* **103**, 501–510 (2012).

12. Kaya, M., Tani, Y., Washio, T., Hisada, T. & Higuchi, H. Coordinated force generation of skeletal myosins in myofilaments through motor coupling. *Nat. Commun.* (2017) doi:10.1038/ncomms16036.

13. Pertici, I. *et al.* A myosin II nanomachine mimicking the striated muscle. *Nat. Commun.* **9**, 1–10 (2018).

14. Baker, J. E. & Thomas, D. D. A thermodynamic muscle model and a chemical basis for A.V. Hill's muscle equation. *J. Muscle Res. Cell Motil.* **21**, 335–344 (2000).

15. Uçar, M. C. & Lipowsky, R. Collective Force Generation by Molecular Motors Is Determined by Strain-Induced Unbinding. *Nano Lett.* **20**, 669–676 (2020).

16. Hooft, A. M., Maki, E. J., Cox, K. K. & Baker, J. E. An accelerated state of myosin-based actin motility. *Biochemistry* **46**, 3513–3520 (2007).

17. Baker, J. E., LaConte, L. E. W., Brust-Mascher, I. & Thomas, D. D. Mechanochemical

coupling in spin-labeled, active, isometric muscle. *Biophys. J.* **77**, (1999).

18. Baker, J. E. Free energy transduction in a chemical motor model. *J. Theor. Biol.* **228**, (2004).

19. Hill, A. V. The heat of shortening and the dynamic constants of muscle. *Proc. R. Soc. London. Ser. B, …* **126**, 136–195 (1938).

20. Fenn, W. O. A quantitative comparison between the energy liberated and the work performed by the isolated sartorius muscle of the frog. *J. Physiol.* **58**, (1923).

21. Fenn, W. O., Brody, H. & Petrilli, A. The tension developed by human muscles at different velocities of muscle shortening. *Am. J. Physiol. Content* (1931) doi:10.1152/ajplegacy.1931.97.1.1.

22. Rayment, I. *et al.* Three-dimensional structure of myosin subfragment-1: A molecular motor. *Science (80-. ).* **261**, 50–58 (1993).

23. Kabsch, W., Mannherz, H. G., Suck, D., Pai, E. F. & Holmes, K. C. Atomic structure of the actin:DNase I complex. *Nature* **347**, 37–44 (1990).

24. Lymn, R. W. & Taylor, E. W. Mechanism of Adenosine Triphosphate Hydrolysis by Actomyosin. *Biochemistry* **10**, 4617–4624 (1971).

25. Sabido-David, C. *et al.* Orientation changes of fluorescent probes at five sites on the myosin regulatory light chain during contraction of single skeletal muscle fibres. *J. Mol. Biol.* **279**, 387–402 (1998).

26. Goldman, Y. E. Kinetics of the actomyosin ATPase in muscle fibers. *Annu. Rev. Physiol.* **49**, 637–54 (1987).

27. Holmes, K. C. & Geeves, M. a. The structural basis of muscle contraction. *Philos. Trans. R. Soc. Lond. B. Biol. Sci.* **355**, 419–31 (2000).

28. Baker, J. E., Brust-Mascher, I., Ramachandran, S., Laconte, L. E. W. & Thomas, D. D. A large and distinct rotation of the myosin light chain domain occurs upon muscle contraction. *Proc. Natl. Acad. Sci. U. S. A.* **95**, 2944–2949 (1998).

29. Ross, J. L., Ali, M. Y. & Warshaw, D. M. Cargo transport: molecular motors navigate a complex cytoskeleton. *Curr. Opin. Cell Biol.* **20**, 41–7 (2008).

30. HUXLEY, A. F. Muscle structure and theories of contraction. *Prog. Biophys. Biophys. Chem.* **7**, 255–318 (1957).

31. Bárány, M. ATPase activity of myosin correlated with speed of muscle shortening. *J. Gen. Physiol.* **50**, Suppl:197-218 (1967).

32. Uyeda, T. Q., Kron, S. J. & Spudich, J. a. Myosin step size. Estimation from slow sliding movement of actin over low densities of heavy meromyosin. *J. Mol. Biol.* **214**, 699–710 (1990).

33. Brizendine, R. K. *et al.* A mixed-kinetic model describes unloaded velocities of smooth, skeletal, and cardiac muscle myosin filaments *in vitro*. *Sci. Adv.* **3**, (2017).

34. Kovács, M., Tóth, J., Hetényi, C., Málnási-Csizmadia, A. & Seller, J. R. Mechanism of blebbistatin inhibition of myosin II. *J. Biol. Chem.* **279**, 35557–35563 (2004).

35. Stewart, T. J. *et al.* Actin sliding velocities are influenced by the driving forces of actin-myosin binding. *Cell. Mol. Bioeng.* **6**, 26–37 (2013).

36. Harris, D. E. & Warshaw, D. M. Smooth and skeletal muscle myosin both exhibit low duty cycles at zero load *in vitro*. *J. Biol. Chem.* **268**, 14764–8 (1993).

37. Taylor, E. W. & Sleep, J. A. Intermediate States of Actomyosin Adenosine Triphosphatase. *Biochemistry* **15**, 5813–7 (1976).

38. Homsher, E., Wang, F. & Sellers, J. R. Factors affecting movement of F-actin filaments propelled by skeletal muscle heavy meromyosin. *Am. J. Physiol.* **262**, C714-23 (1992).

39. Greenberg, M. J. & Moore, J. R. The molecular basis of frictional loads in the *in vitro* motility assay with applications to the study of the loaded mechanochemistry of molecular motors. *Cytoskeleton (Hoboken)*. **67**, 273–85 (2010).

40. Webb, M. *et al.* The myosin duty ratio tunes the calcium sensitivity and cooperative activation of the thin filament. *Biochemistry* **52**, (2013).

41. Sich, N. M. *et al.* Effects of actin-myosin kinetics on the calcium sensitivity of regulated thin filaments. *J. Biol. Chem.* **285**, 39150–9 (2010).

42. Siemankowski, R. F., Wiseman, M. O. & White, H. D. ADP dissociation from actomyosin subfragment 1 is sufficiently slow to limit the unloaded shortening velocity in vertebrate muscle. *Proc. Natl. Acad. Sci. U. S. A.* **82**, 658–62 (1985).

43. Baker, J. E. & Thomas, D. D. Thermodynamics and kinetics of a molecular motor ensemble. *Biophys. J.* **79**, 1731–1736 (2000).

44. Hill, T. L. Theoretical formalism for the sliding filament model of contraction of striated muscle. Part I. *Prog. Biophys. Mol. Biol.* **28**, 267–340 (1974).

45. Highsmith, S. Muscle cross-bridge chemistry and force [1]. *Biophysical Journal* vol. 79 (2000).

46. Amrute-Nayak, M., Antognozzi, M., Scholz, T., Kojima, H. & Brenner, B. Inorganic phosphate binds to the empty nucleotide binding pocket of conventional myosin II. *J. Biol. Chem.* **283**, (2008).

47. Hill, T. L. *Free Energy Transduction and Biochemical Cycle Kinetics*. (Springer-Verlag, 1989).

48. Månsson, A. Hypothesis: Single actomyosin properties account for ensemble behavior in active muscle shortening and isometric contraction. *Int. J. Mol. Sci.* **21**, 1–21 (2020).

49. Pertici, I., Bianchi, G., Bongini, L., Lombardi, V. & Bianco, P. A Myosin II-based nanomachine devised for the study of Ca2+-dependent mechanisms of muscle regulation. *Int. J. Mol. Sci.* (2020) doi:10.3390/ijms21197372.

50. Campbell, S. G., Hatfield, P. C. & Campbell, K. S. A mathematical model of muscle containing heterogeneous half-sarcomeres exhibits residual force enhancement. *PLoS Comput. Biol.* (2011) doi:10.1371/journal.pcbi.1002156.

51. Debold, E. P., Longyear, T. J. & Turner, M. a. The effects of phosphate and acidosis on regulated thin-filament velocity in an *in vitro* motility assay. *J. Appl. Physiol.* **113**, 1413–

22 (2012).

52. Haldeman, B. D., Brizendine, R. K., Facemyer, K. C., Baker, J. E. & Cremo, C. R. The kinetics underlying the velocity of smooth muscle myosin filament sliding on actin filaments *in vitro*. *J. Biol. Chem.* **289**, 21055–70 (2014).

53. Veigel, C., Wang, F., Bartoo, M. L., Sellers, J. R. & Molloy, J. E. The gated gait of the processive molecular motor, myosin V. *Nat. Cell Biol.* **4**, 59–65 (2002).

54. Prochniewicz, E. *et al.* Functional, structural, and chemical changes in myosin associated with hydrogen peroxide treatment of skeletal muscle fibers. *Am. J. Physiol. Cell Physiol.* **294**, C613–C626 (2008).

55. Margossian, S. S. & Lowey, S. Preparation of myosin and its subfragments from rabbit skeletal muscle. in *Methods in Enzymology* (eds. Colowick, S. P. & Kaplan, N. O.) vol. 85 55–71 (Academic Press, 1982).

56. Pardee, J. & Spudich, J. Purification of muscle actin. *Methods Enzymol.* **85**, 164–181 (1982).

57. Smillie, L. B. Preparation and identification of alpha- and beta-tropomyosins. *Methods Enzymol.* **85 Pt B**, 234–41 (1982).

58. Potter, J. D. Preparation of troponin and its subunits. *Methods Enzymol.* **85 Pt B**, 241–63 (1982).

59. Shi, X., Lim, J. & Ha, T. Acidification of the oxygen scavenging system in single-molecule fluorescence studies: in situ sensing with a ratiometric dual-emission probe. *Anal. Chem.* **82**, 6132–6138 (2010).

60. Sakamoto, T., Limouze, J., Combs, C. a, Straight, A. F. & Sellers, J. R. Blebbistatin, a myosin II inhibitor, is photoinactivated by blue light. *Biochemistry* **44**, 584–8 (2005).

61. Fabiato, A. & Fabiato, F. Calculator programs for computing the composition of the solutions containing multiple metals and ligands used for experiments in skinned muscle cells. *J. Physiol. (Paris).* **75**, 463–505 (1979).

62. Huxley, A. F. Muscular contraction. *J. Physiol.* **243**, 1–43 (1974).

63. Huxley, H. E. The mechanism of muscular contraction. *Science* vol. 164 1356–1366 (1969).

64. Finer, J. T., Simmons, R. M., Spudich, J. A. & others. Single myosin molecule mechanics: piconewton forces and nanometre steps. *Nature* **368**, 113–119 (1994).

65. Guilford, W. H. H. *et al.* Smooth muscle and skeletal muscle myosins produce similar unitary forces and displacements in the laser trap. *Biophys. J.* **72**, 1006–21 (1997).

66. Molloy, J. E., Burns, J. E., Kendrick-Jones, B., Tregear, R. T. & White, D. C. S. Movement and force produced by a single myosin head. *Nature* **378**, (1995).

67. Spudlch, J. A. How molecular motors work. *Nature* **372**, 515 (1994).

68. Huxley, H. E. Sliding filaments and molecular motile systems. *J. Biol. Chem.* **265**, 8347–50 (1990).

## Chapter 3

## A Model of Collective Force Generation by Myosin Accounts for Opposing Effects of $P_i$ on Detachment-Limited Actin Sliding Velocities

Vidya Murthy, Travis J. Stewart, Josh E. Baker

**Abstract**

Muscle contraction results from cyclic interactions of actin-myosin binding coupled to the actin-myosin catalyzed hydrolysis of ATP. Although the mechanics and kinetics of muscle myosin are well established at the level of a single molecule, it is less evident how these single molecule behaviors scale up to the collective behaviors of many myosin molecules working together. Recent studies show that $P_i$ inhibits actin sliding velocities, *V*, at low [ATP] and activates *V* at low pH. Both studies are difficult to reconcile with traditional independent force generator models. Here we account for both $P_i$ effects with a simple collective force generator model based on well-established actin-myosin kinetics and mechanics. We show that both effects result from $P_i$ inhibition of internal forces generated collectively at low actin-myosin detachment rates. At low [ATP], $P_i$ slows *V* because decreasing internal forces decreases the amplitude of collective steps. At ADP release rates slowed at low pH, $P_i$ accelerates *V* because decreasing internal forces accelerates the force-dependent ADP release rate. A collective force model predicts that both $P_i$ effects can be attenuated by decreasing internal forces through reducing myosin densities, *N*. To test this prediction, we use an in vitro motility assay to measure the *N*-dependence of *V* at pH 7.4 and pH 6.5 and show that $P_i$-activation of *V* is attenuated at low *N*. Collective force generation by myosin results in unexpected emergent mechanical behaviors that offer new interpretations for how muscle works.

**Introduction**

Muscle generates force and movement when myosin heads undergo a conformational change upon binding actin filaments[1,2,3,4,5] – a chemical step that is repeated through the actin-myosin catalyzed ATP hydrolysis reaction[6,7,8] at a rate, *v* (Fig. 3-1). For over fifty years, muscle mechanics have been described using independent force generator models[9], which assume that mechanical states in muscle are well defined at the level of individual myosin heads (*x* in Fig. 3-2A) and as such describe muscle mechanics as the sum of its molecular mechanical parts[10]. These models allow one, in theory, to extrapolate the behaviors of muscle from the behaviors of its individual myosin components, enabling theoretical biologists to tune hypothesized molecular behaviors to match muscle mechanics data.

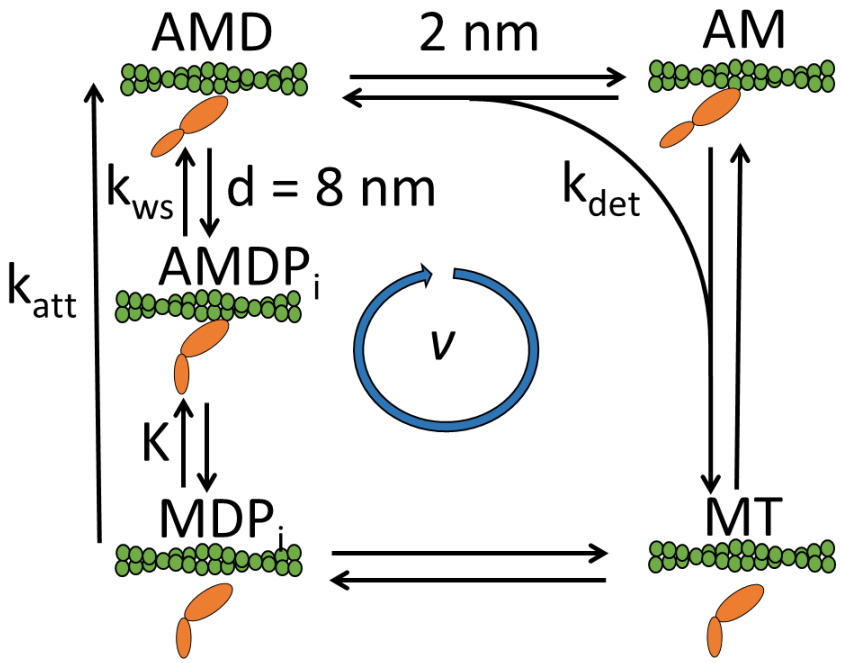


Figure 3-1: A minimal biochemical scheme for force generation through the actin-myosin ATPase reaction. Myosin (M) is weakly associated (K) with actin when bound to ADP (D) and $P_i$ (P). Upon $P_i$ release and strong binding to actin ($k_{att}$) myosin displaces actin a distance of $d_1$ = 8 nm. Myosin detaches from actin ($k_{det}$) in two steps. Upon ADP release, myosin further displaces the actin filament a distance $d_2$ = 2 nm, and upon ATP (T) binding myosin detaches from actin. ATP is hydrolyzed to products ADP and $P_i$ that remain bound to myosin. All these transitions are reversible.

The problem with this approach is that muscle is a dynamic macromolecular complex consisting of many myosin molecules interacting and thermally fluctuating with actin filaments, making it difficult if not impossible to partition mechanical states among different components in this complex. In 2000, based on A.V. Hill's muscle mechanics and energetic studies[11] and on direct measurements of mechanochemical coupling in muscle[12], we developed a thermodynamic model of muscle contraction[13] in which the mechanical state (*x* in Fig. 3-2B) is defined at the level of a muscle filament, and myosin heads collectively generate force in a single equivalent filament spring.

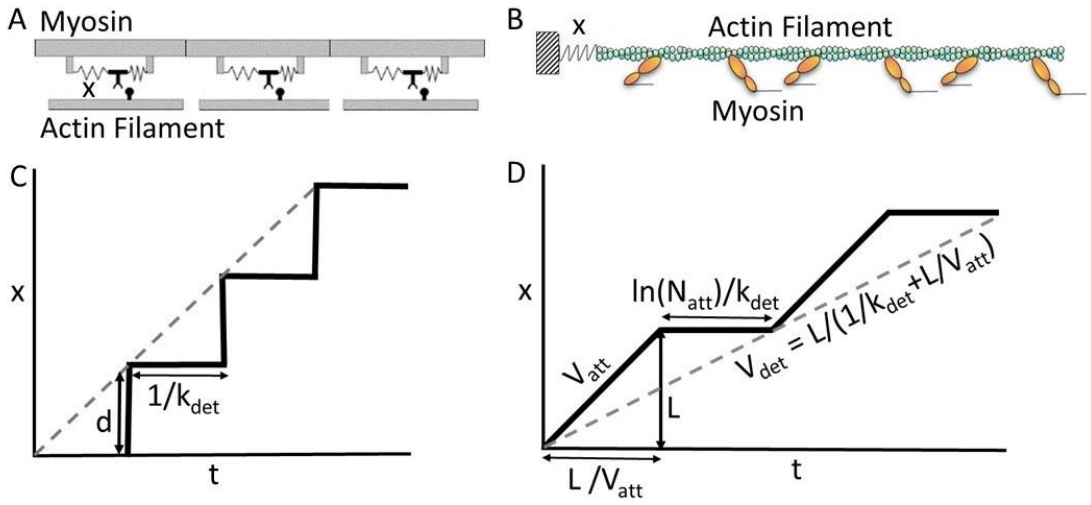


Figure 3-2: Comparison of independent-force and collective-force models. (A) In an independent force generator model, mechanical states, *x*, are defined at the level of an individual myosin head. (B) A collective force model assumes that mechanical states cannot be partitioned among components in a dynamic, thermally fluctuating macromolecular complex, and thus the mechanical state, *x*, is defined at the level of actin-myosin system with a single spring that is collectively displaced by mechanical steps in the actin-myosin ATPase reaction (Fig. 3-1). During unloaded actin sliding, the single spring represents collectively generated intrafilament forces. (C) An independent force generator model requires that actin sliding velocities are detachment-limited and is described in terms of molecular mechanics and chemistry as $V = d \cdot k_{det}$. (D) At low $k_{det}$, high $k_{att}$, and high $N$, collective force generation models approach a detachment-limited $V [= L/(ln(N_{att})/ k_{det} + L/V_{att})]$ where $L$ is a displacement collectively generated by sequential myosin steps of size $d (= d_1 + d_2)$ at a rate $V_{att} (= N \cdot v \cdot d)$, and $N_{att}$ is the number of myosin heads attached to actin at initiation of stall. This resembles our collective movement model for a tethered myosin[17] and is developed here more generally for collective force generation.

In contrast to independent force generator models, in a collective force model, muscle mechanics are an emergent property of the muscle system, which makes modeling muscle mechanics much less intuitive because emergent behaviors are not evident from the mechano-kinetic behaviors of individuals myosin molecules. Using a collective force model to account for experimental data requires almost a blind reliance on model parameters that are a priori well-defined experimentally, trusting the simulations to reveal the emergent behaviors rather than adjusting molecular states and properties to match experimental results.

Collective force models readily account for the observation that under physiological conditions, actin sliding velocities are largely attachment-limited ($V = N \cdot v \cdot d$)[13,14,15,16]. This is clearly at odds with the predictions of independent force generator models, which require detachment-limited velocities ($V = d \cdot k_{det}$). This requirement comes from the fact that if actin movement were formally allowed to occur with the force-generating step of a given myosin head, force would be distributed with that step among all compliant system components stretched by actin movement and would not be localized to that head, violating the basic assumption of independent force generation.

Collective force models show and experimental data support that $V$ can approach a detachment limit under conditions such as slow actin-myosin detachment rates, $k_{det}$, high actin-myosin attachment rates, $k_{att}$, and/or high numbers of myosin heads, $N$[15,17]. Here using a Monte Carlo simulation based on a simple collective force model (Fig. 3-1 and Fig. 3-2B) we show that the transition from attachment toward detachment-limited $V$ involves a transition from staircase steps with variable amplitudes and durations to more periodic steps that stall at repeated, relatively constant amplitudes. The periodic stepping that arises from stochastic kinetics is an example of the emergent behaviors of collective force generation.

Periodic collective steps in a collective force model (Fig. 3-2D) can be used to approximate velocities near the detachment limit, $V_{det} = L \cdot k_{det}/\ln(N_{att})$, in the same way that the steps of single myosin heads in an independent force generator model (Fig. 3-2C) are used to approximate detachment-limited velocities, $V_{det} = d \cdot k_{det}$, with two notable differences. First, the amplitude of a collective step, $L$, is determined by the stall force in an in-

tra filament spring, which is influenced by actin-myosin chemistry as well as mechanics[15,18,19]. In contrast, the relatively fixed molecular step, $d$, in $V_{det} = d \cdot k_{det}$ is defined by a discrete structural change in a single myosin head. Second, the average duration of the collective step, $\ln(N_{att})/k_{det}$, is a bulk property that depends on the number of actin-bound myosin heads, $N_{att}$, which results in steps that are more periodic than the stochastic, exponentially distributed step durations, $1/k_{det}$, of a single myosin head.

Two seemingly contradictory studies provide evidence of emergent behaviors in a collective actin-myosin system. In 2007, Hooft et al.[15] showed that under detachment-limited conditions (low [ATP]) inorganic $P_i$ inhibits $V$ in an in vitro motility assay. This result is difficult to reconcile with independent force generator models since $P_i$ affects neither $d$ nor $k_{det}$. In 2011, Debold et al.[20] showed that under detachment-limited conditions (slow ADP release rate) $P_i$ accelerates $V$ in an in vitro motility assay, which is also difficult to reconcile with independent force generator models. In the latter study, the authors developed an independent force generator model to account for this observation, but it required the addition of states and transitions that are unsupported experimentally[20]. The observation that $P_i$ activates $V$ is remarkable considering that, if anything, $P_i$ inhibits the actin-myosin ATPase reaction. So how does $P_i$ accelerate $V$? And why is this effect completely opposite from the $P_i$ effect observed under similar detachment-limited conditions at low [ATP]?

Here we show that a simple collective force model accounts for these opposing effects of $P_i$. Briefly, as previously proposed, our simulations show that $P_i$ inhibits $V$ at low [ATP] because $P_i$ decreases the intra filament stall or “driving” force through the

same mechanism by which $P_i$ inhibits isometric force[19,21]. The $P_i$-induced decrease in intra filament stall force does not affect the step duration because at low [ATP] $k_{det}$ is limited by ATP binding, which is not a force-dependent transition[22]. Thus at low [ATP], $P_i$ inhibits $V = L \cdot k_{det}/\ln(N_{att})$ by decreasing $L$.

At slow ADP release rates, $P_i$ similarly decreases the step amplitude, $L$, by inhibiting the stall force. However, unlike at low [ATP] here the $P_i$-induced inhibition of stall force significantly accelerates the force-dependent ADP release rate[22], which is rate-limiting for $k_{det}$ under these conditions. The net effect is that $P_i$ accelerates $V = L \cdot k_{det}/\ln(N_{att})$ by decreasing stall force resulting in an increase in $k_{det}$ that is proportionally larger than the decrease in $L$. The basic mechanism by which $P_i$ accelerates $V$ at low ADP release rates is inhibition of an autoinhibition of ADP release. This mechanism resembles that of a finger trap where the forces generated by fingers trying to slide out of the trap prevent finger sliding. Decreasing the force that the finger trap exerts on the fingers enables the fingers to slide.

A collective force model predicts that the high-force, detachment-limited $V$ at low ADP release rates can be transitioned to a low-force, attachment-limited $V$ simply by decreasing $N$. Thus, the model predicts that $P_i$ acceleration of $V$ through a force-dependent autoinhibition mechanism will be attenuated at low $N$. As predicted, using an in vitro motility assay, we show that the effects of $P_i$ on $V$ are significantly diminished at low $N$.

Under physiological conditions, $V$ is attachment-limited[14,15,17], and so it is unlikely that $P_i$-induced acceleration or inhibition of a detachment-limited $V$ has physiological relevance. However, the collective force model that accounts for these data has broad

implications for muscle contraction because it represents a new paradigm of muscle mechanics as emergent behaviors of an ensemble of myosin molecules. These emergent behaviors tend to be unexpected and unintuitive, and so exploring these behaviors will undoubtedly reveal unforeseen mechanisms of muscle contraction and regulation in normal, disease, and therapeutic states.

## Materials and Methods

**Protein Preparations.** Skeletal muscle myosin was prepared from rabbit psoas muscle as previously described and stored in glycerol at –20° C[23,24]. F-actin was purified from rabbit psoas muscle and stored on ice at 4° C[25]. To stabilize and label actin for *in vitro* motility assays, actin (1 µM in actin buffer) was incubated with 1 µM tetramethyl-rhodamine isothiocyanate (TRITC)-phalloidin (Sigma) overnight at 4° C prior to dilution to the experimental concentration (see below). Skeletal tropomyosin and troponin (Tm-Tn) were purified as previously described[26,27]. Regulated thin filaments were reconstituted by combining 250 nM Tm and Tn to 0.015 uM TRITC-actin and incubating on ice for 20 minutes as previously described[28].

**Buffers.** Myosin buffer contained 300 mM KCl, 25 mM imidazole (pH 7.4), 1 mM EGTA, 4 mM $MgCl_2$, and 10 mM DTT. Actin buffer contained 50 mM KCl, 50 mM imidazole (pH 7.4), 2 mM EGTA, 8 mM $MgCl_2$, and 10 mM DTT. Motility buffer contained 50 mM imidazole (pH 7.4), 2 mM EGTA, 8 mM $MgCl_2$, 10 mM DTT, 0.5% methylcellulose and KCl and 1 mM ATP. Motility buffer also contained an oxygen scavenger system (2.9 mg/ml glucose, 1.6 mg/ml glucose oxidase, 2.3 mg/ml catalase) that was added immediately prior to imaging[29].

**In vitro motility assays.** Velocities of TRITC-labeled actin filaments were measured at 30$^{o}$ C as they moved over surface-attached monomeric skeletal muscle myosin. Flow cells were made by attaching a nitrocellulose-coated coverslip to a microscope slide with double-sided 1/4 inch thick tape (3M, St Paul, MN). Different myosin concentra-

tions in myosin buffer were applied to the flow cell followed by 2 x 50 µl aliquots in sequence of 5 mg $ml^{-1}$ BSA in actin buffer, 10 nM TRITC-actin in actin buffer prepared as described above, actin buffer, and motility buffer. Each solution was incubated in the flow cell for 2 minutes before adding the next. Phosphate experiments were performed with 30 mM $P_i$ added to the motility buffer, maintaining a constant ionic strength in the no-$P_i$ with KCl. The pH of all buffers was adjusted after addition of all buffer components. Motility assays were performed using a Nikon TE2000 epifluorescence microscope and images were digitally acquired with a Roper Cascade 512B camera (Princeton Instruments, Trenton, NJ).

**Tracking and Image Analysis**. MetaMorph software (Molecular Devices) was used for image acquisition. For each flow cell, 30 sec image sequences from three different fields were recorded. Actin velocities were manually tracked using the MTrackJ plug-in for ImageJ (NIH, Bethesda, MD). Only smoothly moving filaments with trajectories greater than 3 µm were selected for analysis. An average velocity for a given trajectory meeting the above criteria was determined using ImageJ. For a given experiment (one flow cell) 45 to 100 trajectories were recorded and analyzed (n = 1). Reported *V* values are averages of at least three (n = 3) independent experiments with standard error reported with error bars.

**Calculating N.** Based on previous studies[30], we assume a linear relationship between the surface density of myosin on a motility coverslip and the myosin concentration, [M], used to incubate a flow cell for two minutes. The number, *N*, of myosin available to

bind a unit length (1 μm) of actin is proportional to the myosin surface density. To calculate $N$, we multiply [M] by a conversion factor 1 (myosin per μm actin)/(μg/ml) consistent with estimates in Harris and Warshaw[30].

**Collective Force Computational Model.** Computer simulations are based on a five-state actin-myosin ATPase kinetic scheme (Fig. 3-1) with all forward and reverse rate constants set to values consistent with those measured for skeletal muscle myosin. A single elastic element of stiffness $\kappa$ was collectively displaced by myosin heads a distance $d_1$ = 8 nm for each actin-myosin binding step (referred to as the working step) and $d_2$ = 2 nm for each ADP release step. Strain dependent kinetics are incorporated into the model as described below.

The work performed by mechanical steps is simply $w = E_f - E_i$ where $E_f = ½\kappa\cdot(x + d)^2$ and $E_i = ½\kappa\cdot x^2$ are the energy in the system spring after and before a mechanical step of size, $d$ stretches the spring from an initial displacement, $x$. The strain-dependent contributions to the forward and reverse rate constants are described by the Boltzmann factors $\exp(-\gamma\cdot w/kT)$ and $\exp(-(1-\gamma)\cdot w/kT)$ for forward and reverse steps where $\gamma$ is the fraction of work performed prior to the activation energy barrier[31]; k is the Boltzman constant; and T is temperature. For the attachment working step, $\gamma = a$ and $d = d_1$. For the ADP release step, $\gamma = b$ and $d = d_2$. Here we assume that the stiffness of the force-generating myosin head is much greater than the effective stiffness of the rest of the system, which means that the displacement of the system spring, $x$, equals the distance the actin moves with each myosin step. Deviations from this assumption result in actin displacements that are smaller than $d_1$ and $d_2$.

Model parameters (unless otherwise specified in figure legends are $a = 0.5$; $b = 1$; $\kappa = 0.04$ pN/nm; $N = 50$; second order ATP binding constant, $k_T = 5 \times 10^6$ $M^{-1} \cdot s^{-1}$; [ATP] = 1 mM; ADP release rate, $k_{det} = 500$ $s^{-1}$; ADP binding rate, $[ADP]k_{+D} = 0.0001$ $s^{-1}$; forward hydrolysis rate, $k_{+hyd} = 20$ $s^{-1}$; reverse hydrolysis rate, $k_{-hyd} = 2$ $s^{-1}$; attachment rate, $k_{att} = 30$ $s^{-1}$; second order reverse attachment rate, $k_{-att} = 0.25$ $mM^{-1} \cdot s^{-1}$; contaminating $[P_i]$ = 40 µM. Monte Carlo simulations were run with 1 µs time steps.

Saturation kinetics was incorporated assuming a fixed number of actin binding sites per micron of actin, $N_{actin} = 50$, and an infinite weak-binding actin-myosin association constant, $K$ (Fig. 3-1) such that saturation of myosin binding sites on actin occurred when $N = N_{actin}$.

**Results**

Figure 3-1 shows a well-established five-state mechanokinetic scheme that forms the basis for our Monte Carlo simulations of collective force generation. The model assumes an 8 nm ($d_1$) mechanical displacement of actin by myosin associated with the working step (AMDP to AMD) and a 2 nm ($d_2$) mechanical displacement by myosin associated with the ADP release step (AMD to AM)[4,22] for a total displacement, $d = d_1 + d_2$, of 10 nm. These biochemical steps and corresponding displacements directly move actin filaments, generating force in all compliant elements stretched by that movement (Figs. 3-2B and 3-2D). In a collective force model, we reduce this dynamic elastic network to a single equivalent system spring with an effective stiffness, $\kappa$ (Fig. 3-2B). Because they perform work, both the working step and the ADP release step are strain dependent in both directions (see methods).

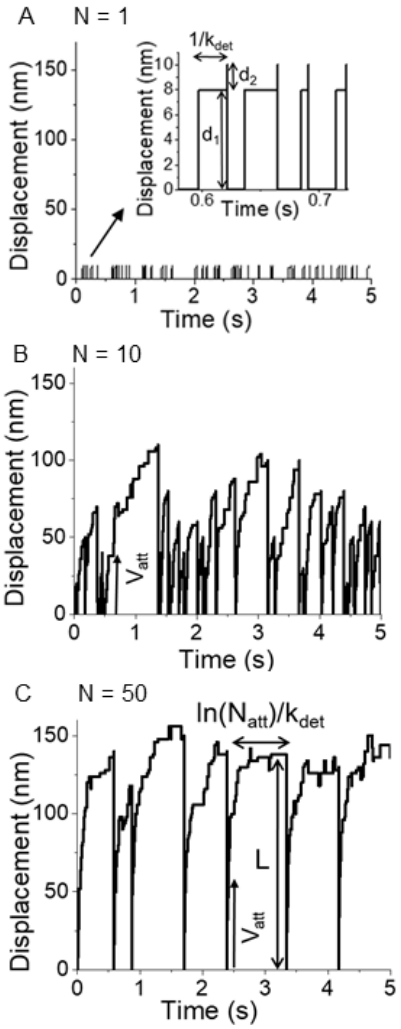


Figure 3-3: Computer simulations of collective force generation illustrating emergent collective behaviors with increasing numbers of myosin heads, *N*. (A) One myosin head takes a step of size $d_1$ at a rate $k_{att}$ and a second step of size $d_2$ associated with ADP release. Upon ATP binding, the step terminates when the myosin head detaches from actin. The total molecular displacement is $d = d_1 + d_2$ and the step durations are exponentially distributed (inset) with an average lifetime $1/k_{det}$. (B) $N = 10$ myosin heads collectively displace a system spring through sequential steps of size d at a rate $V_{att} = N \cdot v \cdot d$, resulting in staircase steps that typically terminate before reaching a stall force. Both amplitudes and durations appear stochastically distributed, and so we refer to this behavior as stochastic, "staircase" stepping. This is the mechanism underlying attachment-limited *V*. (C) $N = 50$ myosin heads collectively displacing a system spring through sequential steps of size *d* at a rate $V_{att} = N \cdot v \cdot d$ result in staircase steps that do not terminate before reaching a stall force at an average displacement, *L*. Both amplitudes and durations appear relatively constant, and so we refer to this as periodic stepping. This collective stepping behavior resembles that illustrated in Fig. 2D and is the mechanism underlying a near detachment-limited $V = L \cdot k_{det}/ln(N_{att})$.

Figure 3-3 shows simulations of collective force-generation performed at three different $N$ values, where $N$ is the number of myosin heads available to bind an actin filament. For $N = 1$, single molecule stepping behaviors resemble those observed in single molecule optical trap studies[14,22]. For $N = 10$, we observe collective stochastic stepping behaviors with a broad distribution of run lengths and durations consistent with those observed in optical trap studies of small myosin ensembles[32,33]. At large $N$ ($N = 50$), the stepping behavior becomes more periodic with relatively constant collectively generated amplitudes and periodicities similar to those observed recently by Kaya and colleagues[34]. Here we describe the in silico mechanism underlying the phase shift from stochastic single molecule steps (Fig. 3-3A, inset) to periodic collective steps (Fig. 3-3C) with increasing $N$.

The stochastic stepping in Fig. 3-3B is generated through sequential displacements, $d$, by myosin heads at a rate $V_{att} = N \cdot d \cdot v$. The step amplitudes and durations are variable because under these conditions the probability is relatively high that all myosin heads detach from actin before a stall force is reached. Because movement occurs at the rate of ATP turnover, $v$, and $v$ is limited by $k_{att}$, this stochastic stepping is the collective force mechanism for an attachment-limited $V$.

The periodic steps in Fig. 3-3C are generated through sequential displacements, $d$, by myosin heads at a rate $V_{att} = N \cdot d \cdot v$ until a stall force is reached. These steps have relatively constant amplitudes, $L$, because the stall force, $F = \kappa \cdot L$, generated by a myosin ensemble is relatively constant. The step duration is relatively constant because it too is a bulk property. Solving $N_{att} \cdot \exp(-k_{det} \cdot t) = 1$ for $t$, we obtain the time that it takes for all but

one of the $N_{att}$ actin-bound myosin heads at initiation of stall to detach from actin, $t = \ln(N_{att})/k_{det}$. For reasons discussed below, here we ignore the additional time required for detachment of the last head, $1/k_{det}$. When $L/V_{att}$ is small relative to the step duration, the duration of these steps is limited by $\ln(N_{att})/k_{det}$. Thus these periodic steps are the collective force mechanism for $V$ near a detachment limit, $V = L \cdot k_{det}/\ln(N_{att})$.

In all models of actin sliding, it is assumed that forward progress is maintained when myosin heads detach from actin (Fig. 3-3, transitions to $x = 0$), and a net velocity is determined by summing mechanical steps (Figs. 3-2C and 3-2D). In a collective force model, the forces generated during actin sliding are intermolecular and are dissipated ($x = 0$) when all but one myosin head detaches from actin. The periodic mechanical steps underlying a detachment-limited $V$ in a collective force model (Fig. 3-2D, Fig. 3-3C) resemble the single molecule mechanical steps underlying a detachment-limited $V$ in independent force generator models (Fig. 3-2C) with two important differences. First the amplitude, $L$, of a collective step (Fig. 3-2D) varies proportionally with changes in stall force, whereas the step size, $d$, is relatively fixed as it is associated with a discrete structural change in the myosin head (Fig. 3-2C). Second, the collective step duration is a bulk property with a distribution centered around an average value, $\ln(N_{att})/k_{det}$, in contrast to the stochastic, exponentially distributed single molecule step durations around an average value $1/k_{det}$ (Fig. 3-3A, inset).

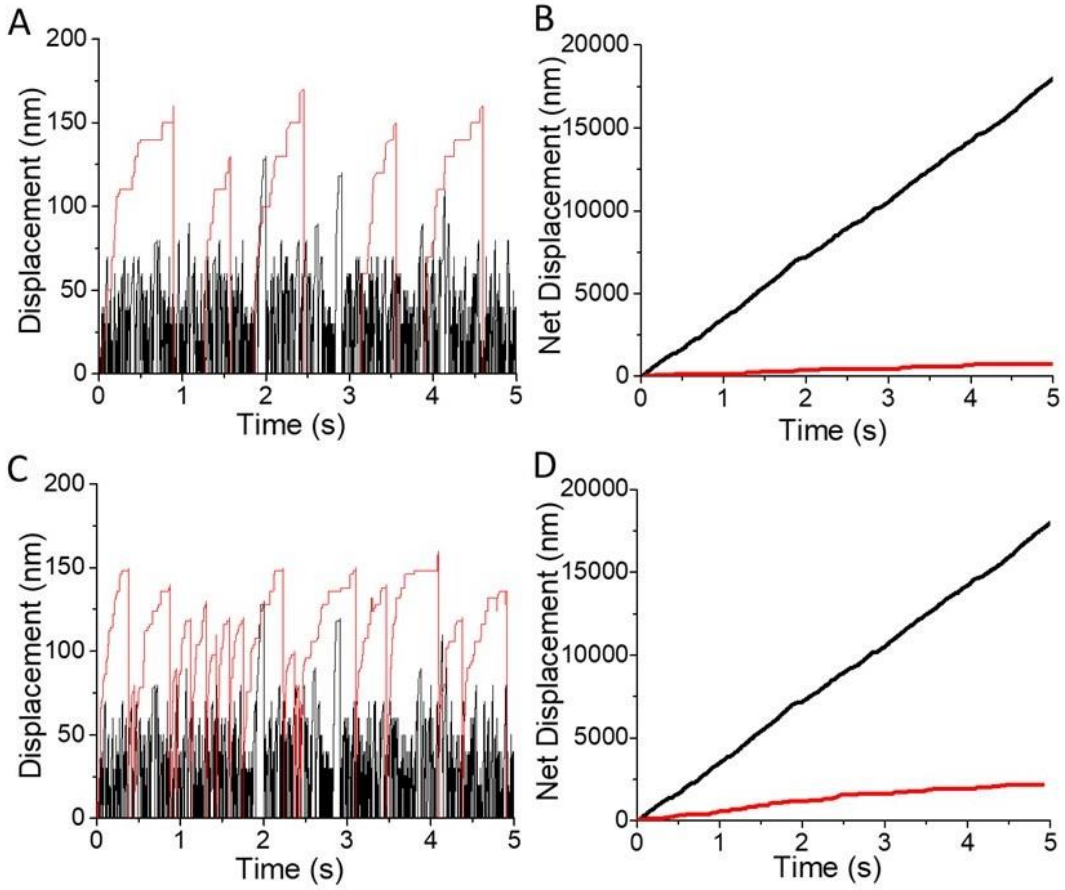


Figure 3-4: Simulations of the effects of decreasing $k_{det}$ on $V$. (A) At relatively high $k_{det}$ collective myosin displacements of actin occur with stochastic, attachment-limited stepping (black). For $k_{det}$ slowed at low ATP (red), collective myosin displacements of actin become periodic and approach a detachment limit. (B) The net displacement of actin filaments is the sum of the stepping behavior in panel A, showing that even though decreasing [ATP] increases the step size, $L$, the increased step duration results in a net decrease in $V$. (C) At relatively high $k_{det}$ collective myosin displacements of actin occur with stochastic, attachment-limited stepping (black). For $k_{det}$ slowed by a decreased ADP release rate, collective myosin displacements of actin become periodic and approach a detachment limit (red). (D) The net displacement of actin filaments is the sum of the stepping behavior in panel C, showing that even though decreasing the ADP release rate increases the step size, $L$, the increased step duration results in a net decrease in $V$. Model parameters (Table 3-1).

Many factors affect the phase, amplitude and duration of collective steps with mechanisms that are discoverable in silico. As an example, Fig. 3-4A shows that decreasing [ATP] makes steps more periodic with higher amplitudes, *L*, and longer durations, since decreasing $k_{det}$ both increases the probability that a stall force is reached before termination of the step and increases the periodic step duration. Fig. 3-4B shows that while the increase in *L* contributes to increasing *V*; the longer step duration has a proportionally larger effect, resulting in a net decrease in *V*. This is consistent with observed effects of [ATP] in in vitro motility[35,36] and unloaded muscle shortening studies[37].

As another example, Fig. 3-4C shows the simulated effects of decreasing the ADP release rate on *V*. Like decreasing [ATP], decreasing the ADP release rate decreases $k_{det}$, which makes steps more periodic, increases the step amplitude *L*, and lengthens step durations. Also, like low [ATP], while the increased *L* contributes to increasing *V*, Fig. 3-4D shows that the longer step duration has a proportionally larger effect resulting in a net decrease in *V*, consistent with studies showing a correlation between ADP release rates and *V* [38].

Because the release of inorganic phosphate, $P_i$, is associated with the working step of the actin-myosin ATPase reaction (Fig. 3-1), many researchers have used $P_i$ as a tool to probe the mechanics and kinetics of muscle contraction. Some of these studies have yielded surprising results. Here we consider two such studies that look at the effects of $P_i$ on *V* measured in an in vitro motility assay at both low [ATP] and slow ADP release rates. Although decreasing [ATP] and ADP release rates both decrease $k_{det}$ and thus have similar mechanistic effects on *V* (Fig. 3-4), the observed effects of $P_i$ on *V* under these

two conditions are completely opposite, and both effects have been difficult to reconcile using independent force generator models.

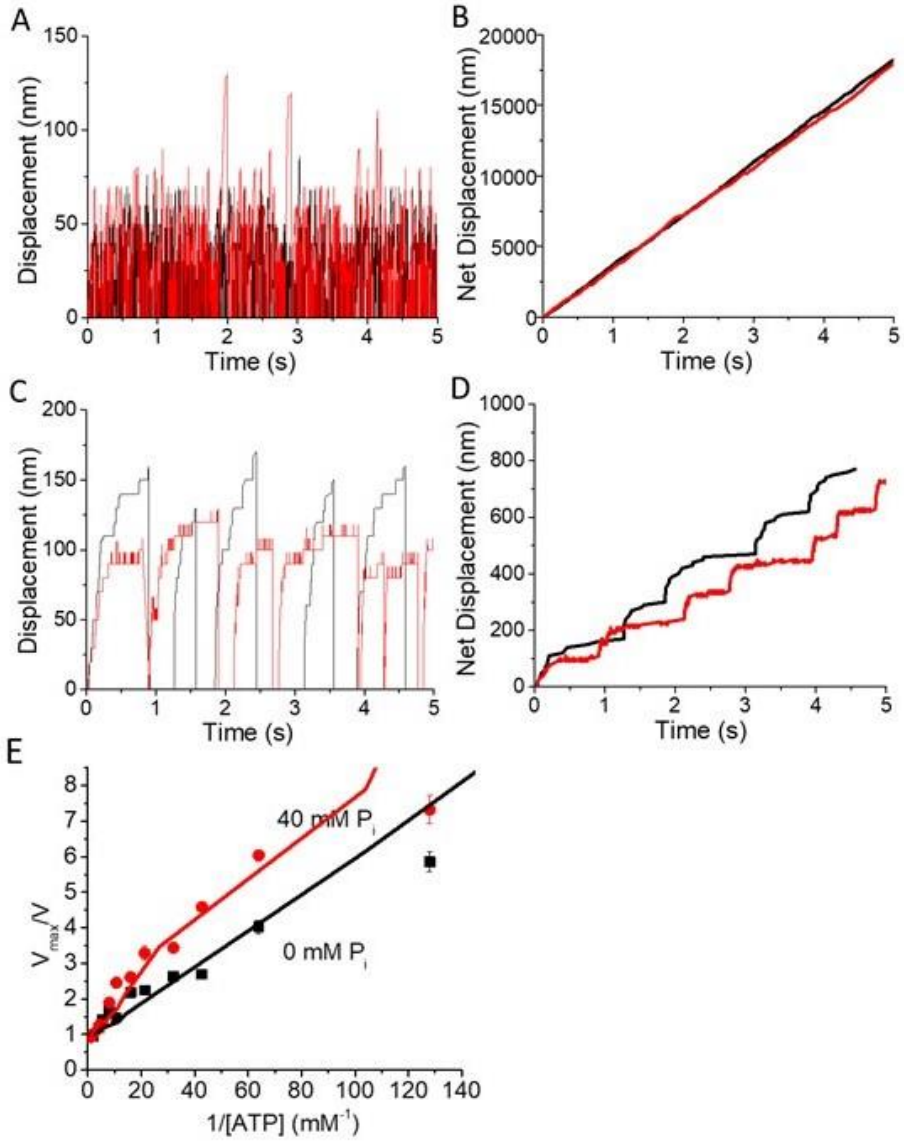


Figure 3-5: The effects of $P_i$ at high and low [ATP]. (A) Simulated attachment-limited staircase stepping of collective displacements at 1 mM ATP both without (black) and with (red) inorganic phosphate show that 40 mM $P_i$ has little effect on attachment-limited stepping. (B) The net displacement of actin filaments in panel A shows that $P_i$ has little effect on *V* at 1 mM ATP. (C) Simulated collective displacements at low ATP both without (black) and with (red) 40 mM $P_i$ (red) show the amplitude of detachment-limited stepping decreases with $P_i$ without significantly affecting step durations. (D) The net displacements of actin in panel C shows that $P_i$ slows *V* at low [ATP]. (E) Simulations of collective force generation (lines) account for the [ATP] dependence of *V* previously measured in an in vitro motility assay (symbols) with (red) and without (black) 40 mM added $P_i$[15]. Model parameters (Table 3-1).

Hooft et al. along with others[15,35] have shown that at high [ATP] the effects of $P_i$ on *V* are relatively minor, proposing that at high [ATP] internal loads in a motility assay are insufficient to reverse the weak-to-strong binding transition. This is similar to observations and interpretations of the effects of $P_i$ on unloaded muscle shortening velocities[37]. A collective force model accounts for these results, showing that at high [ATP], $P_i$ has little effect on attachment-limited stepping (Fig. 3-5A) and *V* (Fig. 3-5B), since the low internal forces, *F*, are insufficient to significantly reverse the working step in the presence of $P_i$ (Fig. 3-5A). At low [ATP], however, Hooft et al. showed that $P_i$ significantly inhibits *V*, proposing that $P_i$ inhibits the high "driving forces" in a motility assay at low [ATP]. A collective force model supports this hypothesis, showing that the higher forces generated with periodic stepping are sufficient to reverse the working step in the presence of $P_i$, decreasing *L* (Fig 3-5C) and thus *V* (Fig. 3-5D). The decrease in intra filament stall force with $P_i$ in Fig. 3-5C is consistent with the observation that $P_i$ decreases isometric muscle force[39]. Figure 3-5E shows that a collective force model (line) accurately describes the effects of 40 mM $P_i$ on the [ATP]-dependence of *V* previously reported by Hooft et al.

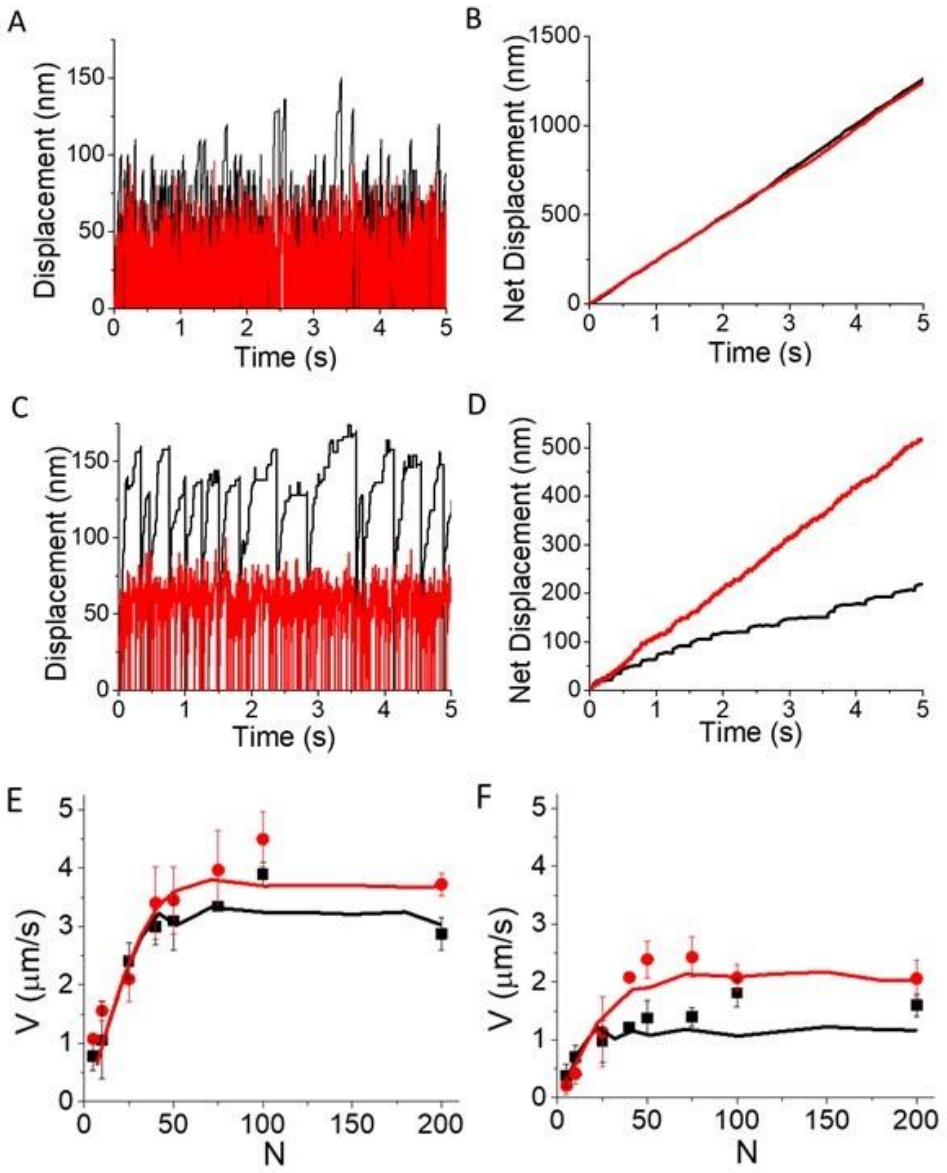


Figure 3-6: The effects of $P_i$ at high and low ADP release rates, $k_{det}$. (A) Simulated attachment-limited staircase stepping of collective displacements at high $k_{det}$ both without (black) and with (red) $P_i$ show that $P_i$ has little effect on attachment-limited stepping. (B) The net displacement of actin filaments in panel A shows that $P_i$ has little effect on *V*. (C) Simulated collective displacements at low $k_{det}$ both without (black) and with (red) added $P_i$ (red) show that both the amplitude and duration of detachment-limited stepping decreases with $P_i$. (D) The net displacements of actin in panel C show that $P_i$ accelerates *V* at low ADP release rates because step durations are decreased with the acceleration of $k_{det}$ that occurs with $P_i$ inhibition of stall force. (E) The N-dependence of *V* was measured in an in vitro motility assay at 0 (red circles) and 30 mM (black squares) added $P_i$ at pH 7.4. Computer simulation (solid lines) follow experimental values and trends. (F) The *N*-dependence of *V* was measured in an in vitro motility assay at 0 (red circles) and 30 mM (black squares) added $P_i$ at pH 6.5. Computer simulation (solid lines) follow experimental values and trends. Model parameters (Table 3-1).

Debold et al.[20] showed that ADP release rates are slowed by decreasing pH from 7.4 to 6.5 and observed that, in contrast to $P_i$-inhibition of *V* observed at low [ATP], $P_i$ activates *V* at a slow ADP release rate. A collective force model accounts for these seemingly contradictory and counterintuitive results. The simulated control experiments in Fig. 3-6A and 6B are similar to those in Figs. 3-5A and 3-5B, showing that $P_i$ has little effect on attachment-limited *V* at high [ATP] and high ADP release rates. Figure 3-6B shows that, like at low [ATP], the higher forces generated with periodic stepping at low ADP release rates are sufficient to reverse the working step in the presence of $P_i$, decreasing the stall force and *L* (Fig. 3-6C). However, unlike at low [ATP], at low ADP release rates $P_i$ also significantly decreases step durations, $\ln(N_{att})/k_{det}$ (Fig. 3-6C). Figure 3-6D shows that the $P_i$ effect on $k_{det}$ is proportionally larger than the effect on *L*, resulting in a net increase in $V = L \cdot k_{det}/\ln(N_{att})$.

The in-silico mechanism for $P_i$-induced acceleration of *V* at low ADP release rates is clear. The high stall forces generated at low ADP release rates significantly slows the force-dependent ADP release rate[22], which is rate limiting for $k_{det}$. This increases the step duration (Fig. 3-6C, black). The inhibition of stall forces by $P_i$ (decreased *L* in Fig 3-6C) dramatically increases the force-dependent $k_{det}$, decreasing the step duration in Fig. 3-6C. In short, the collective force generated by myosin heads upon $P_i$ release autoinhibits ADP release. By decreasing the collective force, $P_i$ inhibits the autoinhibition mechanism, accelerating the ADP release rate. This effect of $P_i$ is not observed in Fig. 3-5, because at low [ATP], ATP binding is rate limiting for $k_{det}$, and ATP binding is not a force dependent kinetic step.

A collective force model predicts that the above $P_i$ effects on *V* can be attenuated by decreasing the internal forces generated in a motility assay. One way to do this is to decrease *N* (Fig. 3-3). Here we used an in vitro motility assay to test the prediction that decreasing *N* attenuates the $P_i$ effect. We measured the effects of 30 mM $P_i$ on the N-dependence of *V* at pH 7.4 (Fig. 3-6E) and pH 6.5 (Fig. 3-6F). The data are accurately described by a collective force simulation (line), modeling the decrease in pH as a decrease in ADP release rates. Both the model and data show that $P_i$ activates *V* at low ADP release rates and that decreasing *N* attenuates this effect.

**Discussion**

Models of collective force generation differ from models of independent force generation in the scale at which a mechanical state is defined. Independent force generator models treat a single myosin head as a thermodynamic system within which forces equilibrate[20] and thus assume the mechanical state (Fig. 3-2A, x) is well defined at the level of a single myosin head. Collective force models treat the protein complex consisting of actin filaments and many myosin molecules as the thermodynamic system within forces equilibrate, and thus assume that the mechanical state of this macromolecular complex (Fig. 3-2B, x) is well-defined only at the level of the complex[40,41,42]. In other words, rather than defining a network of mechanical springs that are independently stretched by actin-myosin force generating events, a single equivalent spring is defined that is collectively stretched by actin-myosin force generating events.

Here we have shown that computer simulations based on a collective force model using well-established actin-myosin kinetics and mechanics (Fig. 3-1) accurately describe single molecule mechanical events (Fig. 3-3A), small ensemble stochastic staircase stepping (Fig. 3-3B), and the more periodic steps (Fig. 3-3C) reported in the literature with increasing *N*. The transition from the stochastic step durations of single molecules (Fig. 3-3A) to the more periodic collective steps of many myosin molecules (Fig. 3-3C) is characteristic of collective force generation. The mechanistic differences between stochastic stepping (Fig. 3-3B) and periodic stepping (Fig. 3-3C) and the factors that influence the transition between them is of particular interest.

Stochastic “staircase” stepping (Fig. 3-3B) results from collective displacements of the system spring by sequential myosin steps at a rate $V_{att} = N \cdot d \cdot v$. This stepping does

not reach a stall force and has broadly distributed run durations and amplitudes because actin-bound myosin heads all detach from actin before a stall force is reached.

Periodic stepping (Fig. 3-3C) occurs when the effective system spring is collectively displaced by sequential myosin steps with the force generated in the spring, $F = \kappa \cdot x$, progressively slowing $v(F)$ until the net flux through the working step and forward actin movement stall (the plateau of the step). This stall force is maintained by actin bound myosin heads for a duration, $\ln(N_{att})/k_{det}$ that is force-dependent when limited by ADP release and not force-dependent when limited by ATP binding (at low [ATP]). This is key to understanding the opposite effects of $P_i$ on $V$ at low [ATP] versus low ADP release rates. When $k_{det}$ limits $V$, $P_i$ inhibition of stall force accelerates $k_{det}$ and $V$ when limited by ADP release but does not accelerate $k_{det}$ when limited by ATP binding.

The assumption that $V$ is the sum of myosin mechanical steps is common to both independent force (Fig. 3-2A) and collective force (Fig. 3-2B) models. In both models, forces are generated (springs are stretched) by individual myosin steps even during unloaded actin sliding (Figs. 3-2A and 3-2B). In independent force generator models of $V$ a spring localized to the force-generating myosin is stretched, generating force, and that force is subsequently balanced against resistive forces in other actin-bound myosin. The detachment of resistive myosin heads allows actin to move at a detachment-limited rate[43]. The same basic argument holds for a collective force model, only the spring in this case is not localized to the force-generating myosin head but is instead a single effective system spring stretched directly by the discrete steps of individual myosin heads. In this case, the effective spring (Fig. 3-2B) is intermolecular[15], and multiple collective steps generate force (Fig. 3-3) within the filament system during unloaded shortening. Forward

progress is not lost when the intra filament force is dissipated, which for internal loads in a motility assay occurs when all but one myosin head detaches from actin.

Stochastic stepping (Fig. 3-3B) is favored when there is a low probability, *P*, that myosin heads reach an intra filament stall force before detaching from actin. Because stochastic stepping occurs at an average velocity, $V_{att} = N \cdot v \cdot d$, actin sliding velocities under these conditions are attachment-limited[13,14,17,44]. Stochastic stepping is strain dependent because *v* is limited by $k_{att}$, which is strain dependent.

Periodic stepping (Fig. 3-3C) is favored when *P* is high, which occurs at high $k_{att}$, low $k_{det}$ (Fig. 3-4), and high *N* (Fig. 3-3). Because periodic stepping includes a period over which *v* is stalled by actin-attached myosin heads (Figs. 3-2B and 3-3C), the time it takes for these myosin heads to detach from actin, $\ln(N_{att})/k_{det}$, limits actin sliding velocities, and thus actin sliding velocities under these conditions are near the detachment limit[9,15,43].

Figure 3-4 shows that decreasing $k_{det}$ by either decreasing [ATP] or slowing the ADP release rate shifts myosin stepping from stochastic to periodic, resulting in a transition from attachment- to detachment-limited *V*. We had previously postulated this transition based on in vitro motility studies showing that detachment-limited *V* at low [ATP] transitioned toward a "hypermotile", attachment-limited *V* at high [ATP][15]. We showed that this "hypermotile" state was associated with lower internal forces indicated by decreased actin filament breaking rates[19]. And we recently observed that the hypermotile, attachment-limited *V* in filament-filament sliding assays is made more pronounced by the myosin S2 tether[17]. Under physiological conditions, actin sliding velocities appear to be

largely attachment-limited[14,15,17], and in a standard in vitro motility assay, *V* is approximately 40% limited by detachment kinetics (*P* = 0.4).

The above statistical arguments for weighting attachment versus detachment components of *V* resemble the approach we used recently to develop a collective movement (no force) model of *V* for tethered myosin[17]. In this model, *L* in Fig. 3-2B is determined by a fixed myosin tether (i.e., the S2 domain) that allows unfettered attachment-limited actin movement while a myosin is bound to actin up until that myosin reaches the end of its tether at which point movement discretely stops. This discretized version of the collective force model presented herein provided a useful approximation for developing a simple analytical expression to account for filament-filament velocities that exceed the detachment limit[16,17]. However, compliance and force in filaments are not discretized as infinite or zero as assumed in this model, and while non-linear compliance can certainly influence *L*, *L* is not strictly defined by the fixed length of a structural tether any more than it is strictly defined by the relatively fixed displacement, *d*, generated by the structural change of a myosin head. A myosin tether model with a structurally defined *L* cannot account for observations such as the $P_i$ effects on *V* in Figs. 3-5 and 3-6, which require that *L* varies proportionally with stall force and is $P_i$ dependent (e.g., Figs. 3-4A, 3-4C, 3-5C, 3-6C).

The independent force generator model describes *V* as a sum of mechanical steps over time (Fig. 3-2A); however, these steps differ fundamentally from the steps in a collective force model (Fig. 3-2B). In the independent force generator model, the step displacement, *d*, is generated by a conformational change of a single myosin head that is thought to be relatively discrete and constant independent of experimental conditions,

which like a fixed *L* in a myosin-tether model (above), renders the model unable to easily account for the effects of $P_i$ on *V* (Figs. 3-5 and 3-6).

The inhibitory effects of $P_i$ at low [ATP] are accounted for by the simulations in Fig. 3-5. As we previously postulated[15,19], at low [ATP] the internal mechanical "driving force" associated with a detachment-limited *V* is inhibited by $P_i$ in the same way that $P_i$ inhibits isometric force[39], resulting in a decrease in *L* and thus *V*. The $P_i$-induced decrease in force at low [ATP] does not affect the step duration because $k_{det}$ is limited by ATP binding which is not force-dependent.

The activating effects of $P_i$ at low ADP release rates are accounted for by the simulations in Fig. 3-6. Similar to low [ATP], $P_i$ inhibits internal forces and decreases *L* at low ADP release rates However, the predominant impact of $P_i$ on *V* comes from the dramatic decrease in step durations. At low ADP release rates, $k_{det}$ is limited by ADP release which is force dependent. The $P_i$-induced decrease in force thus accelerates the ADP release rate, which shortens $k_{det}$, resulting in a net increase in *V*. This is an allosteric mechanism whereby $P_i$ inhibits the autoinhibition of ADP release by inhibiting the internal forces collectively generated by myosin. This mechanism resembles fingers autoinhibited from sliding out of a finger trap, which are then subsequently allowed to slide by inhibiting the force of the trap. This type of allosteric regulation of ADP release has been previously proposed for processive motors and muscle myosin[12,45].

This model is further supported by our measurements of the *N*-dependence of *V* at pH 7.4 (Fig. 3-6E) and pH 6.5 (Fig. 3-6F). Figure 3-3 shows that decreasing *N* results in a shift from a high internal force, near detachment-limited *V* to low internal force, attachment-limited *V*, suggesting that the force-dependent mechanism for acceleration of *V* by

$P_i$ should diminish with decreasing *N*. Our data and corresponding computer simulations show that the $P_i$ effect is attenuated at low *N* because the internal force is no longer sufficient to autoinhibit ADP release or reverse the working step.

Under physiological conditions, unloaded shortening velocities tend to be attachment-limited[17], and so it is unlikely that $P_i$-induced acceleration or inhibition of a detachment-limited *V* has physiological relevance. However, the collective force model that accounts for these data in general has significant implications for muscle contraction because it represents an entirely new way of understanding muscle chemistry and mechanics.

Table 3-1: Model Parameters

| **Parameter** | **Units** | **Fig 3-3** | **Fig 3-4A 3-4B** | **Fig 3-4C 3-4D** | **Fig 3-5A 3-5B** | **Fig 3-5C 3-5D** | **Fig 3-5E** | **Fig 3-6A 3-6B** | **Fig 3-6C 3-6D** | **Fig 3-6E** | **Fig 3-6F** |
|---|---|---|---|---|---|---|---|---|---|---|---|
| $k_T$, ATP binding rate | $s^{-1}$ $M^{-1}$ | 5e6 | 5e6 | 5e6 | 1e6 | 1e6 | 1e6 | 5e6 | 5e6 | 5e6 | 5e6 |
| $k_{Hydf}$, hydrolysis rate | $s^{-1}$ | 100 | 100 | 100 | 100 | 100 | 100 | 100 | 100 | 100 | 100 |
| $k_{Hydr}$, reverse hydrolysis rate | $s^{-1}$ | 10 | 10 | 10 | 10 | 10 | 10 | 10 | 10 | 10 | 10 |
| $k_{att}$, weak-to-strong binding rate | $s^{-1}$ | 30 | 30 | 30 | 60 | 60 | 60 | 30 | 30 | 60 | 30 |
| $k_{-ws}$, reverse binding | $s^{-1}$ $mM^{-1}$ | 0.01 | 0.01 | 0.01 | 0.01 and 10 | 0.01 and 10 | 0.01 and 10 | 0.01 and 10 | 0.01 and 10 | 0.01 and 10 | 0.01 and 10 |
| $k_{det}$, ADP release rate | $s^{-1}$ | 50 | 500 | 500 & 100 | 500 | 500 | 500 | 500 | 500 | 600 | 250 |
| N, number of molecules | | 50 | 50 | 50 | 50 | 50 | 50 | 50 | 50 | 50 | 50 |
| $\kappa$ , spring constant | pN/nm | 0.04 | 0.04 | 0.04 | 0.02 | 0.02 | 0.02 | 0.04 | 0.04 | 0.04 | 0.04 |
| a, work partitioning term | | 0.5 | 0.5 | 0.5 | 0.1 | 0.1 | 0.1 | 0.5 | 0.5 | 0.5 | 0.5 |
| b, work partitioning term | | 1 | 1 | 1 | 1 | 1 | 1 | 1 | 1 | 1 | 1 |
| [ATP] | M | $1e^{-3}$ | $1e^{-3}$ and $1e^{-6}$ | $1e^{-3}$ | $1e^{-3}$ | $1e^{-6}$ | $1e^{-6}$ to $1e^{-3}$ | $1e^{-3}$ | $1e^{-3}$ | $1e^{-3}$ | $1e^{-3}$ |

**References**


1. Reedy, M. K., Holmes, K. C. & Tregear, R. T. Induced changes in orientation of the cross-bridges of glycerinated insect flight muscle. *Nature* **207**, 1276–80 (1965).

2. Baker, J. E., Brust-Mascher, I., Ramachandran, S., Laconte, L. E. W. & Thomas, D. D. A large and distinct rotation of the myosin light chain domain occurs upon muscle contraction. *Proc. Natl. Acad. Sci. U. S. A.* **95**, 2944–2949 (1998).

3. Molloy, J. E., Burns, J. E., Kendrick-Jones, B., Tregear, R. T. & White, D. C. S. Movement and force produced by a single myosin head. *Nature* **378**, (1995).

4. Guilford, W. H. H. *et al.* Smooth muscle and skeletal muscle myosins produce similar unitary forces and displacements in the laser trap. *Biophys. J.* **72**, 1006–21 (1997).

5. Finer, J. T., Simmons, R. M., Spudich, J. A. & others. Single myosin molecule mechanics: piconewton forces and nanometre steps. *Nature* **368**, 113–119 (1994).

6. Lymn, R. W. & Taylor, E. W. Mechanism of adenosine triphosphate hydrolysis by actomyosin. *Biochemistry* **10**, 4617–4624 (1971).

7. Goldman, Y. E. Kinetics of the actomyosin ATPase in muscle fibers. *Annu. Rev. Physiol.* **49**, 637–54 (1987).

8. Cooke, R. Actomyosin interaction in striated muscle. *Physiol. Rev.* **77**, 671–97 (1997).

9. HUXLEY, A. F. Muscle structure and theories of contraction. *Prog. Biophys. Biophys. Chem.* **7**, 255–318 (1957).

10. Baker, J. E. Free energy transduction in a chemical motor model. *J. Theor. Biol.* **228**, 467–476 (2004).

11. Hill, A. V. The heat of shortening and the dynamic constants of muscle. *Proc. R. Soc. London. Ser. B, …* **126**, 136–195 (1938).

12. Baker, J. E., Brosseau, C., Fagnant, P. & Warshaw, D. M. The unique properties of tonic smooth muscle emerge from intrinsic as well as intermolecular behaviors of myosin molecules. *J. Biol. Chem.* **278**, 28533–28539 (2003).

13. Baker, J. E. & Thomas, D. D. A thermodynamic muscle model and a chemical basis for A.V. Hill's muscle equation. *J. Muscle Res. Cell Motil.* **21**, 335–344 (2000).

14. Baker, J. E., Brosseau, C., Joel, P. B. & Warshaw, D. M. The biochemical kinetics underlying actin movement generated by one and many skeletal muscle myosin molecules. *Biophys. J.* **82**, 2134–2147 (2002).

15. Hooft, A. M., Maki, E. J., Cox, K. K. & Baker, J. E. An accelerated state of myosin-based actin motility. *Biochemistry* **46**, 3513–3520 (2007).

16. Brizendine, R. K. *et al.* Velocities of unloaded muscle filaments are not limited by drag forces imposed by myosin cross-bridges. *Proc. Natl. Acad. Sci.* 201510241 (2015) doi:10.1073/pnas.1510241112.

17. Brizendine, R. K. *et al.* A mixed-kinetic model describes unloaded velocities of smooth, skeletal, and cardiac muscle myosin filaments in vitro. *Sci. Adv.* **3**, (2017).

18. Baker, J. E. & Thomas, D. D. Thermodynamics and kinetics of a molecular motor ensemble. *Biophys. J.* **79**, 1731–6 (2000).

19. Stewart, T. J. *et al.* Actin sliding velocities are influenced by the driving forces of actin-myosin binding. *Cell. Mol. Bioeng.* **6**, 26–37 (2013).

20. Debold & Walcott_2011-Pi enhances myosin-powered actin filament velocity under acidic conditions in a motility assay.pdf.

21. Hooft, A. M., Maki, E. J., Cox, K. K. & Baker, J. E. An accelerated state of myosin-based actin motility. *Biochemistry* **46**, 3513–20 (2007).

22. Veigel, C., Molloy, J. E., Schmitz, S. & Kendrick-Jones, J. Load-dependent kinetics of force production by smooth muscle myosin measured with optical tweezers. *Nat. Cell Biol.* **5**, (2003).

23. Prochniewicz, E. *et al.* Functional, structural, and chemical changes in myosin associated with hydrogen peroxide treatment of skeletal muscle fibers. *Am. J. Physiol. Cell Physiol.* **294**, C613–C626 (2008).

24. Margossian, S. S. & Lowey, S. Preparation of myosin and its subfragments from rabbit skeletal muscle. in *Methods in Enzymology* (eds. Colowick, S. P. & Kaplan, N. O.) vol. 85 55–71 (Academic Press, 1982).

25. Pardee, J. & Spudich, J. Purification of muscle actin. *Methods Enzymol.* **85**, 164–181 (1982).

26. Smillie, L. B. Preparation and identification of alpha- and beta-tropomyosins. *Methods Enzymol.* **85 Pt B**, 234–41 (1982).

27. Potter, J. D. Preparation of troponin and its subunits. *Methods Enzymol.* **85 Pt B**, 241–63 (1982).

28. Sich, N. M. *et al.* Effects of actin-myosin kinetics on the calcium sensitivity of regulated thin filaments. *J. Biol. Chem.* **285**, 39150–39159 (2010).

29. Shi, X., Lim, J. & Ha, T. Acidification of the oxygen scavenging system in single-molecule fluorescence studies: in situ sensing with a ratiometric dual-emission probe. *Anal. Chem.* **82**, 6132–6138 (2010).

30. Harris, D. E. & Warshaw, D. M. Smooth and skeletal muscle myosin both exhibit low duty cycles at zero load in vitro. *J. Biol. Chem.* **268**, 14764–8 (1993).

31. Hille, B. Ionic channels of Excitable Membranes 2nd edition. *Journal of The Electrochemical Society* (1987).

32. Kad, N. M., Kim, S., Warshaw, D. M., VanBuren, P. & Baker, J. E. Single-myosin crossbridge interactions with actin filaments regulated by troponin-tropomyosin. *Proc. Natl. Acad. Sci. U. S. A.* **102**, 16990–16995 (2005).

33. Debold, E. P. *et al.* Hypertrophic and dilated cardiomyopathy mutations differentially affect the molecular force generation of mouse alpha-cardiac myosin in the laser trap assay. *Am. J. Physiol. Heart Circ. Physiol.* **293**, H284-91 (2007).

34. Kaya, M., Tani, Y., Washio, T., Hisada, T. & Higuchi, H. Coordinated force generation of skeletal myosins in myofilaments through motor coupling. *Nat. Commun.* **8**, 1–13 (2017).

35. Warshaw, D. M., Desrosiers, J. M., Work, S. S. & Trybus, K. M. Effects of MgATP, MgADP, and $P_i$ on actin movement by smooth muscle myosin. *J. Biol. Chem.* **266**, 24339–43 (1991).

36. Homsher, E., Wang, F. & Sellers, J. R. Factors affecting movement of F-actin filaments propelled by skeletal muscle heavy meromyosin. *Am. J. Physiol.* **262**, C714-23 (1992).

37. Pate, E. & Cooke, R. A model of crossbridge action: the effects of ATP, ADP and $P_i$. *J. Muscle Res. Cell Motil.* **10**, 181–96 (1989).

38. Siemankowski, R. F., Wiseman, M. O. & White, H. D. ADP dissociation from actomyosin subfragment 1 is sufficiently slow to limit the unloaded shortening velocity in vertebrate muscle. *Proc. Natl. Acad. Sci. U. S. A.* **82**, 658–62 (1985).

39. Cooke, R. & Pate, E. The effects of ADP and phosphate on the contraction of muscle fibers. *Biophys. J.* **48**, 789–98 (1985).

40. Hill, T. L. *Free Energy Transduction and Biochemical Cycle Kinetics*. (Springer-Verlag, 1989).

41. Baker, J. E. Free energy transduction in a chemical motor model. *J. Theor. Biol.* **228**, (2004).

42. Baker, J. E., Brust-Mascher, I., LaConte, L. E. W. & Thomas, D. D. Mechano-chemical coupling in muscle. *Biophysical Journal* vol. 78 (2000).

43. How_molecular_motors_work.pdf.

44. Bárány, M. ATPase activity of myosin correlated with speed of muscle shortening. *J. Gen. Physiol.* **50**, Suppl:197-218 (1967).

45. Baker, J. E. *et al.* Myosin V processivity: Multiple kinetic pathways for head-to-head coordination. *Proc. Natl. Acad. Sci. U. S. A.* **101**, 5542–5546 (2004).

## Chapter 4

### Thermodynamics and Kinetics of a Binary Mechanical System: Mechanisms of Force Generation and Beating Patterns.

V. Murthy, J.E. Baker

**Abstract**

With relevance to various biological systems involving proteins, here we have conducted explorative study using statistical mechanics to understand emergent behaviors with muscle as an example. Individual myosin motors in muscle function as molecular mechanical switches. Specifically, a myosin conformational change induced by actin binding displaces elements external to the motor to generate force and movement. As such, an ensemble of myosin motors functions as a binary mechanical system. A binary mechanical model was recently developed that accounts for many mechanical and energetic aspects of muscle contraction such as the muscle force-velocity relationship, muscle work loops (cardiac pressure-volume loops), and muscle force transients following a rapid chemical or mechanical perturbation. In all cases, the chemo mechanical behaviors of muscle are described by adiabatic and isothermal thermodynamic processes that emerge from a single molecular mechanism. Here, based on a binary mechanical model, we develop discrete state simulations of stochastic force generation in a muscle held at a constant length. In particular, we focus on non-ideal behaviors, equilibrium and non-equilibrium conditions, and periodic force generation to define different phases of force generation. This research provides new insights into the chemistry underlying muscle force generation in normal and disease states. The chapter is concluded by proposing further investigations and experiments to deepen our knowledge of force generation dynamics in biological systems.

**Introduction**

I have already established that muscles are a complex and dynamic macromolecular system in chapter 1 of this dissertation. I have mentioned where the muscle field is right now in terms of understanding models of muscle contraction and this chapter aims to show simulation results to account for the development of thermodynamic model of muscle contraction. The model requires a new formulation of reaction free energy in terms of system entropies instead of chemical activities, implying a novel entropic kinetic theory and enabling the development of the first explicit solution to the ensemble mechanochemistry.

All the simulations that follow this chapter are based on the two state mechanochemical transitions (Fig. 4-1A) and we refer to the force generation and phases of force generation to understand the thermodynamics and kinetics in the binary system. Specifically, strong actin binding to myosin is gated by inorganic phosphate, $P_i$, release (MDP to AMD) and induces a conformation change in myosin that displaces the actin filament a distance 8 nm[4,7,8,9] . This conformational change (a large and distinct rotation of the myosin lever arm) displaces elements external to the myosin motor, generating force if those elements are elastic[10,11,7,4,12]. The question remains, how is this simple two-state binding mechanism (Fig. 4-1A) related to the chemistry and mechanics of muscle contraction?

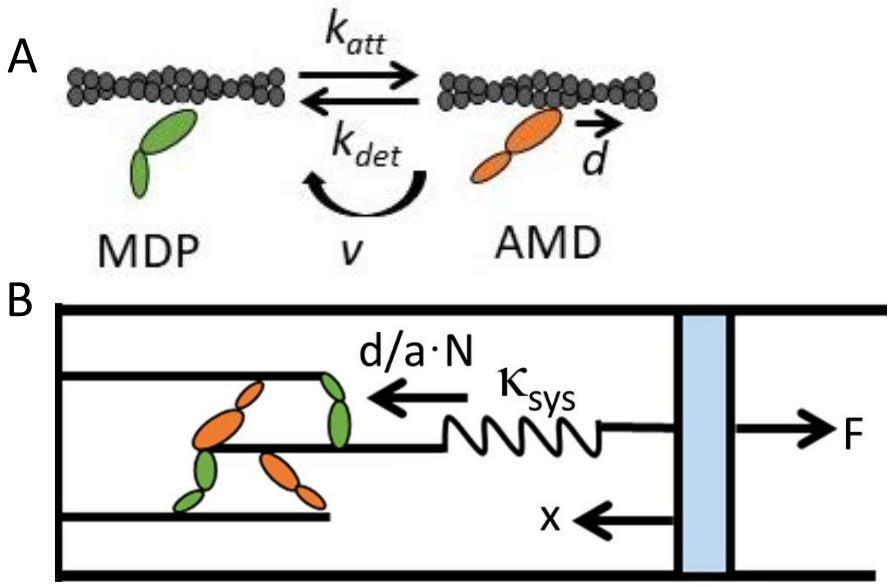


Figure 4-1: Binary mechanical model system. (A) Two-state (MDP and AMD) scheme in which a single motor (ovals) undergoes a discrete conformational change upon binding to a track (black helix; actin), generating a displacement, *d*, at a rate $k_{att}$ (MDP to AMD). The reverse transition occurs at a rate $k_{det}$ (AMD to MDP). Motors can be irreversibly detached (AM to M) through an active (ATP-dependent) process that occurs at a rate *v*. (B) If a single system spring with stiffness $\kappa_{sys}$ equilibrates with the surroundings, *F* determines the distribution of states between MDP and AMD. If force generation either occurs against a fixed length (no movement, *x*, of the blue bar) or occurs much more rapidly than the spring equilibrates with the surroundings, *F* is mechanistically determined by working steps that displace the system spring an effective distance, $d/(a \cdot N)$.

In 1938, A.V. Hill[9] proposed a thermodynamic model of muscle contraction. In 1957, Huxley[1] proposed a molecular mechanic model of muscle contraction that violated the principles of thermodynamics, which is why in 1971 T.L. Hill[13,14,15] was compelled to formalize a new kind of molecular (not ensemble) mechanochemistry. These two theories are fundamentally different. A.V. Hill's model is based on chemical thermodynamics developed by Gibbs. Huxley's model is based on a corpuscular mechanic philosophy proposed by Boyle[16] in the 17th century that has since widely been dismissed as an obsolete scientific idea[17].

An ensemble of molecular mechanical switches constitutes a binary mechanical system – a model that while analogous to classical quantum spin systems was only recently developed. This model accounts for most chemical and mechanical aspects of muscle contraction such as the steady state force-velocity relationship, work loops (e.g., cardiac pressure-volume loops), and the four phases of a force transient following a rapid mechanical or chemical perturbation of muscle.

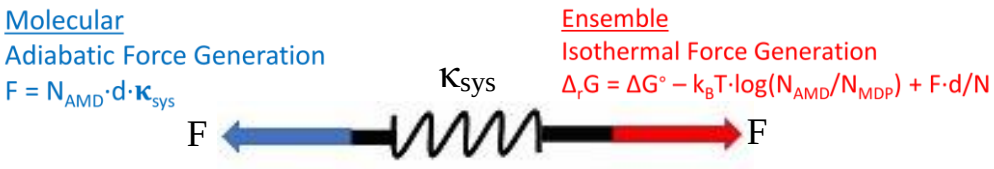


Figure 4-2: Thermodynamic System spring bridges the gap between molecular force generation and Gibbs free energy for binding. $\kappa_{sys}$ is the system stiffness. The spring generates molecular force on its left side when right side of the spring is held constant. Ensemble force generation for Gibbs free energy binding is on the right side of the spring.

Gibbs described thermodynamics as the mechanical laws of a macroscopic system of particles as measured by an observer, not the mechanical laws of thermally fluctuating particles as conjured by a corpuscularian. We have shown that the laws of mechanics of muscle can be described by a single system spring held at a force, *F*. One side of the spring (Fig. 4-2, right red arrow) describes the macroscopic state (force and length) of muscle, while the other side of the spring (Fig. 4-2, left blue arrow) is collectively stretched by myosin motor binding events. When muscle is held at a fixed length (right side of spring), molecular force generation (left side of spring) occurs adiabatically and is described by a simple linear force equation. When the muscle system is at equilibrium, the system force (right side of the spring) is described by the Gibbs free energy equation

for binding. Under one or the other of these idealized conditions, muscle force generation follows one or the other of these thermodynamic pathways (equations in Fig. 4-2). Under non-ideal conditions, muscle force generation is intermediate between these two pathways.

In all cases, mathematical models describe smooth trajectories that do not reflect the stochasticity of molecular motor mechanochemistry. More importantly, mathematical models will never reveal the emergent stochastic mechanics of the muscle system. Therefore, here we develop discrete chemical simulations of muscle force generation based on a binary mechanical model. We show that under ideal conditions (adiabatic or isothermal) simulated force generation follows on average one or the other of the ideal thermodynamic pathways and under non-ideal conditions force generation is intermediate between these pathways. A single muscle force transient explores different thermodynamic pathways over time where each pathway (adiabatic, isothermal, or intermediate) is a different thermodynamic phase of a transient. We perform simulations under a wide range of conditions, and the differences observed in the complexity of each transient is remarkable considering they all emerge from a single molecular mechanism.

Under certain conditions, these simulations exhibit stochastic, periodic force generation resembling spontaneous oscillatory contractions[16,18] (SPOCs) observed under certain conditions in active muscle and small myosin motor ensembles. The mechanism for periodic force generation becomes clear when the simulations are overlaid with the ideal thermodynamic processes. Periodic force generation occurs through a time series of four phases: adiabatic force generation, isentropic force generation, and isothermal force

generation, ending with a catastrophic (dissipative) relaxation of force. Interestingly, periodic force generation exhibits a bifurcation between beating behaviors having relatively constant periodicity and amplitude and beating behaviors having stochastic periodicity and amplitudes depending on the conditions. Again, the mechanism for this bifurcation becomes clear when simulations are overlaid with the ideal thermodynamic processes.

The findings of our investigation shed light on the kinetics of force generation by various myosins as well as the function of ATP turnover in these processes. When a few myosins are interacting with the actin filament, we observe staircase stepping, which is basically single myosins stacked up on each other or summed together to generate force (even here, the behaviors are stochastic in nature). This stepping does not reach a stall force and has broadly-distributed run durations and amplitudes because actin-bound myosin heads all detach from actin before a stall force is reached.

The adiabatic phase, which is characterized by a quick increase in force, is a classical molecular mechanic model where force increases linearly with the number of bound heads. The isothermal phase characterized by a slow increase in force, is a thermodynamic force generation where force increases with a decrease in the number of bound heads (due to entropic force) are the two separate phases of force generation. When all myosins but the final one detaches, a catastrophic shortening event takes place. Interesting complex behaviors emerge when the number of myosins is increased and when the ensemble of myosins generates force; the emergent behaviors are no longer stochastic, rather it creates an order out of disorder (a rhythmic beating is observed). This

type of behavior is observed in cardiac muscle, where the cardiac muscle functions without futile ATP turnover.

Rhythmic force generation emerges from our stochastic computer simulation. The periodicity of these mechanical contractions resembles that of cardiac and phasic smooth muscle contractions with clear implications for muscle efficiency. The relevance of this study can be applied to SPOCs (Spontaneous Oscillatory Contractions)[19] and for non-muscle myosin beating during development.

The effects of system spring stiffness on force generation are twofold: when the system stiffness is low, it gives rise to regular periodic beating with similar amplitudes and beating frequency; when the system stiffness is higher, it gives rise to stochastic beating patterns with irregular amplitude and beating frequency. ATP is crucial in regulating the force generating dynamics, higher ATPase rate is directly related to higher energy utilization and enhanced force generation. Myosin density affects force generation dynamics in that higher the number of myosin, the higher the force generation and periodic behavior, and low numbers of myosin lead to stochastic beating. The findings highlight how crucial myosin coordination, population size, and ATP turnover are for effective force production. These discoveries improve our knowledge of how motor proteins behave and have ramifications for a number of biological processes that depend on motor protein activity.

**Methods**

The computer simulations in this chapter are based on the actin-myosin ATPase kinetic scheme, as shown in Figure 4-1A. All forward and reverse rate constants were set to values that match experimental measurements on skeletal muscle myosin[3, 2, 5, 4, 20, 10, 21]. In the simulations, a single elastic element with a stiffness $\kappa_{sys}$ was collectively displaced by all myosin heads. Each actin-myosin binding step results in an 8 nm displacement of that element[5] at a rate determined by the kinetics of the binding reaction. Based on this simple kinetic scheme, Monte Carlo stochastic modeling with a time step of 1 $\mu s$ were simulated to generate chemical and mechanical transients. In a Monte Carlo simulation with each μs time step, kinetic rate constants which are dynamically changing within the reaction cycle are compared to a random number to determine whether a molecular transition occurs.

Strain dependent kinetics were incorporated into the model by multiplying the unloaded rate constants for the two mechanical steps by the Boltzmann factor, $exp^{(-w/kBT)}$, where $w$ is the work performed by displacing the elastic element, $k_B$ is the Boltzmann constant, and $T$ is temperature. When myosins make a transition from MDP to AMD state, attachment occurs by forming cross-bridge at the rate of $k_{att}$, upon attachment, a discrete lever arm rotation associated with a displacement ($d/a*N$) takes place in strain-dependent manner, where '$d$' is the step size, '$a$' is the fraction of maximal force generated and '$N$' is the numbers of myosin in the cycle. Similarly, detachment of myosin from actin occurs at the rate of $k_{det}$, which is governed by the equations:

$$k_{att} = k_{att}^{o} \cdot exp^{(-w/(k_BT))} \quad \text{Eq (1)}$$

$$k_{det} = k_{det}^{o} \cdot exp^{(-w/(k_BT))} \quad \text{Eq (2)}$$

where $k_{att}^{o}$ is the unstrained attachment rate constant, w is the work done, $k_B$ is the Boltzmann constant, $T$ is the temperature in Kelvin and $k_{det}^{o}$ is the unstrained detachment rate constant.

In a two-state force-generating model, where a discrete conformational change in myosin induced by its attachment to actin leads to actin filament displacement and force generation against a compliant spring in the system, the reaction free energy is given by

$$\Delta G = \Delta G^{o} + \frac{F.d}{a.N} - k_B T \cdot ln \frac{N_{AMD}}{N_{MDP}} \qquad \text{Eq (3)}$$

where, $\Delta G$ is the free energy, $\Delta G^{o}$ is the standard free energy, where ($\Delta G^{o} = \frac{k_{\mathrm{att}}\mathrm{o}}{k_{\mathrm{det}}\mathrm{o}}$), $F$ is the force exerted, and $d$ is the step size. The variable *'a'* is an equilibration factor, which describes the extent to which the reaction is equilibrated. For an equilibrium system, $a$ = 1. At a minimum (the far from equilibrium, molecular mechanic limit), $a = \frac{1}{N}$ ($a \cdot N$ in Eq. 3 equals 1). The parameter $a$ (the extent to which the system is equilibrated) has many different outcomes because there are different mechanisms by which a system can be pulled from equilibrium and different consequences of a system being pulled from equilibrium. According to Eq. 3, the parameter $a$ can describe the numbers of myosin motors that are equilibrated, $a \cdot N$; it can describe an effective step size, $d/a$; it describes the fractional force, $a \cdot F_o$, where $F$ is the maximum isometric force generated when $a$ = 1. In our simulations we define the parameter $a$ as $a = \frac{F}{F_o}$ (fraction of the maximal force generation). In Eq. 3, $N_{MDP}$ is the number of myosins in the detached state (MDP), while $N_{AMD}$ represents the number of myosins in the attached state (AMD).

According to the fist laws of thermodynamics, adiabatic process is the process in which the system neither generates heat or loses heat. The free energy that is available in the system can be used to do work and generate force as long as the available free energy is less than zero. If there is excess of energy available, then the system release heat in order to maintain the system in equilibrium. This process can be expressed in terms of adiabatic force generation using the equation:

$$F_{adiabatic} = \sqrt{\kappa_{sys} \cdot N_{AM} \cdot \left(\frac{dFo}{N}\right)} \qquad \text{Eq (4)}$$

where, $F_{adiabatic}$ is the adiabatic force, $\kappa_{sys}$ is the stiffness of the collective system spring, $N$ is the total numbers of myosin, and $N_{AM}$ is the number of myosins in the AMD state (myosins bound), $d$ is the effective displacement, and $F_o$ is the maximal force that is generated by myosins within the system.

The isothermal process helps describe free energy distribution of the system. The isothermal reaction follows the equation:

$$F_{isothermal} = -\Delta G^{o} \frac{N \cdot a}{d_1} - k_B T \cdot ln \frac{N_{AMD}}{N_{MDP}} \cdot \frac{N \cdot a}{d_1} \qquad \text{Eq (5)}$$

where, $F_{isothermal}$ is the isothermal force, $\Delta G^{o}$ is the standard free energy. As depicted in Figure 4-1A, when a myosin molecule transitions from the biochemical state of MDP (myosin detached state) to AMD (myosin attached state), it generates force by undergoing lever arm rotation. This force causes the myosin to displace the actin filament by a step size represented as *'d/a*N'* in Fig. 4-1B and stretches the compliant element in the system that is in equilibrium with the applied force.

In the simulation, the compliant element is modeled as a spring, and it acts as the opposing force against which the myosins generate movement. The displacement, *d* of the spring represents the effective displacement and is calculated as $\frac{d}{a \cdot N}$, where '*a*' describes the number of myosins taking a step against positively strained elastic elements, and *N* represents the total numbers of myosin.

The work done in displacing the actin filament over a distance '*d*' is determined by the product of the force (*F*) and the distance (*d*), represented as *Work = Force * Distance (F*d)*. This work accounts for the energy utilized by the myosins in generating force and displacing the actin filament. By incorporating these principles into the computer simulation, we are able to simulate the behavior of the actin-myosin system and analyze the mechanical properties and forces involved in muscle contraction.

In Figure 4-1B, the cartoon showcases the coordinated movement of multiple myosin motors that work together to exert sequential forces on a system spring, denoted as $x_{sys}$. The system spring possesses an effective stiffness represented by $\kappa_{sys}$. As the motors undergo incremental steps of size '*d*', they collectively generate a system force denoted as *F*, which can be calculated as the product of $\kappa_{sys}$ and $x_{sys}$ $(F = \kappa_{sys} \cdot x_{sys})$.

**Results**

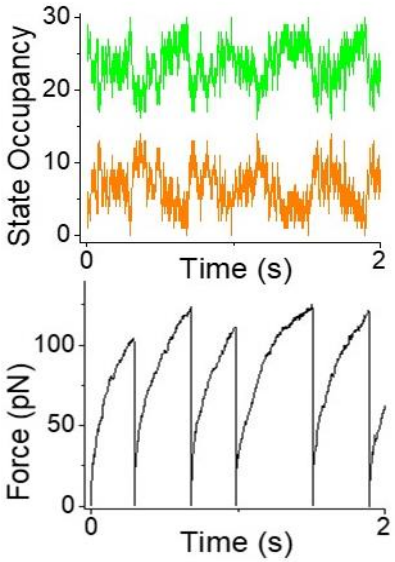


Figure 4-3: The time-dependent variations in the concentration of myosins distributed between the MDP (indicated by the green line) and AMD (indicated by the orange line) states, along with the corresponding Force Generation graph, provide evidence for the chemistry and kinetics of the actomyosin cycle. This graph visually represents the process of myosins transitioning from the detached MDP state to the attached AMD state.

A kinetic diagram of the actin-myosin ATPase reaction is shown in Figure 4-1A. Myosin (MDP) undergoes a conformational change as a result of strong binding to the actin filament (MDP to AMD) at a rate of $k_{att}$ during the process and displaces the actin filament by around 8 nm ($d_1$). The reversal of the binding (AMD to MDP) takes place at a rate of $k_{det}$ reversing the binding step, causing reversal of displacement by 8 nm. The reversal can happen as a non-force dependent transition at the rate of $v$. System force, $F$ is shown in Figure 4-1B, which is the force generated by effective displacements of myosins within the system against the system stiffness, $\kappa_{sys}$. The displacement of the system spring, $x$, while the force exerted on the spring by the surroundings is expressed

by $F = x \cdot \kappa_{sys}$. This equation describes the relationship of force generation within the system.

The chemistry of force generation is shown in the occupancy of molecules in the distributed biochemical states as shown in Figure 4-3. The state occupancy of molecules as a function of time relates to the chemistry of force generation and the color scheme is analogous to the myosins in the biochemical states (Fig. 4-1). Green lines in the state's distribution is analogous to the myosins that are unbound and orange is analogous to the myosins that are bound. Notably, force generation occurs with myosins binding to actin resulting in increase in population of bound state (AMD). Force generation as a function of time is the result of myosins pulling out the spring to generate force stochastically. This figure is helpful in understanding the basic chemistry and mechanics of muscle contraction.

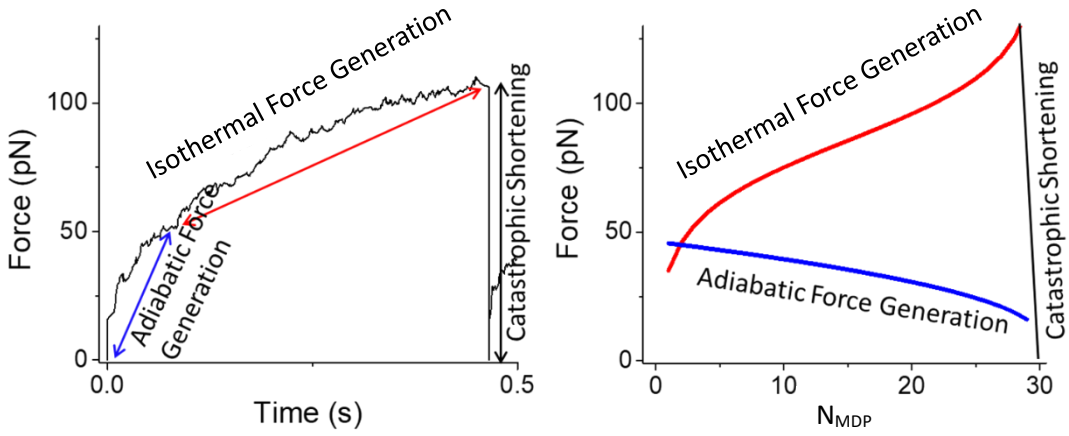


Figure 4-4: Simulations demonstrate the biochemistry of adiabatic and isothermal force generation underlying a single beat. (A) Each beat symbolizes the collective displacement of myosin heads, generating force as they sequentially move a system spring in steps of size d. This process involves adiabatic force generation, followed by isothermal force generation and catastrophic shortening. (B) Force generating loop visually depicts the sequence of adiabatic force generation, isothermal force generation, and catastrophic shortening, with the enclosed area representing the heat dissipated during these processes offering insights into the dynamic nature of myosin force generation.

When we consider a single force generating as shown in Figure 4-4A, we will be seeing three phases of thermodynamic force generation. The initial rapid force generation is the adiabatic force generation (blue arrow in Fig. 4-4A), which is the result of molecular displacements and then there is a force generation process which is the intermediate force generating trajectory before the force generation process becomes purely isothermal force (red arrow). Adiabatic forces are rapid in nature because the available free energy is -5.7 kT and the available free energy becomes gradually low, then the isothermal forces are generated when the system is at equilibrium and the available free energy is zero. The system continues to generate isothermal force despite the minimum free energy, the reason is that the system utilizes the energy from ATP

hydrolysis. This steady and gradual increase continues until the force generation is maximum and all the bound heads detach resulting in catastrophic shortening event(black arrow), where the force ultimately reaches zero. Then the cycle repeats resulting in another force generating pattern with clear thermodynamic phases.

Figure 4-4B shows the force generating loop of the force generating pattern described in Fig. 4-4A. It efficiently describes the underlying biochemistry of adiabatic and isothermal force generation with each beat. Fig. 4-2 describes the system spring and also the two ends of the spring describe molecular force generation and Gibb's free energy. These are the two different behaviors and the that essentially describes the relationship between forces and chemistry. Adiabatic forces are generated (blue line) when the molecular displacements are made to occur by holding the right side of the spring in Fig. 4-2 constant. When the molecular displacements are held constant then the force generation at the equilibrium is the free energy equation and isothermal force generation (red line). These two force generations are ideal conditions in muscle and the majority of the time muscle is a non-ideal system and muscle contraction is functioning somewhere in between these two ideal scenarios. Finally, the black line signifies the occurrence of catastrophic shortening, where all myosins are detached, leading to a force drop to zero. Then the cycle repeats by generating another force loop and the area inside the force generating loop signifies the heat dissipated during the process.

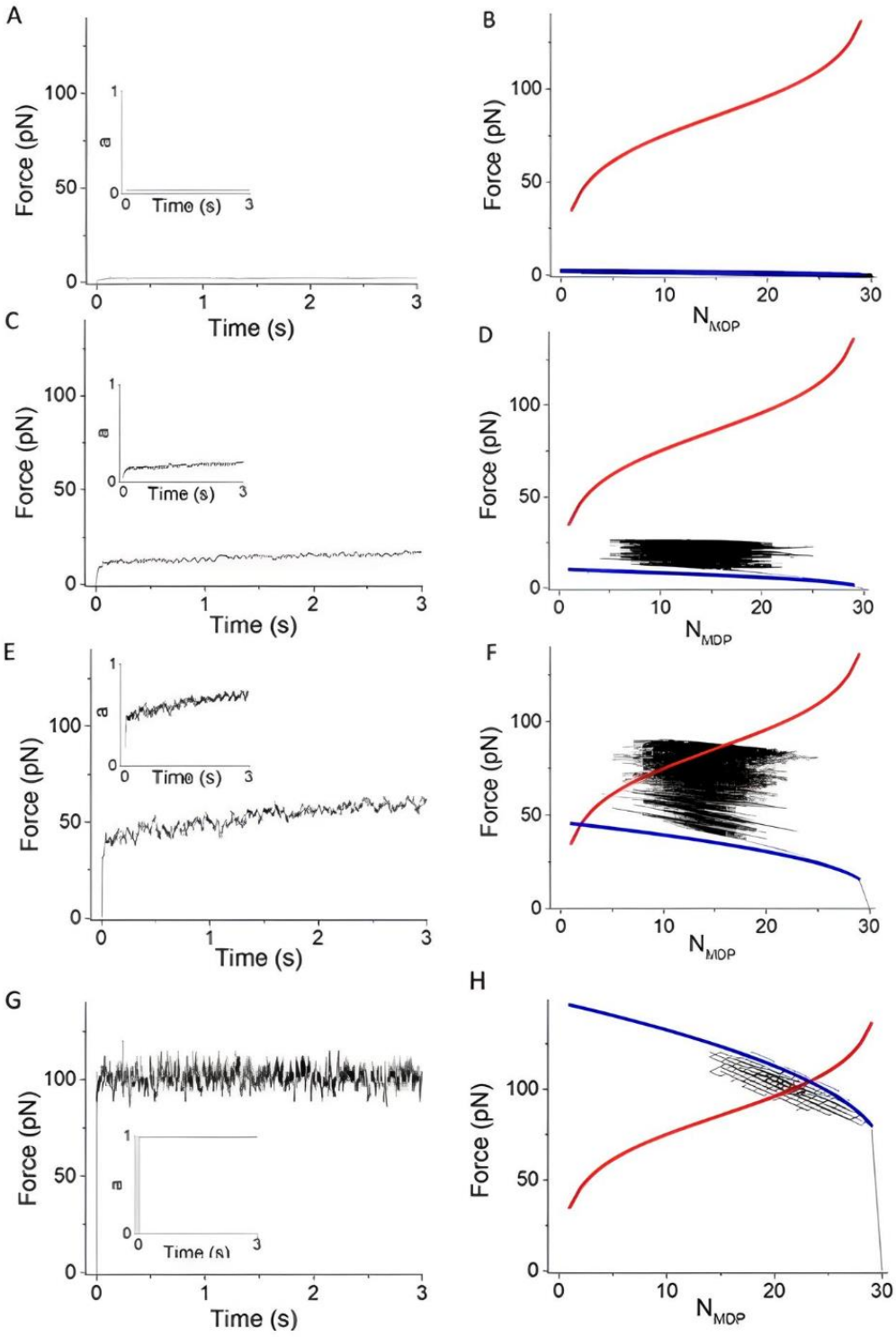
A
B
C
D
E
F
G
H
Force (pN)
Time (s)
a
$N_{MDP}$

Figure 4-5: Equilibration dynamics and Force generation in binding reaction at ATPase rate (0 $s^{-1}$ ) for $N$ = 30 by varying system stiffness (A) System stiffness of 0.01 pN/nm: Investigating the impact on force generation. Inset illustrates the distribution of *'a'* values over time. (B) Simulation of the force generating loop: Adiabatic force generation (blue line) and isometric force generation (red line) (C) System stiffness of 0.16 pN/nm: Examining force generation patterns. Inset displays the distribution of 'a' values over time (D) Simulation of the force generating loop: Adiabatic force generation (blue line) and isometric force generation (red line) (E) System stiffness of 2 pN/nm: Analyzing force generation characteristics. Inset depicts the distribution of *'a'* values over time (F) Simulation of the force generating loop: Adiabatic force generation (blue line) and isometric force generation (red line) (G) System stiffness of 10 pN/nm: Investigating force generation behavior. Inset illustrates the distribution of *'a'* values over time (H) Simulation of the force generating loop: Adiabatic force generation (blue line) and isometric force generation (red line).

Force generation dynamics of the myosins (N = 30) when the ATPase rate is absent demonstrating how the system generate forces when the system stiffness is varied is shown in Figure 4-5. Left panels in the Figure 4-5 (Figures 4-5A ($\kappa_{sys}$ = 0.01 pN/nm), 4-5C ($\kappa_{sys}$ = 0.16 pM/nm), 4-5E ($\kappa_{sys}$ = 2 pN/nm), and 4-5G ($\kappa_{sys}$ = 10 pN/nm)) shows how the forces are generated as we gradually increase system stiffness, and we know theoretically as well as demonstrated by experiments, increased stiffness results in increased force generation as the myosins have to collectively work together to overcome the stiffness and generate force in order to displace actin filaments and to do work. The right side of the panel shows the respective force generating loops for the system stiffnesses with both the adiabatic force generation (blue line) and isothermal force generation (red line). The inset within these figures demonstrates the changes in the *'a'* values, where the *'a'* value less than 1, signifies that the system chemically equilibrates with force, whereas an *'a'* value equal to 1 indicates that the system equilibrates with the maximal force.

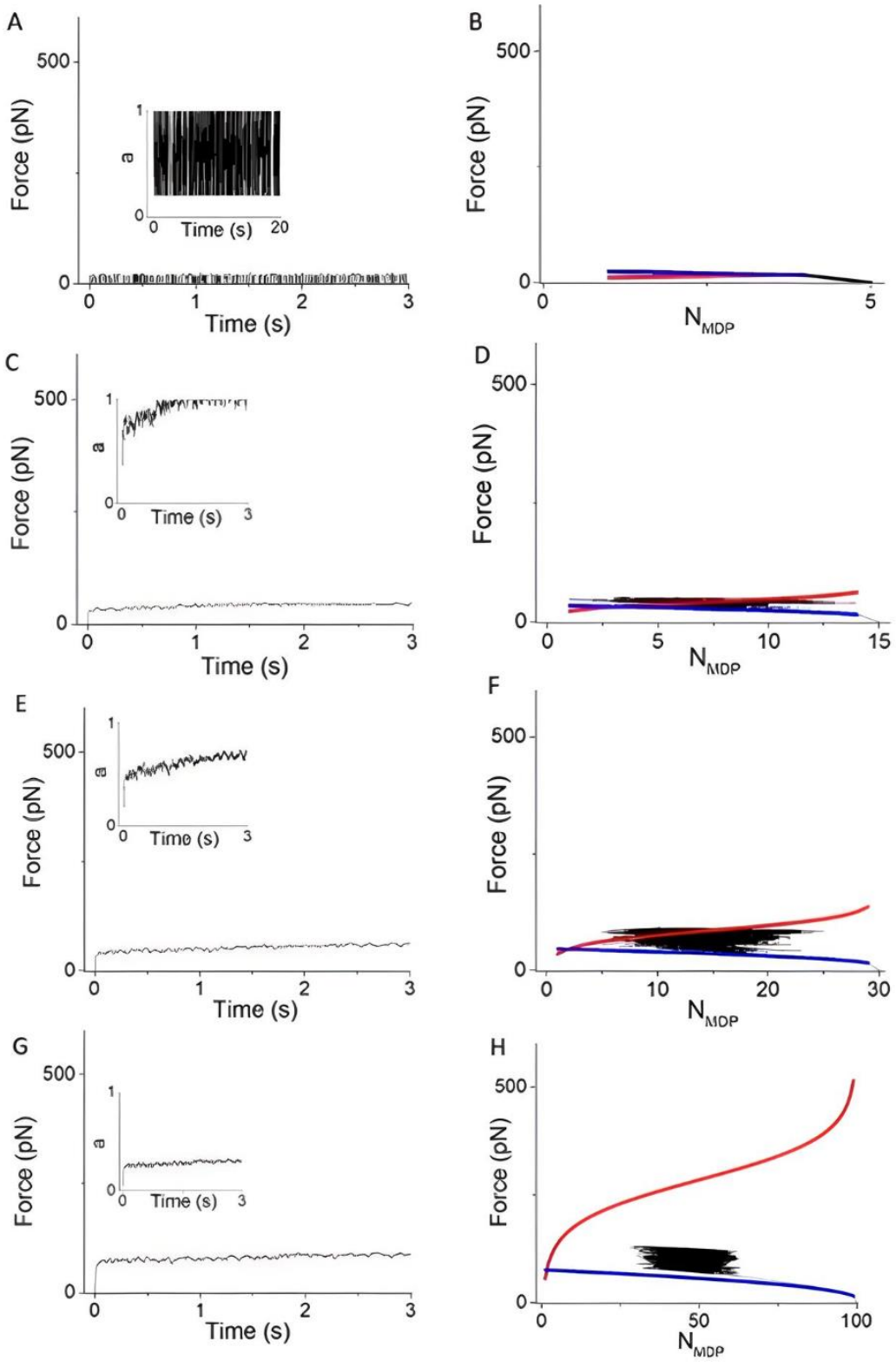
A
Force (pN)
Time (s)
a
B
Force (pN)
N_MDP
C
Force (pN)
Time (s)
D
Force (pN)
N_MDP
E
Force (pN)
Time (s)
F
Force (pN)
N_MDP
G
Force (pN)
Time (s)
H
Force (pN)
N_MDP

Figure 4-6: Investigating the equilibration of the binding reaction at an ATPase rate of 0 $s^{-1}$ and a system stiffness of 2 pN/nm, while varying the number of myosins. (A) N = 5: Analyzing force generation. Inset displays the distribution of 'a' values over time (B) Simulation of the force generating loop: Adiabatic and isometric force generation (C) N = 15: Examining force generation. Inset illustrates the distribution of 'a' values over time (D) Simulation of the force generating loop: Adiabatic and isometric force generation (E) N = 30: Investigating force generation. Inset illustrates the distribution of 'a' values over time (F) Simulation of the force generating loop: Adiabatic and isometric force generation (G) N = 100: Analyzing force generation. Inset depicts the distribution of 'a' values over time (H) Simulation of the force generating loop: Adiabatic and isometric force generation.

Force generation dynamics of the myosins when the ATPase rate is absent at the system stiffness ($\kappa_{sys}$ = 2 pN/nm) when the numbers of myosin available to generate force is varied in the system is shown in Fig 4-6. We know experimentally that by increasing the numbers of myosin results in increasing force generation, however, we want to apply these characteristics to study the interplay between force generation and the myosins in the thermodynamic model. Left panel in Fig. 4-6 ((Fig. 4-6A ($N$ = 5), 4-6C ($N$ = 15), 4-6E ($N$ = 30), and 4-6G ($N$ = 100)) shows low numbers of myosins correspond to low force generation and higher numbers of myosins correspond to higher force generation. Furthermore, we measure the *'a'* value, which characterizes the system's equilibration with force. As the number of myosins increases, the *'a'* value converges towards 1 (which is indicative of system reaching equilibrium forces with the maximal force generation). Remarkably, in the absence of ATPase rate, the *'a'* value exhibits a inverse relationship with the numbers of myosins, which suggests an intricate relationship between myosin population, equilibration dynamics, and force generation in the thermodynamic model of muscle contraction.

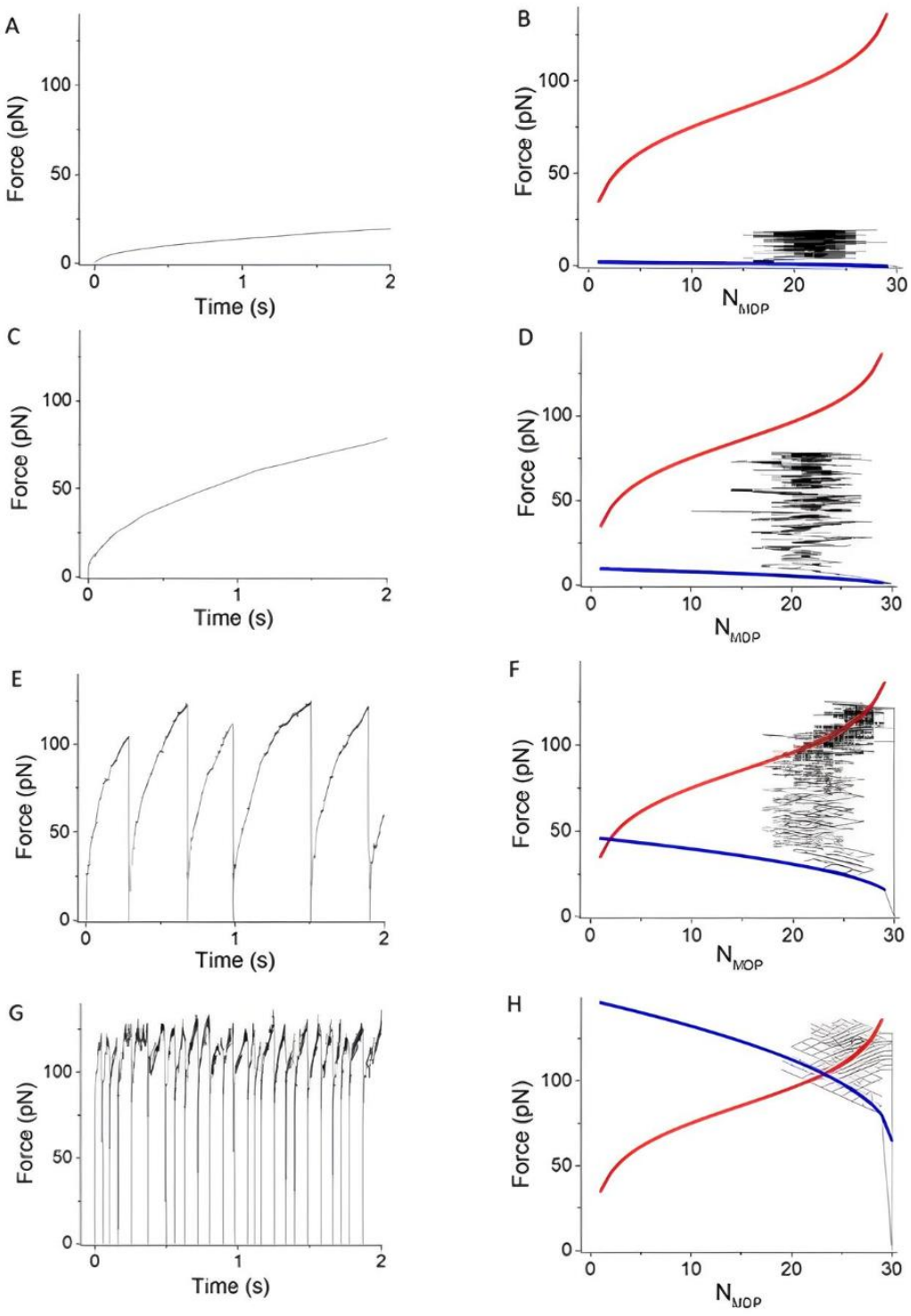
A
Force (pN)
Time (s)
B
Force (pN)
N_MOP
C
Force (pN)
Time (s)
D
Force (pN)
N_MOP
E
Force (pN)
Time (s)
F
Force (pN)
N_MOP
G
Force (pN)
Time (s)
H
Force (pN)
N_MOP

Figure 4-7: Probing Equilibration Dynamics and Force Generation in Binding Reactions at ATPase rate (50 $s^{-1}$) for N = 30 and by varying system stiffness (A) System stiffness of 0.01 pN/nm: Investigating force generation at an ATPase rate of 50 $s^{-1}$ (B) Simulation of the force generating loop: Adiabatic and isometric force generation (C) System stiffness of 0.16 pN/nm: Examining force generation at an ATPase rate of 50 $s^{-1}$ (D) Simulation of the force generating loop: Adiabatic and isometric force generation (E) System stiffness of 2 pN/nm: Analyzing force generation at an ATPase rate of 50 $s^{-1}$ (F) Simulation of the force generating loop: Adiabatic and isometric force generation (G) System stiffness of 10 pN/nm: Investigating force generation at an ATPase rate of 50 $s^{-1}$ (H) Simulation of the force generating loop: Adiabatic and isometric force generation.

We investigated the force generating dynamics in the presence of ATPase rate. Figure 4-7 shows the investigation of equilibration dynamics of force generation of the binding reaction at ($N$ = 30), with the ATPase rate (50 $s^{-1}$) and varying system stiffness ($\kappa_{sys}$). Unlike in the Fig. 4-5 and Fig. 4-6, the presence of ATPase rate results in force generating loops which help us to investigate the relationship between force generation and system stiffness in accordance with the mechanochemical cycle. Left panels in Figure 4-7 (4-7A ($\kappa_{sys}$ = 0.01 pN/nm), 4-7C ($\kappa_{sys}$ = 0.16 pM/nm), 4-7E ($\kappa_{sys}$ = 2 pN/nm), and 4-7G ($\kappa_{sys}$ = 10 pN/nm)) shows that with the increasing stiffness there is increasing force generation revealing a direct relationship between force generation and stiffness. The right panels (4-7B, 4-7D, 4-7F, and, 4-7H) shows the corresponding force generating loops with three phases of force generation in the thermodynamic model of muscle contraction; adiabatic forces (blue line), isothermal forces (red line) and catastrophic shortening (black line) which shows the underlying chemistry, energetics, work done, and heat dissipated in the system. Notably, under the presence of ATPase rate, the increase in stiffness leads to the periodic force generating steps that results in interesting beating patterns resembling rhythmic contractions. These rhythmic oscillations represents an intricate mechanochemical coupling processes underlying the binding reaction. We have to note that, the lower stiffness leads to bigger force generating loops and the periodicity

of beats are noticed. While the stiffness is being reduced, we notice a change of beating patterns to more stochastic beats and the force generating loops are much smaller.

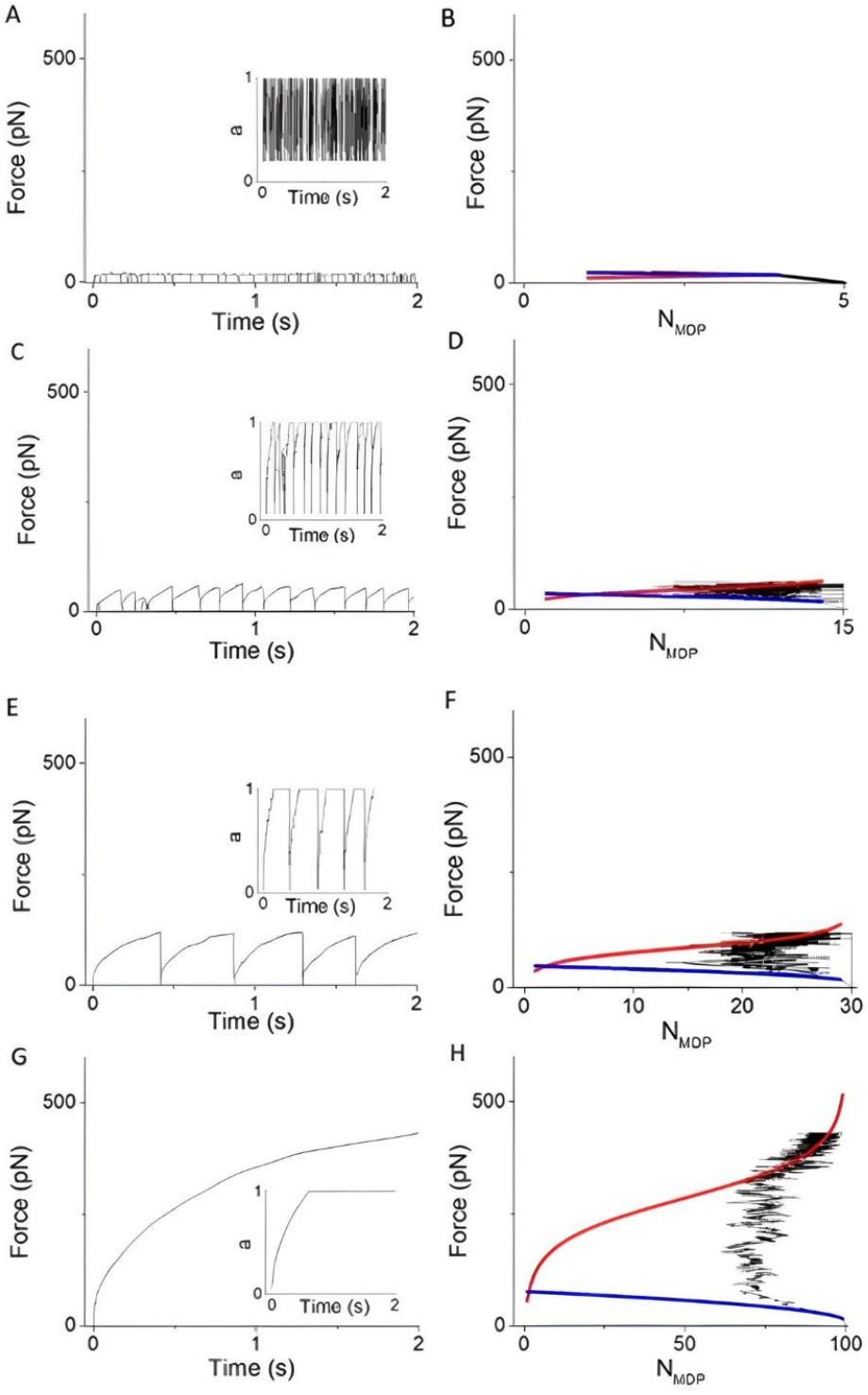
A
B
C
D
E
F
G
H
Force (pN)
Time (s)
a
$N_{MDP}$

Figure 4-8: Equilibration of the binding reaction at ATPase rate (50 $s^{-1}$) with varying numbers of myosin at system stiffness of 2 pN/nm (A) N = 5: Force generation (inset: 'a' value distribution over time) (B) Force generating loop simulation: Adiabatic force generation (blue line) and isometric force generation (red line) (C) N = 15: Force generation (inset: 'a' value distribution over time) (D) Force generating loop simulation: Adiabatic force generation (blue line) and isometric force generation (red line) (E) N = 30: Force generation (inset: 'a' value distribution over time) (F) Force generating loop simulation: Adiabatic force generation (blue line) and isometric force generation (red line) (G) N = 100: Force generation (inset: 'a' value distribution over time) (H) Force generating loop simulation: Adiabatic force generation (blue line) and isometric force generation (red line).

We continued to develop our thermodynamic model by simulating the intriguing equilibration dynamics of the binding reaction at the system stiffness ($\kappa_{sys}$ = 2 pN/nm*)* in the presence of ATPase activity (50 $s^{-1}$) by varying the numbers of myosins that are available to interact with the actin filaments. As we expected, when we increase the numbers of myosin, there was increase in force generation which insists a direct relationship between the two. Left panels in Figure 4-8 (4-8A (*N* = 5), 4-8C (*N* = 15), 4-8E (*N* = 30), and 4-8G (*N* = 100)) shows that with the increasing numbers of myosin there is increasing force generation revealing a direct relationship between force generation and numbers of myosin. The right panels (4-8B, 4-8D, 4-8F, and, 4-8H) shows the corresponding force generating loops with three phases of force generation in the thermodynamic model of muscle contraction; adiabatic forces (blue line), isothermal forces (red line) and catastrophic shortening (black line) which shows the underlying chemistry, energetics, work done, and heat dissipated in the system. Notably, under the presence of ATPase rate, the increase in numbers leads to the periodic force generating steps that results in interesting beating patterns resembling rhythmic contractions. These rhythmic oscillations represents an intricate mechanochemical coupling processes underlying the binding reaction. We have to note that, the lower numbers of myosin leads to smaller force generating loops and the stochastic beating behavior is noticed. At lower

numbers of myosin, a lower force generation is observed, however the system frequently approaches maximal force which is indicated by parameter (*'a'*) approaching 1. Interestingly, as the numbers of myosins available in the cycle increases, there is a transition from random, stochastic beats to periodic beats. This shift in behavior is accompanied by a significant increase in force generation, as shown by the larger force generating loops. This relationship indicates the existence of intricate mechanochemical coupling within the muscle system. Furthermore, the *'a'* value exhibits a continuous rise until the forces reach a maximum force, beyond which the adiabatic force equilibrates and starts generating isothermal forces, leading to the saturation of the *'a'* value at 1.

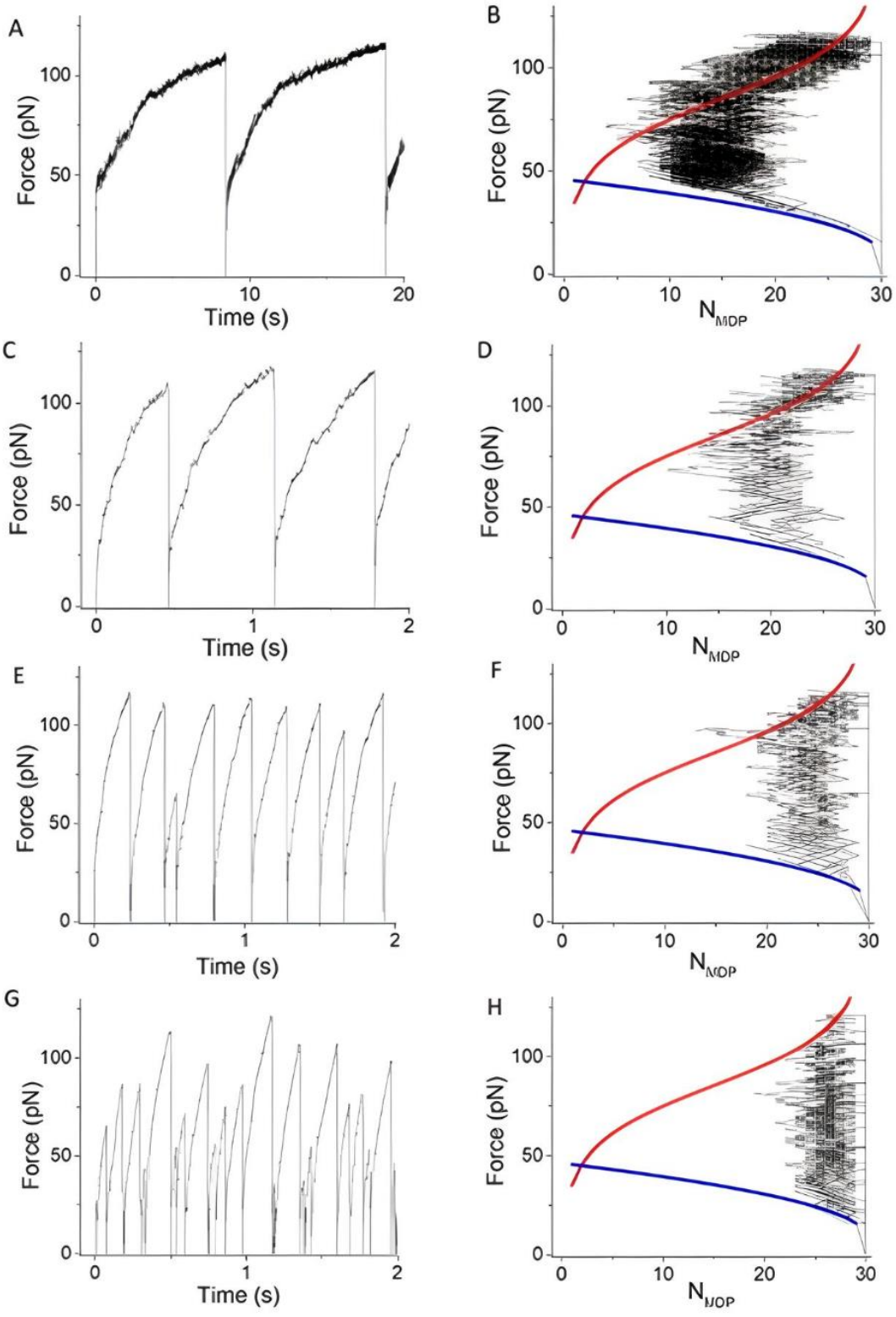
A
Force (pN)
Time (s)
B
Force (pN)
N_MDP
C
Force (pN)
Time (s)
D
Force (pN)
N_MDP
E
Force (pN)
Time (s)
F
Force (pN)
N_MDP
G
Force (pN)
Time (s)
H
Force (pN)
N_MDP

Figure 4-9: Equilibration of the binding reaction at N = 30 and system stiffness of 2 pN/nm, showcasing force generation and force generating loop analysis at varying ATPase rates. (A) Force generation at ATPase rate of 1 $s^{-1}$ (B) Force generating loop with adiabatic force generation (blue line) and isometric force generation (red line). (C) Force generation at ATPase rate of 25 $s^{-1}$ (D) Force generating loop with adiabatic force generation (blue line) and isometric force generation (red line). (E) Force generation at ATPase rate of 100 $s^{-1}$ (F) Force generating loop with adiabatic force generation (blue line) and isometric force generation (red line). (G) Force generation at ATPase rate of 200 $s^{-1}$ (H) Force generating loop with adiabatic force generation (blue line) and isometric force generation (red line).

When the presence of ATPase showed us valuable information regarding the mechanochemical chemistry and energetics, we were compelled to understand the force generating equilibrium dynamics by varying the ATPase rates at $N = 30$ and $\kappa_{sys} = 2$ pN/nm. We gradually increased the ATPase rates in Figure 4-9. The left panel of the Fig. 4-9 (Fig. 4-9A (1 $s^{-1}$), Fig. 4-9C (25 $s^{-1}$), Fig. 4-9E (100 $s^{-1}$), and Fig. 4-9G (200 $s^{-1}$) show a steady increase in force generation with the increasing ATPase rate. Right panels in the Fig. 4-9 (Fig. 4-9B, Fig. 4-9D, Fig. 4-9F, and Fig. 4-9H) illustrate the force generating loops (when force is plotted as a function of numbers of myosins bound) in correspondence with the force generation as a function of time at each ATPase rate providing insights into the energetics and efficiency of force generation by showing the phases of adiabatic force generation (blue line) and isometric force generation (red line). The force generating loops provide a relationship between ATP hydrolysis, force generation, and the equilibrium dynamics within the binding reaction. Each force generating beat exhibits a three-phase behavior: a fast adiabatic phase, a slow isothermal phase and the phases in between these two ideal scenarios. The ATPase plays a crucial role in modulating the frequency and periodicity of the beats.

**Discussion**

Myosins are involved in performing diverse biological functions such as vesicle transport, cell division, wound healing, and muscle contraction. The mechanochemistry of individual motors is well characterized in terms of molecular mechanics using the most advanced single molecule experiments; however, when many myosins work together, the force generated by a given motor equilibrates with other motors in this macromolecular assembly and not just locally within that one motor [22, 23, 24, 25, 26]. This leads to emergent mechanochemical behaviors that are described by the thermodynamics model of muscle contraction and not by molecular mechanics model of muscle contraction[27, 7]. For decades, muscle contraction has been widely modeled as a simple sum of molecular mechanics of individual myosin molecules interacting with actin filaments, where each myosin motor is assigned a system spring and the system force that is generated is simply the sum of individual forces. However, recent studies indicate that the forces generated by individual myosin heads are thermally equilibrated with the system force, which requires a thermodynamic model of muscle contraction[28,29, 26, 30].

To develop the thermodynamic model, we use the key mechanochemical steps (MDP and AMD) with key biochemical transitions. The discrete stochastic simulations are used, where myosin binds to actin, which is a key mechanical step that involves force generation, chemical step and the energetics of actin myosin strong binding that drives the force generation. The goal of the thermodynamic model is to bridge the gap between molecular mechanics and muscle mechanics.

An interesting feature of the thermodynamic model is that the stochastic simulations give rise to emergent rhythmic force generating patterns. This mechanical

phenomenon is similar to the rhythmic contractions seen in cardiac muscle and phasic smooth muscle. The observation here has implications for how effectively muscles work and the same can be used to explain phenomena like Spontaneous Oscillatory Contractions (SPOCs) and the beating of non-muscle myosin during developmental processes. Despite being simple, the thermodynamic model provided in this research accurately describes our existing understanding of myosin behavior[28, 29, 31, 32, 33, 30] and accurately describes other complex muscle behaviors like Force-Velocity relationship, transient stretch responses.

**Force Generation:** In isometric muscle, energy generated is exchanged between the system spring and its surroundings to generate system force. System springs are a depiction of a physical relationship rather than a physical description of the system. They are helpful for describing molecules' reversible alterations to force and displacement[30]. The binding of the system's motors produces mechanical forces against a system spring, and the stepping causes incremental movements represented by effective displacement ($d/a \cdot N$) (Fig 4-1A). As myosins binds to actin filaments it generates force and displaces the actin filament[9,1, 33]. In the thermodynamic model, the system spring is an effective spring which represents all compliant elements in an ensemble motor system, including those in the myosin heads that determine the relationship between force, energy, and displacement[28]. Force generation occurs in various phases. The force generated during these phases is denoted as *'F'*, while the maximal force that can be generated is represented by *'$F_o$'*, known as the maximal isothermal force. The effective displacement, *'$d/a \cdot N$ '*, is the displacement of actin filaments by individual myosin, which is divided by the product of *'a'* (the fraction of maximal force) and *'N'* (the total number of myosins).

**Adiabatic Force Generation:** The initial force generation in the force generating beating pattern is the adiabatic force generation which is due to molecular displacements of myosins. The initial increase in force is fast and it quickly transitions into intermediate pathways and this pattern arises interesting questions about the available free energy to do work and what are the underlying mechanisms for this fast force generating phase and how would the force generation affect when the ATP is absent. These questions persuade us to look into the processes of adiabatic force generation and the modulatory effect of ATP at equilibrium.

There are several ways to test the effects of ATP on adiabatic force generation. We can vary the concentration of ATP to determine force generation dynamics with respect to maximum force generated. We can conduct experiments using inhibitors like Blebbistatin which prevents ATP binding and in turn decreases velocities. We can determine adiabatic force generation and the equilibrium dynamics. Single-molecule techniques such as optical tweezers or atomic force microscopy can be used to study individual myosin behavior and provide insights into ATP-dependent transitions. Our understanding of adiabatic force generation will be improved by these targeted experiments to understand molecular mechanisms within the muscle system.

**Isothermal Force Generation:** When the ensemble myosins are generating force that is based on available Gibb's free energy under equilibrium conditions is the isothermal force generation. During adiabatic force generation, the system spring does not exchange energy with its surroundings, however, when maximal forces are reached in the isometric muscle, the system reaches a equilibrium condition with isothermal force

generation during which there is exchange of energy with the surrounding. Following adiabatic force generation and myosins continue to generate force along the isotherm, then maximal force is reached where all the myosins detach from actin and force drops to zero leading to catastrophic shortening event. This event marks the end of one force generating cycle and the process repeats for the next force generating cycle. The area enclosed within the force generating loop in this process is the heat dissipated[17].

Force generation as a function of time over a time course of 0.5 seconds is shown in Figure 4-4A. The adiabatic force generation is highlighted by the blue arrow which begins at zero force and increases quickly due to the available free energy of -5.7 *kT*. In contrast, the red arrow refers to the isothermal force generation, in which myosins gradually increase the force along the isotherm in spite of having limited available free energy. The black arrow denotes the occurrence of catastrophic shortening. Figure 4-4B is a complementary explanation of the force generating beat, this we represent the force generating phases with the force-generating loop where force is plotted as a function of myosins bound. These distinct phases of force generation gives us insights into the equilibration dynamics.

When there is no ATPase rate as shown in the figures (Fig. 4-5 and Fig 4-6), there is lack of force generating loops and the observation highlights the critical role of ATP in the force generation. By varying the system stiffness, which is a representation of a physical spring, offers us insights into high force generation when there is lower system stiffness. The emergent rhythmic beating patterns demonstrate that force generation is progressively difficult as the system stiffness increases. The beating pattern is more

periodic and regular with similar frequency of beats and amplitude of the beats are similar within a time frame which is indicative of a predictable and regular force generation. However, as the stiffness rises, the beats turn into stochastic beating pattern, with irregular amplitude and beating frequencies which indicates irregularity in the force generating behavior.

In Fig. 4-5, we observed that there was no force generating loop in the absence of ATPase rate. We therefore wanted to observe the behaviors of myosins when we vary the numbers of myosins (Fig. 4-6) in the system available to generate force in the absence of ATPase rate and its effects on force generating dynamics. In the absence of ATPase rate, there is no heat dissipation, the system does not reach its maximal force generation, as we increase the numbers of myosin, the force generation starts generating isothermal force, however, never reaches a maximal force to complete the force generating cycle. These findings highlight the importance of ATPase rate for the formation of force-generating loop and the dissipation of heat, both of which are essential components of force generation dynamics. Another finding is that that intermediate pathways between adiabatic forces and isothermal forces are populated and the distribution of myosins show that they are equally distributed in bound and unbound states. These results advance our understanding of driving mechanical forces and the relationship between mechanochemistry, force generation and ATPase rate for equilibration dynamics.

We continued our investigation for understanding the force generation beating patterns when there is ATP turnover rate (ATPase = 50 $s^{-1}$) by varying the system stiffness and numbers of myosin. Figures 4-7 and 4-8 show the outcomes of these

simulations and offer insights into how the ATP turnover rate influences the equilibration dynamics. When we gradually increased the stiffness of the system (similar to Fig. 4-5), a clear pattern emerged. When the system stiffness was lower, it generated adiabatic forces which are a result of molecular displacements. The force generation then started on the isotherm. When the ATPase rate is present, the available free energy is higher at the beginning of the cycle, this is effectively utilized to generate adiabatic forces and then the system reaches a equilibrium condition, where the energy from ATP hydrolysis is utilized to generate isothermal forces and reaches a maximum before catastrophic shortening. During these processes, there is heat dissipation and exchange of energy.

These results showed that, with the increase of system stiffness, the force generating patterns changed from regular periodic beats to a more random stochastic beat. The adiabatic forces became more quicker, and the isothermal force generation decreased, and the system was not in equilibrium conditions for a long period and these results provide correlation between mechanochemical interaction and equilibrium dynamics. Similarly, in Fig. 4-8, with the increase in numbers of myosin, the force generating patterns changed from irregular random stochastic beats to a more periodic force generating beat. The forces followed adiabatic force generation and force generation in the intermediate pathways before generating isothermal forces. Force generating patterns became more robust by transitioning from stochastic to a more periodic beat by synchronization of myosins in the binding isotherm. These results provide correlation between mechanochemical interaction, coordinated population of myosins and equilibrium dynamics.

Figure 4-9 is the explorative simulations when the available ATPase rate is varied with the system stiffness of 2 pN/nm and the numbers of myosins available to generate force is 30. This gives us the relationship of ATP hydrolysis in the force loops and the work performed and heat dissipated. When the ATPase rate was low, the force generated followed adiabatic force generation and then started generating isothermal forces. The force generating cycles were more periodic with a sustained mechanical output which used minimal available free energy from ATP hydrolysis. The bigger the force generating loop, the higher the heat dissipated. With increasing ATPase rate, we observed a smaller force generating loops and the periodicity of the beats diminished and the force generating beats became more stochastic which indicates that there is decreased heat dissipation.

The thermodynamic model of muscle contraction that we are developing will have the observations of the explorative simulations. The discoveries will have implications for biological processes involving motor proteins, that aid us to interpret mechanochemical effects of the diseases in normal states and in diseased states that involve force generation and heat dissipation.

**Conclusion**

We have been developing the thermodynamic model which has significant advancements to understand muscle contraction by considering system force, entropy, temperature and free energy available to do work. Single molecule experiments with well-established biochemical states and biochemical transitions with key mechanical steps are taken into account to develop this model. The simulations are the myosins generating force, displacing actin filaments and stretching the system spring to generate system force. We take the macroscopic force of the system into consideration and the system properties lead to the kinetics and temperature of the molecular motors which enables us to explore the force generating dynamics of the rate of binding. The chapter provides details into how adiabatic forces and isothermal forces are generated, and we simulate pathways in between these ideal conditions. Overall, our model takes into account the influence by both mechanochemical investigations of single molecules and thermodynamic principles to bridge the gap between molecular mechanics and muscle mechanics. The findings presented here act as a guiding framework for understanding chemical thermodynamics of muscle contraction by considering chemistry of force generation to the mechanism of force generation and beating patterns.

**References**


1. HUXLEY, A. F. Muscle structure and theories of contraction. *Prog. Biophys. Biophys. Chem.* **7**, 255–318 (1957).

2. Guilford, W. H. H. *et al.* Smooth muscle and skeletal muscle myosins produce similar unitary forces and displacements in the laser trap. *Biophys. J.* **72**, 1006–21 (1997).

3. Finer, J. T., Simmons, R. M., Spudich, J. A. & others. Single myosin molecule mechanics: piconewton forces and nanometre steps. *Nature* **368**, 113–119 (1994).

4. Molloy, J. E., Burns, J. E., Kendrick-Jones, B., Tregear, R. T. & White, D. C. S. Movement and force produced by a single myosin head. *Nature* **378**, (1995).

5. Lymn, R. W. & Taylor, E. W. Mechanism of Adenosine Triphosphate Hydrolysis by Actomyosin. *Biochemistry* **10**, 4617–4624 (1971).

6. Cremo, C. R. & Geeves, M. A. Interaction of actin and ADP with the head domain of smooth muscle myosin: Implications for strain-dependent ADP release in smooth muscle. *Biochemistry* **37**, 1969–1978 (1998).

7. Baker, J. E., Brosseau, C., Joel, P. B. & Warshaw, D. M. The biochemical kinetics underlying actin movement generated by one and many skeletal muscle myosin molecules. *Biophys. J.* **82**, 2134–2147 (2002).

8. White, H. D. & Taylor, E. W. Energetics and Mechanism of Actomyosin Adenosine Triphosphatase. *Biochemistry* **15**, (1976).

9. Hill, A. V. The heat of shortening and the dynamic constants of muscle. *Proc. R. Soc. London. Ser. B, …* **126**, 136–195 (1938).

10. Linari, M. *et al.* Force generation by skeletal muscle is controlled by mechanosensing in myosin filaments. *Nature* **528**, (2015).

11. Reedy, M. K., Holmes, K. C. & Tregear, R. T. Induced changes in orientation of the cross-bridges of glycerinated insect flight muscle. *Nature* **207**, 1276–80 (1965).

12. Warshaw, D. M. *et al.* The light chain binding domain of expressed smooth muscle heavy meromyosin acts as a mechanical lever. *J. Biol. Chem.* **275**, (2000).

13. Huxley, A. F. & Simmons, R. M. Proposed mechanism of force generation in striated muscle. *Nature* **233**, 533–538 (1971).

14. Huxley, A. F. Muscular contraction. *J. Physiol.* **243**, 1–43 (1974).

15. Huxley, A. F. Review Lecture : Muscular Contraction. *J. Physiol.* **243**, 1–43 (1974).

16. Boyle, R. A Defence of the Doctrine Touching the Spring and Weight of the Air. (1662).

17. Baker, J. E. Thermodynamics and Kinetics of a Binary Mechanical System: Mechanisms of Muscle Contraction. *Langmuir* **38**, 15905–15916 (2022).

18. Duke, T. A. J. Molecular model of muscle contraction. *Proc. Natl. Acad. Sci. U. S. A.* **96**, 2770–2775 (1999).

19. Harris, S. P. Making waves: A proposed new role for myosin-binding protein C in regulating oscillatory contractions in vertebrate striated muscle. *J. Gen. Physiol.* **153**, 1–16 (2020).

20. Veigel, C., Molloy, J. E., Schmitz, S. & Kendrick-Jones, J. Load-dependent kinetics of force production by smooth muscle myosin measured with optical tweezers. *Nat. Cell Biol.* **5**, (2003).

21. Kaya, M., Tani, Y., Washio, T., Hisada, T. & Higuchi, H. Coordinated force generation of skeletal myosins in myofilaments through motor coupling. *Nat. Commun.* **8**, 1–13 (2017).

22. Baker, J. E., Brosseau, C., Joel, P. B. & Warshaw, D. M. The biochemical kinetics underlying actin movement generated by one and many skeletal muscle myosin molecules. *Biophys. J.* **82**, 2134–47 (2002).

23. Baker, J. E., Brust-Mascher, I., Ramachandran, S., Laconte, L. E. W. & Thomas, D. D. A large and distinct rotation of the myosin light chain domain occurs upon muscle contraction. *Proc. Natl. Acad. Sci. U. S. A.* **95**, 2944–2949 (1998).

24. Baker, J. E., LaConte, L. E. W., Brust-Mascher, I. & Thomas, D. D. Mechanochemical coupling in spin-labeled, active, isometric muscle. *Biophys. J.* **77**, 2657–2664 (1999).

25. Baker, J. E., Brust-Mascher, I., Ramachandran, S., LaConte, L. E. & Thomas, D. D. A large and distinct rotation of the myosin light chain domain occurs upon muscle contraction. *Proc. Natl. Acad. Sci. U. S. A.* **95**, 2944–9 (1998).

26. Baker, J. E. & Thomas, D. D. Thermodynamics and kinetics of a molecular motor ensemble. *Biophys. J.* **79**, 1731–6 (2000).

27. Baker, J. E. & Thomas, D. D. A thermodynamic muscle model and a chemical basis for A.V. Hill's muscle equation. *J. Muscle Res. Cell Motil.* **21**, 335–344 (2000).

28. Baker, J. E. A chemical thermodynamic model of motor enzymes unifies chemical-Fx and powerstroke models. *Biophys. J.* **121**, 1184–1193 (2022).

29. Baker, J. E. The Work Performed By Biological Motors. *bioRxiv* (2019) doi:10.1101/580241.

30. Baker, J. E. Mechanics , Energetics , Entropy and Kinetics of a Binary Mechanical Model System.

31. Baker, J. E. & Thomas, D. D. Thermodynamics and kinetics of a molecular motor

ensemble. *Biophys. J.* **79**, 1731–1736 (2000).

32. Stewart, T. J. *et al.* Actin sliding velocities are influenced by the driving forces of actin-myosin binding. *Cell. Mol. Bioeng.* **6**, 26–37 (2013).

33. Brizendine, R. K. *et al.* Velocities of unloaded muscle filaments are not limited by drag forces imposed by myosin cross-bridges. *Proc. Natl. Acad. Sci.* 201510241 (2015) doi:10.1073/pnas.1510241112.

# Chapter 5

## Dissertation Conclusion

### Summary.

In 1999[1], Dr. Baker developed a steady state thermodynamic model of muscle contraction based on the chemical thermodynamics' foundation laid by A.V. Hill in 1938[8] and recently published the statistical mechanical version required to simulate non-equilibrium muscle force transients. Compared to the well-known molecular mechanics formalism proposed by Huxley-Hill[2,3], thermodynamic model of muscle contraction is a theory purely based on chemical thermodynamics and offers new perspective into the understanding of muscle contraction by considering system force, temperature, entropy and free energy available to do work.

Muscle is an extraordinary structure which is one of the most efficient machines on earth. We have used a combination of theory, in vitro motility experiments, and stochastic mathematical modeling to understand the workings of this complex machinery. The implications of this study will help us to answer basic mechanism of muscle contraction in normal and diseased states. We are developing a model that bridges the gap between molecular mechanics and muscle mechanics by considering system force, and chemistry of force generation to force generation dynamics. This work is about developing a simple framework for analyzing experimental data and to advance our knowledge of muscle mechanics and provide insights into muscle mechanisms by focusing on macroscopic forces.

**Chapters Summary**

Chapter 2 is focused on a combination of experiments[4], theory[5,6,7,8,2,9,10,11,12] and simulations[13] to understand the mechanisms underlying the ensemble myosin. We conducted experiments using in vitro motility assay, in which we investigated the N-dependence of actin sliding velocities, ATPase activity, force generation, and calcium sensitivity. Our results showed that the velocity and ATPase activity reaches its maximum when myosin-binding sites on actin become saturated. Interestingly, saturation of binding sites on actin is influenced by both attachment and detachment kinetics, challenging the notion of independent force generation. These findings support a chemical thermodynamic model muscle contraction by testing the hypothesis of molecular mechanics model and experimentally showing that the kinetics of force generation is not separated by the kinetics of actin binding. This chapter has provided several important results to demonstrate that the thermodynamic model is the right approach to understanding the complex mechanisms of muscle contraction.

In Chapter 3, we continued to understand the collective behaviors of myosin by investigating the effects of phosphate[14,15,16,17,18] on actin-sliding velocities. The results in chapter has experimental data and the simulation results that help us to successfully challenge the independent force generator model theory (molecular mechanisms)[2] and supports a thermodynamic model by testing the hypothesis of molecular mechanics. We have conducted experiments that offer fresh perspectives on the effects of phosphate at low ATP concentrations[19] and at low pH[20]. By incorporating a simple collective force generator model based on well-established actin-myosin kinetics and mechanics. The experimental results showing the opposing effects of phosphate is clearly explained by

the thermodynamics model. Our findings suggest that $P_i$ inhibits *V* by reducing internal forces at low [ATP], while it accelerates *V* by increasing the force-dependent, rate limiting ADP release at low pH. Furthermore, this chapter gives experimental data and simulation results to account for the velocities of actin filament which are measured as a function of numbers of myosin and demonstrates the correctness of the thermodynamic model. This chapter also shows emergent mechanical behaviors resulting from collective force generation by myosin as the rhythmic beating pattern observed during force generation, providing new insights complex behaviors exhibited by muscles.

In chapter 4, we have continued developing the thermodynamic model[21,22] by considering the key mechanical and chemical transitions in the enzymatic ATPase cycle which accounts for the energetics and mechanics of the ATPase cycle. The model is a simplified and minimal model that aligns with the well-established states in the single molecule experiments of muscles. We have considered isometric muscle and studies the adiabatic force generation, isothermal force generation and the intermediate pathways in between ideal trajectories. Force generation dynamics and the equilibration dynamics provide an intricate relationship between the ATP turnover rate, force generating mechanisms in the thermodynamic model. The simulations showing the chemistry of force generation to the system force generation help us in understanding the force loops when system stiffness, numbers of myosins are varied.

**Overall Implications**.

The work detailed in the dissertation contributes to our understanding of muscle contraction and tests the hypothesis of molecular mechanics description and provides thorough experiments and modeling data to show the necessity to interpret muscle data

by considering the thermodynamic perspective of muscle contraction. This dissertation has given a historical difference in the formalism of molecular mechanics and thermodynamics theories by providing a timeline of historical scientific events which is elaborated by Baker[21] to put the theories into historical scientific context. We know that since 1957, after Huxley proposed molecular mechanics models, almost all the models of muscle contraction till today have been following the molecular mechanics theory to explain their scientific findings and the thermodynamic models have been completely abandoned. We discovered that the 60-year-old molecular mechanics models that have dominated the field have never been accurate and are completely obsolete. We have used the knowledge of molecular mechanics of single molecules which are well established and experimentally proven in single molecule experiments like optical laser traps, chemistry of force generation by the molecules within the muscle system, muscle force that is generated as a system force, the protein interactions of actin and myosin, free energy available to do work by using Gibb's free energy equations, entropy of the system by considering the randomness of the system, temperature and used the knowledge from the most advanced technologies to develop the thermodynamic model that accounts for several experimental results and bridges the gap between different theories of muscle contraction.

This paradigm change has significant effects. We will now understand that muscle contraction as a thermodynamic system which cannot be simplified by assigning springs to molecular motors and the summation of individual forces generated by myosins do not give rise to system force, rather molecular properties give rise to system properties and the system property is the mathematical variable that is used to describe what the system

is doing, thereby offering a very unique understanding. Since myosins are widely studied as a potential drug target in treating several diseases, this framework will aid in understanding the effects of drugs on muscle function in normal and diseased states. Thermodynamic model will provide novel insights in comprehending complex muscle functions by offering fresh perspectives on investigating mechanochemical effects of muscle contraction and advancing our knowledge of muscle mechanics.

## Recommendations

### Future Directions

Our thermodynamic model of muscle contraction considers the foundation laid by A.V. Hill and applies the concept to understand muscle contraction from a thermodynamic perspective. Continuing further on the stochastic simulations, force loops and the pathways in the force loops are the next areas to investigate. Spontaneous Oscillatory Contractions are observed in the myofibrils, expanding the model, we can investigate these mechanisms by incorporating the workings of sarcomeres in myofibrils. By developing the model to incorporate other proteins to simulate the muscle, we can simulate the tension-transient experiments, stretch response experiments and other complex behaviors exhibited by muscle.

In the current model, we have not been able to fully explore the capacity of the ‘a’ parameter. In addition to carefully developing the model, it is a necessity to expand the knowledge of the ‘*a*’ (defined as the fraction of maximal force generated) parameter. This ‘*a*’ parameter will play a key role in determining heat dissipation, the equilibrium dynamics, force generation dynamics and the transition between three phases of force generation.

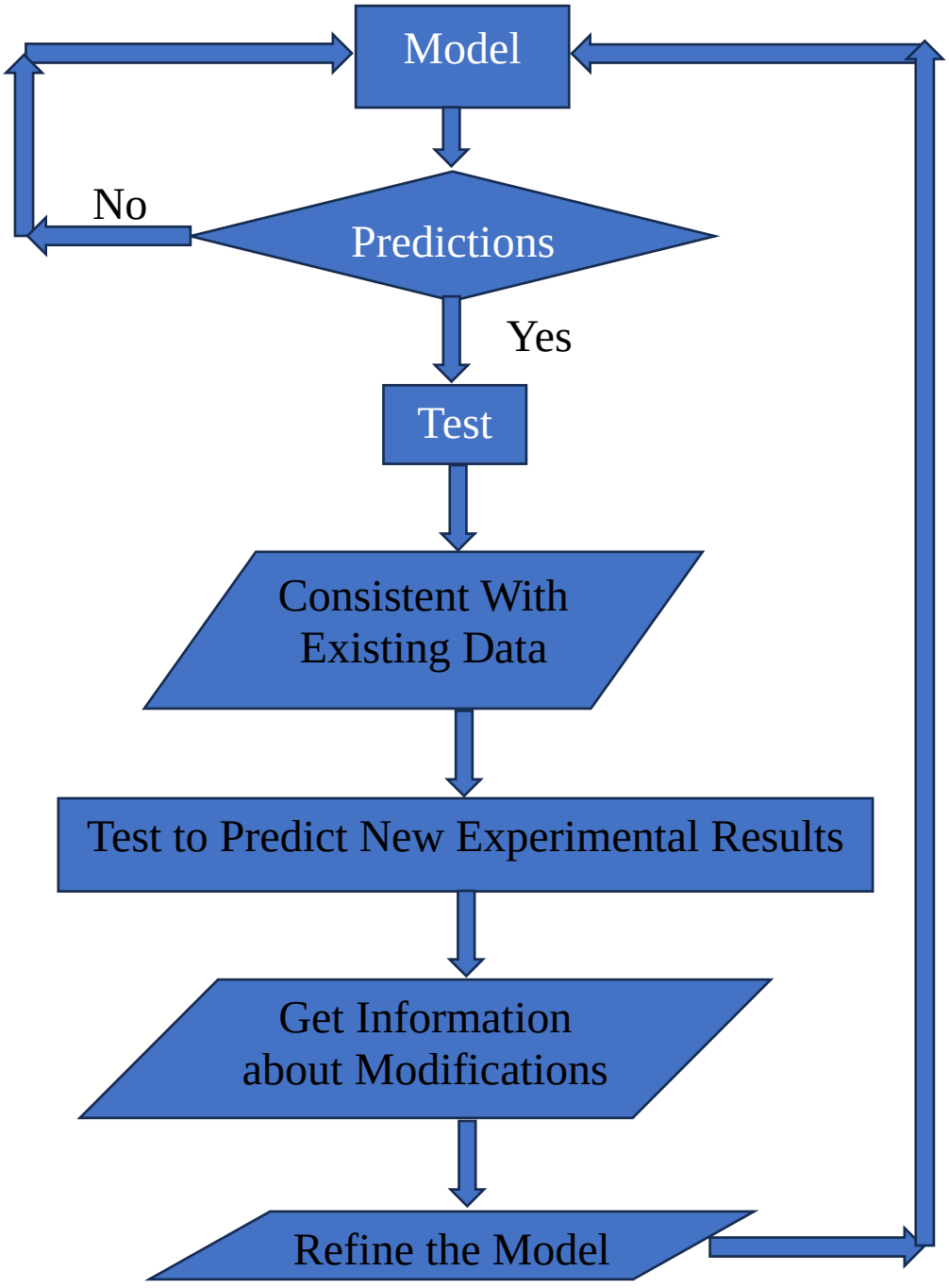


Figure 5-1: Flowchart showing iterative process of model refinement using testing, predicting, and modifying.

Figure 5-1 shows the iterative process used in developing the thermodynamic algorithm using the scientific method of agile process development to refine the model. The flowchart concisely depicts the steps involved in constructing the model to evaluate its effectiveness. One of the classic ways to test the model is to use the experimental data in the literature or by conducting experiments to reproduce some of the classic experiments and feed the model. Since muscle is one of the extensively studied biological systems, we have experimental data that are available from 1920s which provides valuable information that can be used to assess the model's ability to account for experiments such as heat output of the shortening muscle. Hence, accounting for existing data serves as a crucial means to validate the model.

The flowchart depicts that the two state mechanochemical transitions allow variables in the system to be varied in tuning the model; the simulations that are performed in non-ideal trajectories reveal mechanical pathways in different phases of force generation. Even though our detailed work has given a significant insight into the workings of several parameters used within the system, there are several other components that still need to be extensively tested, for example '*a*' parameter. Since 'a' parameter reveals interesting outcomes in non-equilibrium and non-steady state systems, this should serve as the focal point in future studies including isotonic and isometric contractions, stochastic and continuous simulations, force production, and tension transient simulations.

**Next steps.** Expanding the model to simulate tension-transient responses, stretch responses and recovery of muscle in sarcomeres and myofibrils to understand force generation dynamics, equilibration dynamics and spontaneous oscillatory contractions (SPOCs), we will be able to reveal new insights about their mechanochemical effects.

**Reflections on integrating wet lab studies with mathematical and computational modeling.**

I want to emphasize that by integrating wet lab investigations with computational models, we were able to narrow the gap between single molecule mechanics and muscle mechanics by combining theory, experiments, and simulation results. We modeled the muscle as the mechanical system with constructs (system spring), and macroscopic force. These experimental results challenged preexisting ideas and offered critical insights on the ensemble myosin behavior which will offer a paradigm shift in understanding the workings of muscle.

**References**


1. Baker, J. E., LaConte, L. E. W., Brust-Mascher, I. & Thomas, D. D. Mechanochemical coupling in spin-labeled, active, isometric muscle. *Biophys. J.* **77**, (1999).
2. HUXLEY, A. F. Muscle structure and theories of contraction. *Prog. Biophys. Biophys. Chem.* **7**, 255–318 (1957).
3. Hill, T. L. Theoretical formalism for the sliding filament model of contraction of striated muscle. Part I. *Prog. Biophys. Mol. Biol.* **28**, 267–340 (1974).
4. Stewart, T. J., Murthy, V., Dugan, S. P. & Baker, J. E. Velocity of myosin-based actin sliding depends on attachment and detachment kinetics and reaches a maximum when myosin-binding sites on actin saturate. *J. Biol. Chem.* **297**, 101178 (2021).
5. Stewart, T. J. *et al.* Actin sliding velocities are influenced by the driving forces of actin-myosin binding. *Cell. Mol. Bioeng.* **6**, 26–37 (2013).
6. Lymn, R. W. & Taylor, E. W. Mechanism of Adenosine Triphosphate Hydrolysis by Actomyosin. *Biochemistry* **10**, 4617–4624 (1971).
7. Huxley, A. F. Review Lecture : Muscular Contraction. *J. Physiol.* **243**, 1–43 (1974).
8. Hill, A. V. The heat of shortening and the dynamic constants of muscle. *Proc. R. Soc. London. Ser. B, …* **126**, 136–195 (1938).
9. Cremo, C. R. & Geeves, M. A. Interaction of actin and ADP with the head domain of smooth muscle myosin: Implications for strain-dependent ADP release in smooth muscle. *Biochemistry* **37**, 1969–1978 (1998).
10. Webb, M. *et al.* Cooperative Activation of the Thin Filament. (2013).
11. Webb, M. *et al.* The myosin duty ratio tunes the calcium sensitivity and cooperative activation of the thin filament. *Biochemistry* **52**, (2013).
12. Brizendine, R. K. *et al.* Velocities of unloaded muscle filaments are not limited by drag forces imposed by myosin cross-bridges. *Proc. Natl. Acad. Sci.* 201510241 (2015) doi:10.1073/pnas.1510241112.
13. Stewart, T. J., Murthy, V., Dugan, S. P. & Baker, J. E. Velocity of myosin-based actin sliding depends on attachment and detachment kinetics and reaches a maximum when myosin binding sites on actin saturate. *J. Biol. Chem.* 101178 (2021) doi:10.1016/j.jbc.2021.101178.
14. Hooft, A. M., Maki, E. J., Cox, K. K. & Baker, J. E. An accelerated state of myosin-based actin motility. *Biochemistry* **46**, 3513–3520 (2007).
15. Debold & Walcott_2011-$P_i$ enhances myosin-powered actin filament velocity under acidic conditions in a motility assay.pdf.

16. Debold, E. P., Patlak, J. B. & Warshaw, D. M. Slip sliding away: Load-dependence of velocity generated by skeletal muscle myosin molecules in the laser trap. *Biophys. J.* **89**, L34–L36 (2005).

17. Walcott, S., Warshaw, D. M. & Debold, E. P. Mechanical coupling between myosin molecules causes differences between ensemble and single-molecule measurements. *Biophys. J.* **103**, 501–510 (2012).

18. Debold, E. P., Beck, S. E. & Warshaw, D. M. Effect of low pH on single skeletal muscle myosin mechanics and kinetics. *Am. J. Physiol. - Cell Physiol.* **295**, 173–179 (2008).

19. Debold, E. P., Longyear, T. J. & Turner, M. a. The effects of phosphate and acidosis on regulated thin-filament velocity in an in vitro motility assay. *J. Appl. Physiol.* **113**, 1413–22 (2012).

20. Debold, E. P., Turner, M., Stout, J. C. & Walcott, S. Phosphate enhances myosin-powered actin filament velocity under acidic conditions in a motility assay. *Am. J. Physiol. Regul. Integr. Comp. Physiol.* (2011) doi:10.1152/ajpregu.00772.2010.

21. Baker, J. E. Thermodynamics and Kinetics of a Binary Mechanical System: Mechanisms of Muscle Contraction. *Langmuir* **38**, 15905–15916 (2022).

22. Baker, J. E. Chemical Relaxation of a Binary Mechanical Model System. 1–22.

23. Baker, J. E. & Thomas, D. D. A thermodynamic muscle model and a chemical basis for A.V. Hill's muscle equation. *J. Muscle Res. Cell Motil.* **21**, 335–344 (2000).

**Supplement**

This chapter supplements the description of the Thermodynamic model of force generation description in this dissertation. This documentation provides more details regarding the implementation of the model in an iterative stochastic framework for Thermodynamic Collective Force Generation Model code. For the sake of avoiding redundancy, this supplement does not discuss specifics about the theoretical considerations.

**Description of code in model**

To mimic the kinetics, energetics, and mechanics of the chemical and molecular interactions in an ATPase cycle, the algorithm for Thermodynamic Collective Force generation is implemented in Python. Here, we model the behavior of molecules and their interactions using discrete random simulations. Algorithm is designed to allow for user to change parameters according to the type of muscle being used. The model considers a system with four biochemical states: AM (Strongly bound Actin and Myosin without any nucleotides), MT (Myosin with the nucleotide ATP), MDP (Myosin weakly bound to Actin with nucleotides ADP and $P_i$), and AMD (Myosin strongly linked to Actin with the nucleotide ADP). It keeps track of how many molecules are present in each state and mimics their transitions over a predetermined number of steps.

The program performs calculations and generates outputs for a quantity at each stage of the simulation, including the distribution of molecules in each biochemical state, net displacement, free energy values, net force generated, net flux, rates, '*a*' values and other parameters of interest. This kinetic model's distinctive quality is that it is designed

to give users the freedom to adjust the simulation parameters and examine the molecular mechanisms in the ATPase cycle.

Complex systems like muscle are viewed as a series of well-defined events in an ordered sequence. The flow chart shows the steps involved in the design of the stochastic collective force model of muscle contraction. At the start of each time step during the simulation, dynamic variables (the rate constants) are determined. The stochastic evolution of the system over time causes these variables to change. Each head is analyzed to see if a transition has taken place at each time step. For each time step (in our case 1 microsecond step), we generate random numbers for each myosin and the transition probabilities are determined and defined by the rate constants. For instance, let us consider if the myosin is in AM state, how will the myosin make the transition from AM to either MT or AMD? The chance that the myosin will move from state AM to state MT is known as $P_{MT}$, and it depends on the rate of second-order ATP binding and the time step. The probability that the myosin will move from state AM to AMD is known as $P_{AMD}$, and it is also influenced by the rate of ADP binding and the step size. If the random number is less than the sum of $P_{MT}$ and $P_{AMD}$, then the myosin stays in the same state (here, in AM state); if the random number is greater than the sum of $P_{MT}$ and $P_{AMD}$; then the second random number which is generated will be checked for the condition whether random number 2 is greater than $P_{MT} / (P_{MT} + P_{AMD})$; if the condition is yes, then the myosin enters the MT state (meaning a forward transition has occurred); if the condition is ‘no’; then the myosin enters the AMD state, that is the reverse transition has occurred. Hence, this way each myosin in the system will be tracked to identify the transitions and the states will be determined; accordingly, we output all the required

components to visually analyze the results. The model captures all statistics of the system. These include velocity of actin, force generation of myosin, average kinetic rates, time spent in each state, average displacements, net flux, and provides flexibility to plot any required dynamically changing term.

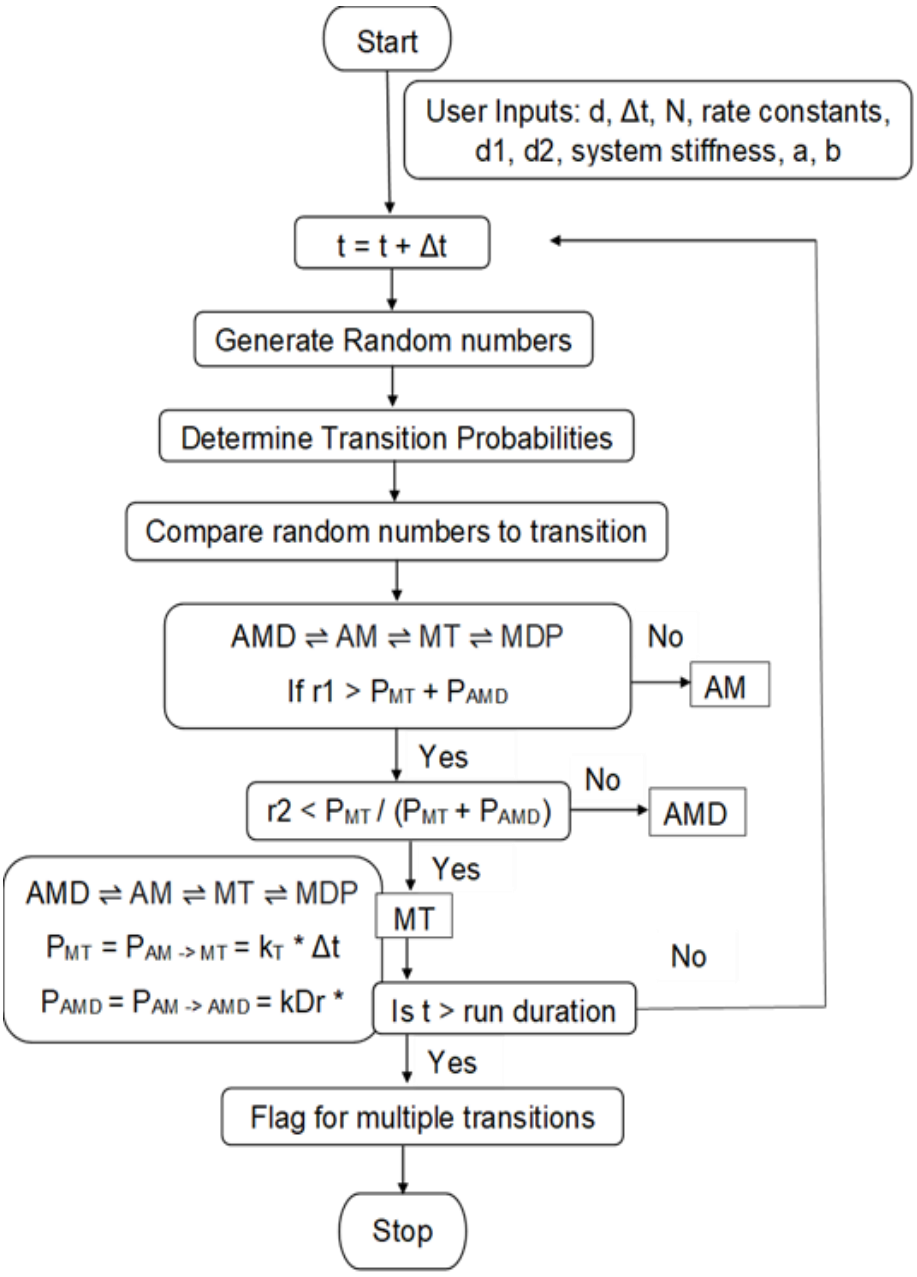


Figure 0-1: Flow chart to show the detailed steps taken to design the algorithm of thermodynamics in muscle contraction with example of biochemical states transition from AM state.

Table 0-1: Simulation constants

| Constants | Name | Value | Unit |
|---|---|---|---|
| Time step | t_step | 1e-6 | s |
| ATP | T | 1 | mM |
| ADP | D | 1 | μM |
| $P_i$ | P | 1 | μM |
| Number of Myosin | Molecules | 50 | |
| Force | F | variable | pN |
| Maximum Force | $F_o$ | variable | pN |
| System Stiffness | κ | 0.04 | $pNnm^{-1}$ |
| Displacement | x | variable | Nm |
| Weak to strong binding step size | $d_1$ | 8 | nm |
| ADP release step size | $d_2$ | 2 | nm |
| Free energy | dG | variable | KT |
| Standard free energy | $dG_o$ | –5.8 | KT |
| ‘a’ term for binding free energy | a_value | 1/N < a < 1 | |
| ‘a’ term for ADP release free energy | a_Prime_val | 1/N < a_Prime<1 | |
| Boltzmann Constant | kT | 4 | pN nm |
| Work partitioning term for binding | a | 0.5 | |
| Work partitioning term for ADP release | b | 0.5 | |
| [AM] -> [A+MT] | $p_{34}$ | 1E6·T | $s^{—1}$ |

| | | | |
|---|---|---|---|
| [A+MT] -> [AM] | $p_{43}$ | 0 | $s^{-1}$ |
| [MT] -> [$MDP_i$] | $p_{41}$ | 20 | $s^{-1}$ |
| [$MDP_i$] -> [MT] | $p_{14}$ | 2 | $s^{-1}$ |
| [$MDP_i$] -> [AMD] | $p_{12}$ | 30 | $s^{-1}$ |
| [AMD] -> [$MDP_i$] | $p_{21}$ | 0.1 | $s^{-1}$ |
| [AMD] -> [AM] | $p_{23}$ | 500 | $s^{-1}$ |
| [AM] -> [AMD] | $p_{32}$ | 0.01 | $s^{-1}$ |

**Code**

```
# -*- coding: utf-8 -*-
"""Created by Vidya Murthy
@author: vmurthy
"""
import numpy as np
class Kinetics_model:
def workingstep(self, number_of_steps: int): #molecules: int):
molecules = int(input('Enter number of molecules: '))
init_molecules_MDP = int(input('Enter number of molecules in MDP: '))
init_molecules_AMD = int(input('Enter number of molecules in AMD: '))
    init_molecules_AM = int(input('Enter number of molecules in AM: '))
    n_actin = 100
    #resetting molecules to not exceed n_actin
    if molecules > n_actin:
        print('N_actin = ', n_actin)
        print('Resetting molecules to n_actin')
        molecules = n_actin
        print('Molecules now is: ', molecules)
    t_step = 1e-6
    kDfo = 250 #s-1
    kTf = 1e6 #s-1 M-1 (per second per molar)
    kHYDf = 20 #s-1
    kHYDr = 2 #s-1
    kDr = 0.1 #s-1
    kTr = 0.000001  #s-1
    displacement = []
    energy = []
```

WS_array = []

t4_mechstep = []

WSr_array = []

t5_mechstep = []

kDf_array = []

t7_ADP = []

disp = []

t8_disp = []

freeenergy = []

t11_dG = []

delG = []

t13_dG = []

force = []

t12_force = []

a_value = [] #array to output 'a' values in d = $d_1$/(a*N)

t15_a = []

a_val = []

t16_a = [] #'a' value time points

a_Prime_value = [] #array to output 'a' values in d = $d_2$/(a*N)

t17_a = []

a_Prime_val = []

t18_a = [] #'a' value time points

K = 0.0138

T = 297

x = 0

$kf_o$ = 30

$kr_o$ = 10

ATP = 1e-5

a = 0.5

```
b = 0.5
L = 0 #Tether length; Units: nm
k = 0.04
p14 = kHYDr * t_step
p34 = kTf * ATP * t_step
p32 = kDr * t_step
p43 = kTr * t_step
p41 = kHYDf * t_step
mol_state = []
state_count={'MDP': 0, 'AMD': 0, 'AM': 0, 'MT':0}
state_count_2={'MDP':init_molecules_MDP, 'AMD':init_molecules_AMD,
'AM':init_molecules_AM}
for i in range(number_of_steps):
    mol_state.append([])
   displacement.append(x)
    dG_o = -(np.log(kf_o/kr_o))
    dG_o_Prime = -(np.log(kDf_o/kDr)) #units of kT ; 1 kT = 4 pNnm
    state_count['MDP'] = mol_state[i].count('MDP')
    state_count['AMD'] = mol_state[i].count('AMD')
    state_count['AM'] = mol_state[i].count('AM')
    state_count['MT'] = mol_state[i].count('MT')
    F = k * x #Force genernated at every time step; 5 pN force is generally generated
    force.append(F)
    t12_force.append(i)
    if state_count['MDP'] ==0 and state_count['AMD'] == 0 :
       Fo = ((-dG_o*molecules)/8 )/4 #maximum isothermic force when a = 1;
    else:
       Fo = ((-dG_o*(state_count['MDP'] + state_count['AMD']))/8)/4
    if state_count['AMD'] == 0 and state_count['AM'] == 0:
       Fo_Prime = ((-dG_o_Prime*molecules)/2)/4
```

```
else:
    Fo_Prime = ((-dGo_Prime*(state_count['AMD'] + state_count['AM']))/2)/4
a1 = F/(Fo)
if a1 < (1/molecules) :
    a1 = 1/molecules
    # a1 = 0.3
    a_value.append(a1)
    t15_a.append(i)
    if len(a_val) >= 0:
        if a1 != a_value[i-1]:
            a_val.append(a1)
            t16_a.append(i)
    else:
        a_val.append(a1)
        t16_a.append(i)
    if state_count['MDP'] ==0 or state_count['AMD'] == 0:
        d1 = 8
    else :
        d1 = 8/(a1*(state_count['MDP'] + state_count['AMD']))
    if d1 > 8:
        d1 = 8
elif a1 >= (1/molecules) and a1 <= 1 :
    a1 = F/(Fo)
    a_value.append(a1)
    t15_a.append(i)
    if len(a_val) >= 0:
        if a1 != a_value[i-1]:
            a_val.append(a1)
            t16_a.append(i)
```

```
    else:
        a_val.append(a1)
        t16_a.append(i)
    if state_count['MDP'] ==0 or state_count['AMD'] == 0:
        d1 = 8
    else :
       d1= 8/(a1*(state_count['MDP'] + state_count['AMD']))
        print('N_AMD+MDP is :', state_count['MDP'] + state_count['AMD'])
    if d1> 8:
        d1 = 8
elif a1 > 1:
    a1 = 1
    a_value.append(a1)
    t15_a.append(i)
    if len(a_val) >= 0:
        if a1 != a_value[i-1]:
            a_val.append(a1)
            t16_a.append(i)
    else:
        a_val.append(a1)
        t16_a.append(i)
    if state_count['MDP'] ==0 or state_count['AMD'] == 0:
        d1 = 8
    else :
        d1 = 8/(a1*(state_count['MDP'] + state_count['AMD']))
    if d1 > 8:
        d1 = 8
#defining a_Prime parameter
a_Prime = F/(Fo_Prime)
```

```
if a_Prime < (1/molecules) :
    a_Prime = 1/molecules
    # a1 = 0.3
    a_Prime_value.append(a_Prime)
    t17_a.append(i)
    if len(a_Prime_val) >= 0:
        if a_Prime != a_Prime_value[i-1]:
            a_Prime_val.append(a_Prime)
            t18_a.append(i)
    else:
        a_Prime_val.append(a_Prime)
        t18_a.append(i)
    if state_count['AM'] ==0 or state_count['AMD'] == 0:
        d2 = 2
    else :
       d2= 2/(a_Prime*(state_count['AM'] + state_count['AMD']))
    if d2 > 2:
        d2 = 2
elif a_Prime >= (1/molecules) and a_Prime <= 1 :
    a_Prime = F/(Fo_Prime)
    a_Prime_value.append(a_Prime)
    t17_a.append(i)
    if len(a_Prime_val) >= 0:
        if a_Prime != a_Prime_value[i-1]:
            a_Prime_val.append(a_Prime)
            t18_a.append(i)
    else:
        a_Prime_val.append(a_Prime)
        t18_a.append(i)
```

```
    if state_count['AM'] ==0 or state_count['AMD'] == 0:
      d2 = 2
    else :
       d2 = 2/(a_Prime*(state_count['AM'] + state_count['AMD']))
    if d2 > 2:
       d2 = 2
elif a_Prime > 1:
    a_Prime = 1
    a_Prime_value.append(a_Prime)
    t17_a.append(i)
    if len(a_Prime_val) >= 0:
       if a_Prime != a_Prime_value[i-1]:
          a_Prime_val.append(a_Prime)
          t18_a.append(i)
    else:
       a_Prime_val.append(a_Prime)
       t18_a.append(i)
    if state_count['AM'] ==0 or state_count['AMD'] == 0:
      d2= 2
    else :
       d2 = 2/(a_Prime*(state_count['AM'] + state_count['AMD']))
    if d2 > 2:
       d2 = 2
else:
    d2 = 2/(a_Prime*(state_count['AM'] + state_count['AMD']))
if d2 > 2:
    d2 = 2
#defining free enegry
if state_count['MDP'] == 0 or state_count['AMD'] == 0:
```

```
            dG = dG_o + (np.log(state_count_2['AMD'] / state_count_2['MDP'])) + ((F*
d_1)/(K*T)) #units of energy in kT
            freeenergy.append(dG)
            t11_dG.append(i)
            if len(delG) >= 0:
               if dG != freeenergy[i-1]:
                  delG.append(dG)
                  t13_dG.append(i)
            else:
               delG.append(dG)
               t13_dG.append(i)
         else:
            dG = dG_o + (np.log(state_count['AMD'] / state_count['MDP'])) + ((F*
d_1)/(K*T)) #units of energy in kT
            freeenergy.append(dG)
            t11_dG.append(i)
            if len(delG) >= 0:
               if dG != freeenergy[i-1]:
                  delG.append(dG)
                  t13_dG.append(i)
            else:
               delG.append(dG)
               t13_dG.append(i)
         #defining rates
         if x < (L- d_1):
            e = (1/2) * 0.001* (x**2)
            energy.append(e)
            kWSf = kf_o * np.exp((-1.0)*(a)*(((0.5*0.001*(((x) + d_1)**2)) -
(0.5*0.001*((x)**2)))/(K*T)))
```

```
            WS_array.append(kWSf)

            t4_mechstep.append(i)

            kWSr = kr_o*np.exp((-1.0)*(1-a)*(((0.5*0.001*((x)**2)) - (0.5*0.001*(((x)+
d_1)**2)))/(K*T)))

            WSr_array.append(kWSr)

            t5_mechstep.append(i)

            kDf = kDf_o * np.exp((-1.0) * (b) * (((0.5 * 0.001 * (((x)+d_2)**2)) - (0.5 * 0.001
* ((x)**2))) / (K*T)))

            kDf_array.append(kDf)

            t7_ADP.append(i)

        else:

            L > x >= (L- d_1)

            kWSf = kf_o * np.exp((-1.0)* (a) * (((0.5 * 0.001* (L**2)) + (0.5 * k * (d_1-
L+x)**2)) - (0.5 * 0.001 * (x**2))))

            WS_array.append(kWSf)

            t4_mechstep.append(i)

            kWSr = kr_o * np.exp((-1.0) * (1-a) * ((0.5*0.001*(x**2)) - ((0.5 * 0.001 *
(L**2)) + (0.5 * k * (d_1-L+x)))))

            WSr_array.append(kWSr)

            t5_mechstep.append(i)

            kDf = kDf_o * np.exp((-1.0) * (b) * (((0.5*0.001 * (L**2)) + (0.5 * k * (d_2-
L+x)**2)) - (0.5 * 0.001 * (x**2))))

            kDf_array.append(kDf)

            t7_ADP.append(i)

        p12 = kWSf * t_step

        p21 = kWSr * t_step

        p23 = kDf * t_step

        for j in range(molecules):

            mol_state[i].append(j)

            r1 = np.random.rand()

            r2 = np.random.rand()
```

```
if i==0:
    mol_state[i][j] = 'AM'
    self.increment_statecount('AM', state_count)
else:
    if mol_state[i-1][j] == 'MDP':
        if r1 >= (p12 + p14):
            mol_state[i][j] = 'MDP'
        elif r2 < (p12 / (p12+p14)):
            mol_state[i][j] = 'AMD'
            disp.append(x)
            t8_disp.append(i)
            x = x + d1
            disp.append(x)
            t8_disp.append(i)
        else:
            mol_state[i][j] = 'MT'
    if mol_state[i-1][j] == 'AMD':
        if r1 >= (p21 + p23):
            mol_state[i][j] = 'AMD'
        elif r2 < (p23 / (p21 + p23)):
            mol_state[i][j] = 'AM'
            x = x + d2
            disp.append(x)
            t8_disp.append(i)
        else:
            mol_state[i][j] = 'MDP'
            self.increment_statecount('MDP', state_count)
```

```
                    x = x - d1

                    disp.append(x)
                    t8_disp.append(i)
                if mol_state[i-1][j] == 'AM' :
                    if r1 >= (p34 + p32):
                        mol_state[i][j] = 'AM'
                    elif r2 < (p34 / (p32 + p34)):
                        mol_state[i][j] = 'MT'
                    else:
                        mol_state[i][j] = 'AMD'
                        x = x - d2
                        disp.append(x)
                        t8_disp.append(i)
                if mol_state[i-1][j] == 'MT':
                    if r1 >= (p41 + p43):
                        mol_state[i][j] = 'MT'
                    elif r2 < (p41 / (p41 + p43)):
                        mol_state[i][j] = 'MDP'
                    else:
                        mol_state[i][j] = 'AM'
        return
def main():
    pass
if __name__ == '__main__':
    main()
```